Conversion of MX Nitrides to Modified Z-Phase in 9-12%Cr Ferritic Steels

Cipolla, Leonardo; Somers, Marcel A. J.; Hald, John

Publication date:
2010

Document Version
Publisher's PDF, also known as Version of record

Conversion of MX Nitrides to Modified Z-Phase in 9-12%Cr Ferritic Steels

PhD Thesis

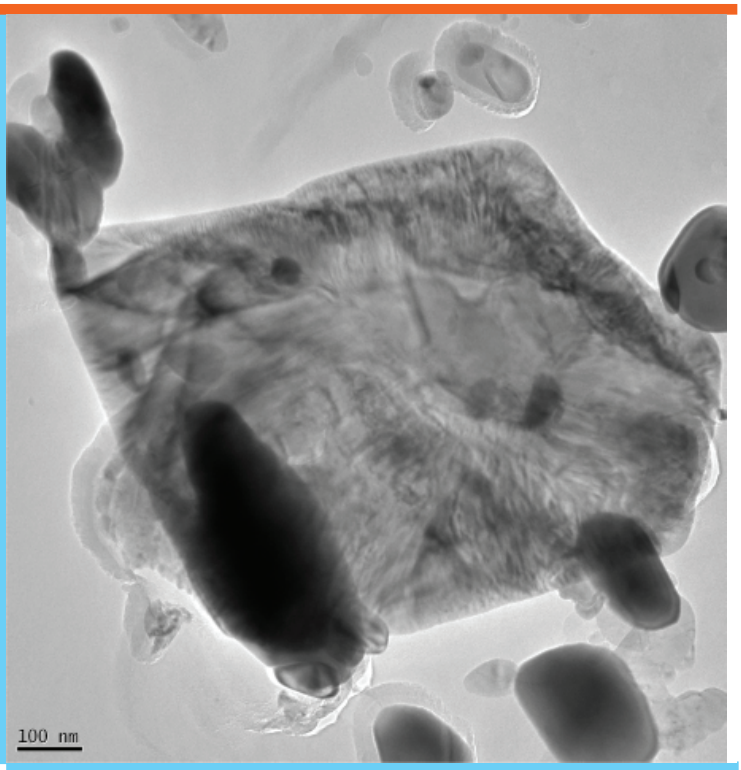

Leonardo Cipolla
DCAMM Special Repport No. S116
March 2010

DTU Mechanical Engineering
Department of Mechanical Engineering

Conversion of MX Nitrides to Modified Z-phase in 9-12%Cr Ferritic Steels

Leonardo Cipolla

Ph.D. Thesis

Department of Mechanical Engineering
Technical University of Denmark
Kgs. Lyngby, Denmark

March 2010

This page was left blank on purpose

To my lovable wife Valentina

This page was left blank on purpose

Preface

This thesis is part of the official requirements for acquiring the Ph.D. degree at the Technical University of Denmark (DTU).

The thesis is the result of a strong and fruitful three-years collaboration between DTU and Centro Sviluppo Materiali (CSM), an Italian private company active in the field of materials science, which financially supported the research activities.

Indeed, as metallurgical researcher enrolled in CSM at Steel Metallurgy Department, I run several research activities at CSM unit in Rome.

The main coordination of the Ph.D. project was taken by the Department of Mechanical Engineering (DTU), under the supervision of Prof. Marcel A. J. Somers and Associated Professor John Hald.

The Ph.D. studies have been carried out in the period of January 1st 2007 to March 31th 2010.

The following papers are included in the thesis:

1. L. Cipolla, H. K. Danielsen, D. Venditti, P. E. Di Nunzio, J. Hald, M. A. J. Somers, *Conversion of MX Nitrides to Z-Phase in a Martensitic 12%Cr Steel*, Acta Materialia 58 (2010) 669-679.
2. L. Cipolla, H. K. Danielsen, D. Venditti, P. E. Di Nunzio, J. Hald, M. A. J. Somers, *On the Role of Nb in Z-Phase Formation in a 12%Cr Steel*, Scripta Materialia 63 (2010) 324-327
3. P.E. Di Nunzio, L. Cipolla, M. A. J. Somers, S. Tiberi Vipraio, *Quantitative X-ray Diffraction Analysis of Development of Z-Phase in 12%Cr-Nb-V-N Steel*, Materials Science and Technology, in proof, DOI 10.1179/026708309X12567268926687.
4. L. Cipolla, S. Caminada, D. Venditti, H. K. Danielsen, A. Di Gianfrancesco, *Microstructural Evolution of ASTM P91 after 100,000 hours exposure at 550℃ and 600℃*, 9th Liège Conference on Materials for Advanced Power Engineering, September 27th-29th, 2010, Liège, Belgium.

31 March 2010 Leonardo Cipolla

Rome, Italy

This page was left blank on purpose

Conversion of MX Nitrides to Modified Z-phase in 9-12%Cr Steels

Leonardo Cipolla
Department of Mechanical Engineering
Technical University of Denmark

Abstract

The 9-12%Cr ferritic steels are extensively used in modern steam power plants at service temperature up to 620℃. Currently the best perform ing ferritic creep resistance steel is the ASTM Grade 92, whose high temperature strength has recently been assessed by European Creep Collaborative Committee in 2005 as 600℃/113MPa/10^5h.
All previous attempts made in the last twenty years to develop ferritic steels for 650℃ applications have failed due to the incapacity to combine the superior oxidation resistance, given by 12%Cr content, with excellent creep resistance of high-alloyed ferritic steels.
Indeed the fast conversion of finely distributed MX nitrides, which highly promote creep strengthening, to larger and thermodynamically more stable modified Z-phase, Cr(V,Nb)N, led to an unforeseen drop of creep resistance of 12%Cr steels. Since chromium content was confirmed to be the main driving force for Z-phase formation, this explains why 12%Cr steels (i.e. P122, VM12, NF12) suffer from fast and abundant Z-phase precipitation, while 9%Cr steels (i.e. Grades 91, 92, 911) do not.

In this thesis the role of vanadium and niobium nitrides in the formation of Z-phase in 9-12%Cr steels is investigated. With this purpose in mind, two 12%Cr model alloys, 12CrVNbN and 12CrVN, with ultra low carbon content, were manufactured. Both model alloys consisted of Cr-, V- and Nb-nitrides only.
The first model alloy, 12CrVNbN, was especially designed to quickly convert the complex V- and Nb-nitrides into modified Z-phase. The second model alloy, 12CrVN, was selected to investigate the transformation of pure V-nitride into V-based Z-phase, CrVN, and through comparison to understand the effect of Nb.
Thus, without the disturbing interferences of carbides and intermetallic phases (i.e. $M_{23}C_6$, NbC, $Fe_2(Mo,W)$) it was possible to identify all stages of MX conversion to Z-phase particle during ageings at 600℃, 650℃ and 700℃ up to 10^4 hours.

Transmission Electron Microscopy (TEM) and X-Ray powder Diffraction (XRD) were applied to follow the microstructural evolution of the nitrides of model alloys during ageings: morphology, crystal structure, chemical composition and equivalent diameter of precipitates were assessed over times and temperatures.

The mechanism of Z-phase formation was identified in the model alloys; hybrid MX/Z particles were found as mid-stage phases of this conversion. The key-role of niobium as accelerator for Z-phase formation was highlighted during the studies.

Several 9-12%Cr commercial steels with prolonged high-temperature exposures have been investigated, too. The same mechanism of Z-phase formation observed in 12%Cr model alloys was identified in industrial 9-12%Cr steels after thousands of hours of high-temperature service. The first MX/Z-phase hybrid particles in Grade P91 and P92 were identified during the Ph.D. project.

Omdannelse af MX Nitrider til Modificeret Z-fase i 9-12%Cr Stål

Leonardo Cipolla
Institut for Mekanisk Teknologi
Danmarks Tekniske Universitet

Resumè

9-12%Cr ferritiske stål er meget brugt I moderne damp kraftværker ved drifts temperaturer op til 620℃. Det nuværende ferritiske stål med den bedste krybestyrke er ASTM stål P92, hvilke højtemperatur styrke for nylig er blevet vurderet af European Creep Collaborative Committee i 2005 som 600℃/113MPa/10^5h.

Alle forrige forsøg som er gjort de sidste tyve år for at udvikle et ferritisk stål til brug ved 650℃ har slået fejl på grund af at man ikke har ku nne kombineret høj oxidation modstand, givet ved 12%Cr indhold, med høj krybestyrke i højt legerede ferritiske stål.

Den hurtige omdannelse af fint fordelte MX nitrider, som giver høj krybestyrke, til større og mere termodynamisk stabile modificerede Z-faser, Cr(V,Nb)N, gav et uforudset tab af krybestyrke af 12%Cr stål. Siden da er krom indholdet blevet identificeret til at være hoved drivkraften bag Z-fase udskillelse, hvilket forklarer hvorfor 12%Cr stål (såsom P122, VM12, NF12) rammes af hurtig og massiv Z-fase udskillelse, imens 9%Cr stål (såsom stål 91, 92, 911) ikke gør.

I denne afhandling vil rollen af vanadin og niob nitriders rolle i udskillelsen af Z-fase blive undersøgt. Med dette formål er to 12%Cr model legeringer, 12CrVNbN og 12CrVN med meget lave kulstof indhold, blevet fremstillet. Begge model legeringer indeholder kun af Cr, V- og Nb-nitrider.

Den første model legering, 12CrVNbN, er specielt udviklet til hurtigt at omdanne de komplekse V- og Nb-nitrider om til Z-fase. Den anden model legering, 12CrVN, var udvalgt til at undersøge omdannelsen af rene V-nitrider til V-baserede Z-faser, CrVN, og igennem sammenligning at forstå effekten af Nb.

Således, uden forstyrrelser af karbider og intermetalliske faser (såsom $M_{23}C_6$, NbC, $Fe_2(Mo,W)$), var det muligt at identificere alle stadier af MX omdannelsen til Z-fase partikler under ældning ved 600℃, 650℃ og 700℃ u p til 10^4 timer.

Transmission Elektron Mikroskopi (TEM) og røntgen stråle pulver diffraktion (XRD) var det muligt at følge den mikrostrukturelle udvikling af nitrider i model legeringerne igennem ældningen: morfologi, krystal struktur, kemiske sammensætninger og ækvivalent diameter af udskillelserne blev vurderede over tid og temperatur.

Mekanismen af Z-fase dannelsen var identificeret i model legeringerne; hybride MX/Z partikler blev fundet som halvvejs faser af denne omdannelse. Nøgle rollen af Niob som accelerator for Z-fase dannelse var fremhævet igennem studierne.

Flere 9-12%Cr erhversmæssige stål der har været udsat for høje temperaturer ved længere tider er også blevet undersøgt. Den samme mekanisme af Z-fase dannelse set i 12%Cr model legeringerne blev også fundet i industrielle 9-12%Cr stål udsat for tusindvis af timer ved høje temperaturer. De første MX/Z-fase hybrid partikler in stål P91 og P92 blev set igennem dette PhD projekt.

Table of Contents

CHAPTER 1

INTRODUCTION

This Ph.D. project focused on the understanding the role of Nb and V-nitrides on the formation of modified Z-phase, Cr(V,Nb)N, in ferritic 9-12%Cr creep resistant steels.

Modern 9-12%Cr creep resistance steels develop modified Z-phase, Cr(V,Nb)N, during high-temperature service. The formation of Z-phase occurs at the expense of finely distributed MX nitrides, which greatly contribute to matrix creep strengthening as opposed to Z-phase, resulting in a net loss of creep strength. Since the substitution of MX nitrides with more stable Z-phase particles is much faster in 12%Cr steels, this caused the breakdown of all promising developments for new ferritic steels for 650℃ applications, where superior oxidation resistance given by 12%Cr could be combined with high creep resistance.

At the start of the project various research activities were ongoing worldwide regarding Z-phase behaviour in 9-12%Cr steels. It was clearly demonstrated that MX nitrides were not thermodynamically stable and that the chromium content constituted the main driving force for Z-phase formation. In particular, major progress on understanding of Z-phase development was made by my H. K. Danielsen during his PhD at DTU [ref. H. K. Danielsen: “Z-phase in 9-12%Cr steels” Ph.D. Thesis, 2007, Technical University of Denmark].

The crystal structure of modified Z-phase was revealed for the first time and a thermodynamic model including Z-phase was developed for 9-12%Cr steels. However, unsolved questions concerned the time-temperature regions of stability, the role of hybrid MX/Z particles, the mechanism of MX conversion and the role of Nb.

It is very difficult and likely impossible to reveal the mechanism of Z-phase formation in common 9-12%Cr steels, since this nitride forms in aged steels with several other precipitating phases (carbides, intermetallic phase, other nitrides), which generally *obscure* the MX/Z conversion stages. Hence, it was recognised that in order to understanding the development of Z-phase in 12%Cr steels, with and without Nb, model alloys without carbides and Laves phase should be investigated.

With this purpose two model alloys containing Cr, V, Nb and N only, and with C, Mo and W contents are low as possible, were produced. Accordingly, after normalising and tempering heat treatment, the model alloys contained of Cr-, V- and Nb-nitrides only, dispersed in a tempered martensitic microstructure.

The model alloys were specially designed to quickly form modified Z-phase during ageings. The first model alloy was produced to study the conversion of complex V- and Nb-based nitrides into Z-phase; the second model alloy is Nb-free and it was produced to focus on the transformation of V-nitride to V-based Z-phase only.
Aged samples of both model alloys at 600℃, 650℃ a nd 700℃ up to 10,000 hours were investigated during the project.

Several 9-12%Cr commercial steels with prolonged high-temperature exposure were analysed, too: P91 samples exposed over 100,000 hours at 550℃ and 600℃ as well as P92 samples after 60,000 hours at 650℃ were analys ed with the purpose of indentifying all stages of the mechanism for Z-phase formation in aged industrial steels.

Transmission Electron Microscopy (TEM) and X-Ray powder Diffraction (XRD) were mainly applied to follow the microstructural evolution of the nitrides during ageing: morphology, crystal structure, chemical composition and equivalent diameter of precipitates were assessed over times and temperatures.

CHAPTER 2

METALLURGY OF 9-12%CR CREEP FERRITIC STEELS

2.1 Historical Development of 9-12%Cr Steels for Power Generation

Up to the 1920s it was general practice to use non-alloyed steels for power plant components in the steam admission zone exposed to maximum temperatures of 350℃ and pressures of about 15 bar. At the beginning of the 1920s, operation at steam temperatures of 450℃ and pressures of 35 bar called for the development of low-alloyed heat resistant steels [1].

The 2¼Cr-1Mo steel (nominally 2.25Cr-1.0Mo-0.3Si-0.45Mn-0.12C composition), designated by ASTM as Grade 22[1], was introduced in the 1940s and it is still widely used nowadays; along with Grade 22, the 9Cr-1Mo steel, designed by ASTM as Grade 9 (nominally 9.0Cr-1.0Mo-0.6Si-0.45Mn-0.12C composition), was developed by additional chromium for superior corrosion resistance [2].

Since then, there has been a continual push to increase operating temperatures of fossil fired power-generation systems. This led to the development of several "generations" of steels with improved high-temperature strengths, obtained by addition of several alloying elements, such as Mo, V, Nb, N, W, Co, also in large amounts.

The evolution of compositions of 9-12%Cr steels, which began with T9 Grade (zeroth generation) with 100,000 h creep-rupture strength at 600ºC of about 40 MPa, has allowed an overall increase of the operating steam temperatures and pressures [2].

Three successful generations of steels have been developed since the introduction of T9, leading to worldwide used 9%Cr steels, such as ASTM Grade 91 and 92. This latter is currently the best performing ferritic creep resistant steel for power plant applications up to 620℃, with a creep resistance at 600℃ of about 11 3MPa within 100,000 hours [3].

A fourth generation of ferritic creep resistant steels turned out a failure, with lack of all expectations, due to unexpected instability of steel microstructure (i.e. NF12, VM12).

Nowadays a fifth generation of new ferritic creep resistant steels is under development.

[1] Grade 22 and the other commercial steels discussed in this thesis are given designations by ASTM (i.e. Grade 9 is 9Cr-1Mo and Grade 91 is modified 9Cr-1Mo). The steels are further distinguished as T22 or T91 for tubing, P22 and P91 for piping, F22 and F91 for forgings, etc. The "T" and "P" designations will mainly be used in this thesis, since many of the steels were developed for boiler tubing and steam piping, although they are also used as other product forms.

Table 1 summarises the chemical compositions of the most popular 9-12%Cr commercial steels developed for power generation industry in past and recent years.
Table 2 shows the evolution of 9-12%Cr ferritic steels over the years, in terms of steel modifications with respect to T9 basic composition (zeroth generation).

Table 1 – Nominal composition of commercial and laboratory 9-12%Cr steels [1] [2].

Designation	C	Si	Mn	Cr	Mo	W	Co	Ni	V	Nb	N	B
T9	0.12	0.60	0.45	9.0	1.0							
X20	0.20	0.35	0.50	12.0	1.0				0.25			
12Cr1MoV (HT91)	0.20	0.40	0.50	12.0	1.0			0.70	0.25			
HCM12	0.10	0.3	0.55	12.0	1.0	1.0			0.25	0.05	0.03	
T91	0.10	0.35	0.45	8.75	1.00	/		0.20	0.21	0.08	0.050	
T911	0.10	0.35	0.45	9.0	1.0	1.0		0.20	0.20	0.08	0.050	0.003
T92 (NF616)	0.10	0.40	0.50	9.0	0.45	1.8		0.15	0.20	0.06	0.045	0.003
P122 (HCM12A)	0.10	0.50	0.50	11.0	0.40	2.0	1.0Cu	<0.40	0.22	0.06	0.06	0.003
TB12	0.10	0.06	0.50	12.0	0.50	1.8		0.1	0.20	0.05	0.06	0.004
TB12M	0.13	0.25	0.50	11.0	0.50	1.8		1.0	0.20	0.06	0.06	
VM12	0.12	0.50	0.35	11.5	0.30	1.5	1.6	0.30	0.25	0.05	0.065	0.005
NF12	0.10	0.35	0.50	10.2	0.15	2.5	2.0	<0.10	0.22	0.07	0.02	0.005
SAVE12	0.10	0.30	0.20	11.0		3.0	3.0	<0.10	0.20	0.07	0.04	0.07Ta 0.04Nd
MARBN 9-3-3	0.08			9.0		3.0	3.0		0.20	0.05	0.008	0.014

Table 2 – Evolution of 9-12%Cr ferritic steels for power generation industry [1] [2].

Generation	Years	Steel Modification	10^5 h Rupture Strength, 600℃ (MPa)	Steels	Max Use Temperature (℃)
0	1940-60		40	T9	538
1	1960-70	Addition of Mo, Nb, V to T9. Introduction of 12%Cr	60	EM12, HT9, HT91, X20	565
2	1970-85	Optimisation of C, Nb, V. Introduction of N.	95	T91, HCM12	593
3	1985-95	Partial Substitution of Mo for W and addition of Cu, B	115	NF616, E911, HCM12A	620
4	1985-2000	Increase of W and addition of Co	<95	NF12, SAVE12, VM12	610
5	2000-Nowadays	NIMS steels: suppression of N and B addition Z-steels: very low C, addition of Ta	>120	NIMS Steel 9-3-3, Z-steels	650

High temperature resistant steels belonging to the zeroth generation contained mainly 9%Cr for improved corrosion and oxidation resistance for elevated-temperature operating conditions, up to maximum temperature of 538℃.

The first generation mainly involved the addition of vanadium and niobium as carbide formers to T9 base composition, with the purpose of obtaining precipitate strengthening. In some cases, a small tungsten addition was made for further solid solution strengthening, in addition to that provided by molybdenum. Where higher oxidation was requested, the chromium content was raised up to 12-wt%.

Generally since the first generation, the microstructures of the 9-12% Cr steels are designed by balancing austenite and ferrite stabilizers to produce 100% martensite when cooling after normalising heat treatment, although small amounts of δ-ferrite (<2%) may be present in some cases, especially in the 12% Cr steels. Nevertheless some duplex steels containing martensite and δ-ferrite have been developed and used; however unless otherwise stated, the microstructures discussed here are assumed to be ≈ 100% martensite.

This first generation of high-temperature steels, introduced in the 1960s for applications to 565ºC, included HT9 (12.0Cr-1.0Mo-0.25V-0.5Ni-0.5W-0.6Mn-0.4Si-0.2C), HT91 (12.0Cr-1.0Mo-0.25V-0.5Ni-0.6Mn-0.4Si-0.2C), X20 (12Cr-1.0Mo-0.25V-0.2C) and EM12 (9.5Cr-2.0Mo-0.30V-0.40Nb-1.1Mn-0.4Si-0.10C); this latter is a duplex steel, with about 50% δ-ferrite because of the 2% Mo in the alloy composition. The steels belonging to the first generation increased the 100,000 h rupture strengths at 600ºC of up to 60 MPa [2].

For the second generation, developed between 1970-1985, carbon, niobium, and vanadium contents were optimized, together with the addition of nitrogen (0.03-0.05-wt%), thus the maximum operating temperature was raised to 593ºC. These steels included modified 9Cr-1Mo, designated T91 (9.0Cr-1.0Mo-0.2V-0.08Nb-0.05N-0.40Mn-0.40Si-0.10C) and HCM12 (12.0Cr-1.0Mo-1.0W-0.25V-0.05Nb-0.55Mn-0.30Si-0.03N-0.10C); they exhibit 100,000 h rupture strengths at 600ºC of about 95 MPa. Among them, T91 has been used most extensively in the power-generation industry throughout the world [2].

The third generation of steels was developed based on the previous generation, primarily by the substitution of tungsten for some of the molybdenum. These steels, which will be discussed in detail further, are well represented by NF616 (9.0Cr-1.8W-0.5Mo-0.20V-0.05Nb-0.45Mn-0.06Si-0.06N-0.004B-0.07C), designated by ASTM as Grade 92, E911

(9.0Cr-1.0Mo-1.0W-0.20V-0.08Nb-0.40Mn-0.40Si-0.07N-0.11C), TB12 (12.0Cr-0.5Mo-1.8W-1.0Ni-0.20V-0.05Nb-0.50Mn-0.10Ni-0.06Si-0.06N-0.004B-0.10C) and HCM12A (12.0Cr-0.5Mo-2.0W-1.0Cu-0.25V-0.05Nb-0.30Ni-0.60Mn-0.10Si-0.06N-0.003B-0.10C), designated as ASTM Grade 122.

The 9%Cr steels of the third generation – NF616 (T92) developed in Japan, and E911 developed in Europe – are both simple modifications of T91. In the NF616, half the molybdenum was replaced by tungsten, whereas in the E911 a 1% W was added to the T91 composition. Both steels contain slightly more nitrogen (0.04-0.07%) than T91 (≈0.05%), and the NF616 contains a small boron addition (10-60ppm) [2].

The TB12 steel, an advanced third-generation 12%Cr steel, is a similar modification of T91 as NF616 with regard to the W, Mo, N, and B, and it has a duplex structure of δ-ferrite and martensite because the extra ferrite-stabilizing element (chromium) is not offset by enough austenite-stabilizing element. It contains only 0.1% Ni to offset the 3% Cr addition (it also contains 0.05% N, an austenite stabilizer). In TB12M, up to 1% Ni is added to produce a 100% martensitic steel.

The HCM12A steel is a somewhat similar 12%Cr composition to that of TB12M, but with a 1% Cu addition as the austenite stabilizer. Copper was used instead of nickel, which was generally used in the past (as it was for TB12M, HT9 and HT91), because nickel reduces creep strength.

More recently, by the beginning of the 3rd millennium, even more alloyed 12%Cr steels were produced, by the addition up to 3% W, balanced by Co in about the same quantity. This further development was explained by the fact that W was found to be very effective (more than Mo) in stabilising the precipitation. Hence steels belonging to the fourth generation (Table 2) were realised for aiming to 650℃ applications: VM12 (0.12C-11.5Cr-0.3Mo-1.5W-1.6Co-0.25V-Nb-N-B), SAVE12 (0.12-11Cr-3W-3Co-0.2V-Nb-N-Ta-Nb) and NF12 (0.10C-10.2Cr-0.15Mo-2.5W-2Co-0.22V-Nb-N-B) [1].

Unfortunately, the promising expectations to combine oxidation resistance, obtained by 12%Cr content, with the excellent creep resistance given by addition of V, Nb, N, W, broke against the unpredicted microstructural evolution of all 12%Cr steels of the third and fourth generation (P122 included), which showed a dramatic drop of creep resistance after 10,000 hours at 650℃, to below or equal to that of T91 steel. In fact, the higher Cr content, together with the V- and Nb-alloying for precipitating nitrides, promoted a fast

degradation of the 12%Cr microstructure, thus cancelling more than twenty years of material development and shattering all expectations to have a new ferritic creep-resistant steel ready for 650℃ service temperature in modern power plants [4] [5] [6].

The reason for the unpredicted degradation of creep properties was found in the transformation of Nb- and V-nitrides into more stable Cr-rich nitrides, known as modified Z-phase, which are less effective in strengthening the matrix [4] [7].

The understanding of the metallurgical reasons of the failure of modern 12%Cr steels due to Z-phase formation is the main goal of the present Ph.D. thesis and will be thoroughly assessed in the following chapters.

Since the drop in creep resistance of P122 and similar 12% Cr steels was explained by the unexpected evolution of their V- and Nb-nitrides, the steels under current development, belonging to the next generation of ferritic steels for 650℃ applications (fifth generation), are based on two different metallurgical approaches:

1) suppressing or delaying the Z-phase formation [8] [9]
2) use of Z-phase for precipitate strengthening [10] [11].

The suppression of Z-phase precipitation was obtained in Japanese new steels by suppression of nitrogen (maintained at minimum level, as scrap element). This class of steels was developed by Japanese National Institute of Material Science (NIMS) in the last ten years; they are 9-12%Cr steels, strengthened mainly by Cr-carbides, adopting the beneficial effect of boron addition, which is believed to stabilise the precipitation, especially along grain boundaries. Due to their martensitic microstructure and the addition of boron, these steels are known as MARBN steels. Recent creep-strength evaluation of the NIMS MARBN steel 9Cr-3W-3Co is 650℃/100MPa/3 $\cdot 10^4$h [8] [9].

On the opposite side, the alloying concept to use Z-phase as precipitate strengthener was developed by Danish researchers in more recent years and it is currently under development. These are low carbon steels and their precipitates consist of nitrides and intermetallic phases only, such as Z-phase and Laves phase [11].

2.2 Recent Assessments of Creep-Rupture Strength

European Creep Collaborative Committee (ECCC) has recently published new creep-rupture predictions of 9-12%Cr steels currently used in power plants during the ECCC Conference on April 2009, in Zurich (CH) [12].

The conference was the occasion to remark the high reliability of European creep-rupture assessments of advanced 9%Cr steels, such as Grades 91 and 92, due to the availability of wide creep databases which allow predictions up to 200,000 hours at 600℃.

The creep resistance of Grades 91, 911 and 92 to have rupture within 600℃ at 10^5h were respectively assessed as follows: 90MPa in 2009 [13] [14], 98 [15] and 113MPa in 2005 [3] [16]. Figure 1 shows the comparison of the 100,000 h creep-rupture strength of Grades 91, 911 and 92.

On the other hand the drop of creep strength of 12%Cr steels, such as P122 (HCM12A) and HCM12, was recently confirmed by long-term creep tests [17].

Figure 1 shows the 100,000 h creep rupture strength of Grades 91, 911 and 92, compared with old 12Cr1MoV steel. Grade 92 is confirmed to be the best promising 9%Cr creep resistance steel available until now. Figure 2 shows the creep-rupture isotherms of the most popular 9-12%Cr creep resistant steels at 650°C.

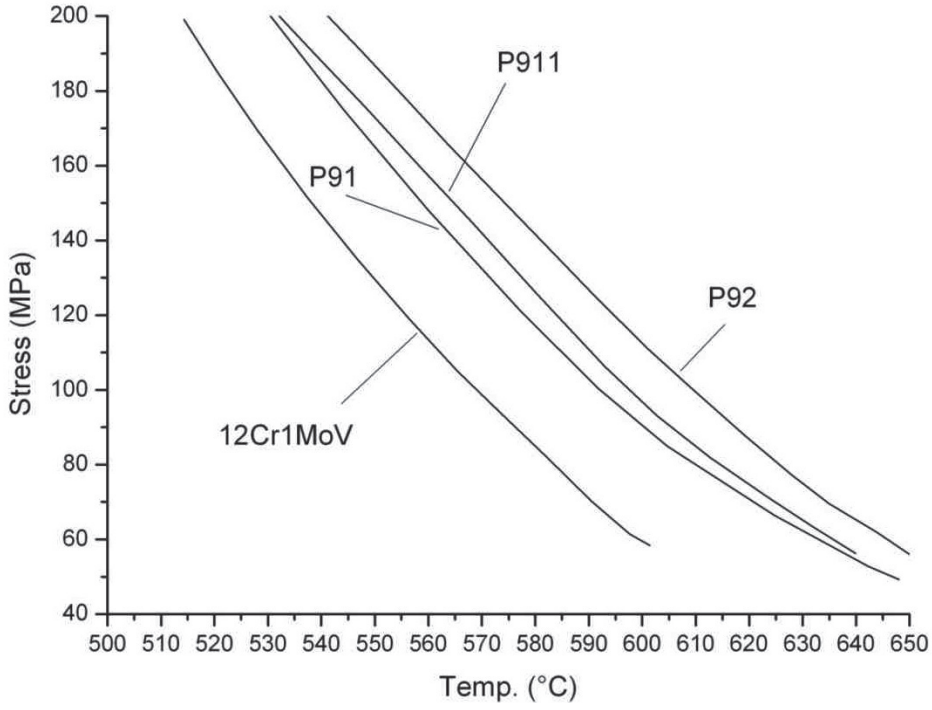

Figure 1 – 100,000 h creep rupture strength of steam plant piping steels as a function of test temperature [13] [3].

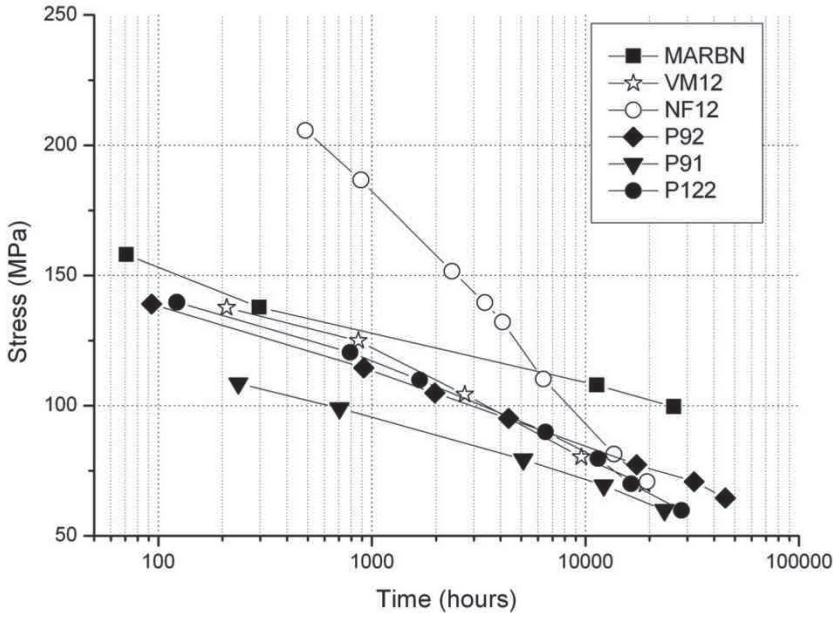

Figure 2 – Creep-rupture lines at 650℃ of most popular 9-12%Cr creep resistant steels [13] [3] [17].

2.3 Metallurgy of 9-12%Cr creep resistance steels

This paragraph describes the metallurgy of 9-12%Cr steels. The basic contribution to the creep strength of any steel comes from its alloying elements, which can determine, together with heat treatment, the forming microstructure and the precipitating phases, which promote the high temperature resistance. The strength therefore comes from dissolved elements, the base microstructure, and the precipitates.

Components of 9-12%Cr creep resistant steels for tube/pipe, forging and casting applications are always furnished after normalising and tempering heat treatments. Normalising is usually performed in the temperature range 1040-1080℃ [18].

Tempering is preferred in the temperature range 730-800℃ [18].

2.3.1 Alloying Elements

Alloying elements determine the type of microstructure formed; heat treatment then leads to formation of different kinds of precipitates. Final chemical compositions shown in Table 1 were achieved only after several attempts and trial & error optimisation process, since even a small variation of element content, can lead to a significant change of the creep resistance. Moreover the synergetic effects of several elements must be always be taken into consideration.

In order to stabilise the structure of 9-12%Cr steels it is mandatory to operate in the γ loop of the Fe-Cr equilibrium phase diagram during austenitizing heat treatment, as shown in Figure 3. It is evident that the austenite field is narrow for steels having Cr concentration higher than 9-wt%. The presence of δ-ferrite, which is promoted for 12%Cr, is considered deleterious for the creep strength and toughness in the final microstructure. With the addition of alloying elements, the gamma loop could be either extended or restricted, thus avoiding the formation of δ-ferrite during austenitizing.
Some beneficial effects of elements are described as follows.

Chromium. This is a ferrite stabilising element and a carbide former. The concentration 8.5-9.0-wt% provides a good combination of creep strength and oxidation resistance [19]; levels greater than 11-wt% chromium were found to markedly increase the corrosion resistance at 650℃, however at that concentration chromium promotes the formation of undesirable δ-ferrite, so that it is usually balanced with austenite stabilising elements, like Ni, Cu and Co [20]. Levels of Cr at 11-12-wt% promote the Z-phase formation which causes a drop in creep properties [4] [17].

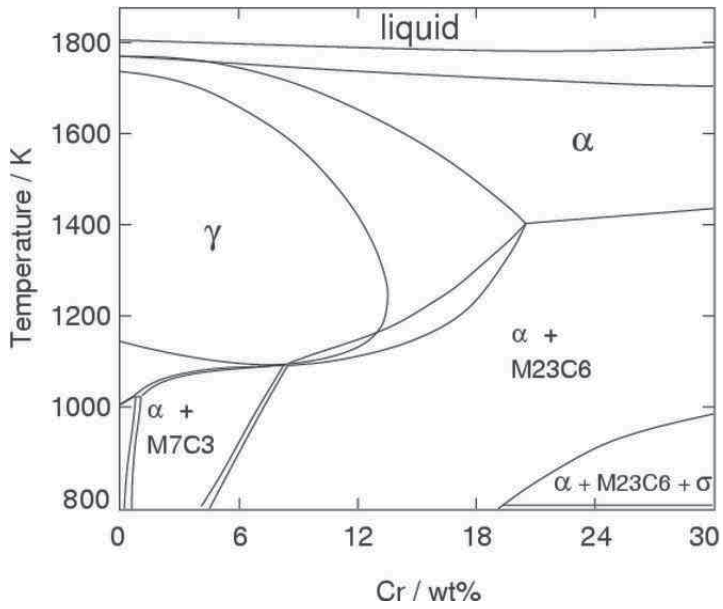

Figure 3 – Pseudo-binary Fe-Cr diagram for 0.1C-wt% [21] [22].

Carbon and *Nitrogen* are not only austenite stabilisers, but fundamental in precipitation reactions. Carbon and nitrogen in balanced quantities promote the formation of carbides,

nitrides and carbonitrides, which provide creep-resistance after heat treatment.
Both elements are used to precipitate a fine distribution of Nb- and V-rich carbonitrides, also active (especially NbC) in the control of grain size during austenitizing.
It was found that a level of 0.15-wt% carbon was optimum in 12-wt%Cr steels and that greater level of carbon may lead to unacceptable reductions in mechanical properties such as toughness [23]. Moreover a level of carbon higher than 0.2-wt% may cause cracking after normalising and also after welding.
Fujita and Asakura [24] examined the effect of carbon in creep rupture strength of a 9-10%Cr-2Mo-V-Nb steel: it was found that the creep rupture resistance of a 10-wt% Cr steel increases with C content (0.05-0.23 wt% C range tested), while there was no discernable increase with C for the 9-wt% Cr steel (0.02-0.14-wt% C range tested).
Concentrations of nitrogen are generally below 0.05 wt% since larger amounts require special steel-making procedures.

Molybdenum and Tungsten contribute to solution strengthening. Both elements also stabilise δ-ferrite and lead to the precipitation of intermetallic Laves phase, $(Fe,Cr)_2(W,Mo)$ during creep service.
Generally, Mo and W are added to the 9-12%C steels at levels of 0.5-1.5% for Mo and 1-2% for W. Tungsten is preferred to molybdenum since it stabilises the Cr-carbides ($M_{23}C_6$ type) and forms more stable Laves phase against coarsening [25] [26].

Nickel, Copper and Cobalt are austenite stabilising elements. Nickel is known to have an adverse effect on the creep strength of 9-12%Cr steels, by enhancing the coarsening rate of precipitates, especially $M_{23}C_6$ type [27] [28]. Nickel accelerates also the formation of M_6X. It was found that nickel concentrations higher than 0.4-wt% in a 11Cr-2W-0.4Mo-1Cu steel deteriorated the creep strength appreciably, see Figure 4. The copper concentrations were also varied in this system and were found to have no effect on the creep resistance [28] [29]. Copper is used as a precipitation hardener, with copper particles forming on martensite lath boundaries, thereby retarding the recovery of martensite [30].
Cobalt strengthens the ferritic matrix and stabilises the fine MX precipitates [31]. It remains in solid solution in 12-wt% Cr steels and enhances the creep strength [32]; an example of this in 12CrWCoB wt% steel at 650℃ is shown in Fig ure 5 [33].

Recent results concluded that cobalt could promote the formation of Z-phase also [34].

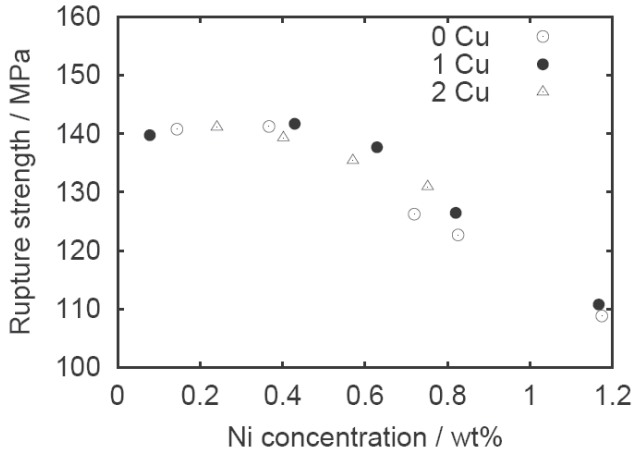

Figure 4 – Effects of Ni and Cu on the extrapolated 10^5 h creep rupture strength of 0.12C-11Cr-2W-0.4Mo-Cu wt% steels at 600℃ [28] [29].

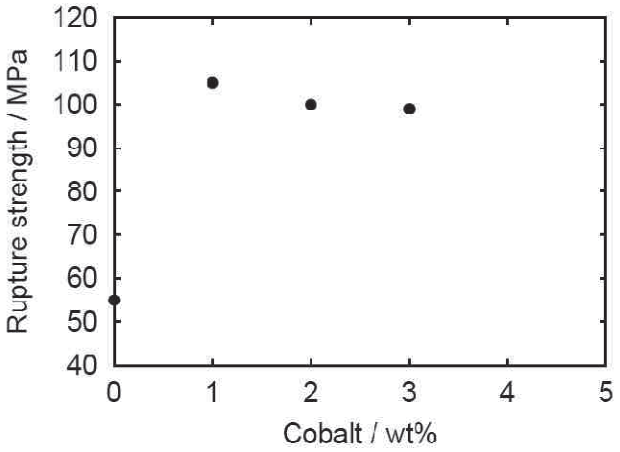

Figure 5 – 10^5 h creep rupture strength at 650℃ as a function of cobalt for 12-wt% CrWCoB steel [33].

Vanadium, Niobium and Tantalum combine with C and N to form carbides, nitrides and carbonitrides which precipitate as finely distributes particles during tempering (with the exception of primary Nb(C,N) which can be present after normalising). Both V and Nb are generally present in the 9-12%Cr steels; they form extremely stable nitrides at creep temperatures and have a major creep strengthening effect in 9%Cr steels. In 12%Cr steels both V- and Nb-nitrides can transform relatively quickly into modified Z-phase, Cr(V,Nb)N, which is deleterious for creep resistance [12].

Tantalum forms stable nitrides too in 9%Cr steels and this can be a valid substitute of vanadium and niobium [35] [36]. Recently Ta-based Z-phase has been discovered in 12%Cr steels [37].

Boron improves hardenability and enhances grain boundary strength, and hence it can contribute to the creep strength. Boron is soluble in Cr-carbides, thus forming $Cr_{23}(C,B)_6$. A recent study showed that boron improves the creep-resistance of 9-12%Cr steels by stabilising Cr-carbides. However, large concentrations of boron can lead to the formation of dangerous boron nitrides (BN), which are detrimental for creep resistance and toughness especially [38].

Silicon is a ferrite stabilising element and can influence the kinetics of carbide precipitation. Silicon additions to 9%Cr steels have been found to increase the precipitation and coarsening of Laves phase [39].

Aluminium. The addition of aluminium is considered to be detrimental to the creep rupture strength since it leads to the formation of deleterious AlN, at the expenses of VN and NbN. Aluminium nitride is a coarse phase, thus it is not useful to the creep strengthening [40]. Recently maximum aluminium content in 9-12%Cr steels has been reduced to 0.02-wt% [18] and the N/Al ratio to prevent formation of AlN has been fixed greater than 3 (N/Al>3.5) [41].

Phosphorus. Significant levels of phosphorus can lead to segregation to grain boundaries and embrittlement of the steel. Phosphorous additions up to 0.023-wt% to a 9Cr-1Mo steel have also been found to lead to a significant loss of ductility [42].

Sulphur. Formation of sulphides, such as MnS, can provide preferential nucleation sites for cavitation. Precipitation of MnS occurs on prior austenite grain boundaries when cooling from the austenite phase. The cavitation is caused by the low interfacial adhesion between MnS and the ferrite matrix [43]. Thus the S content in 9-12%Cr is limited within 0.010-wt%.

Titanium is a strong nitride and carbide former and can improve the creep rupture strength of ferritic steels [44]. However titanium may result in a large reduction in rupture ductility

due to titanium based inclusions (mainly Ti-oxides) preventing deformation at grain boundaries. Titanium, together with niobium, is also very efficient in controlling the austenite grain growth [45]. Typically Ti content in 9-12%Cr steels is limited within 0.01-wt%.

Figure 6 shows the scheme for the design philosophy of heat-resistant steels [46], which can be summarised as follows:

- Martensite microstructure as best creep resistance matrix;
- Limited carbon content (0.14-wt% maximum) to promote easier weldability;
- Alloying optimisation of vanadium, niobium and tantalum, together with carbon and nitrogen, to maximise precipitation strengthening;
- Alloying with molybdenum and tungsten to promote solution and precipitation (Laves) strengthening;
- Alloying with boron to stabilise the precipitates and grain boundary.

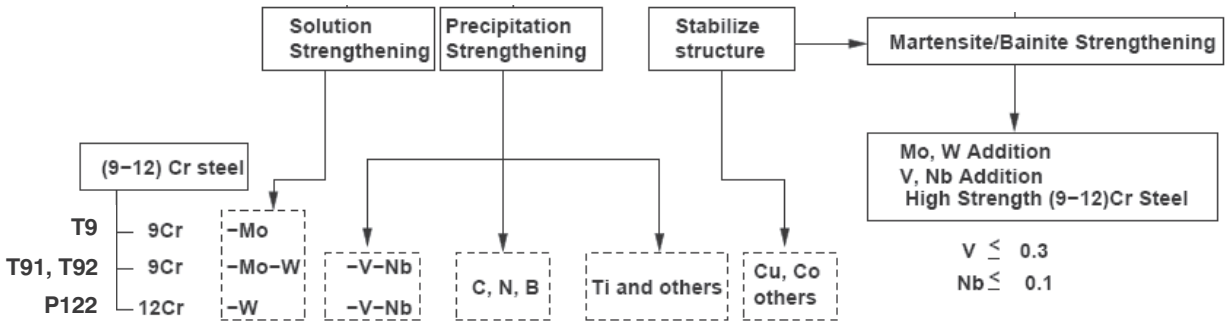

Figure 6 – Alloy philosophy of 9-12Cr steels [46].

2.3.2 Austenite

A normalising heat treatment is performed in the temperature range 1040℃-1080℃, according to ASTM Standard [18]. Generally, the microstructures of the 9-12% Cr steels are designed by balancing austenite and ferrite stabilizers to produce 100% austenite during austenitisation.

The normalising temperature is chosen to give a complete dissolution of elements in the matrix, without excessive grain growth and formation of δ-ferrite. Indeed during normalising most precipitates dissolve, with Nb-rich carbonitrides as only exceptions. Nb-rich carbonitrides remain and prevent uncontrolled grain growth.

The amount of δ-ferrite which could be formed depends on temperature and chemical composition. As a general rule, by raising the normalising temperature, the tendency to form δ-ferrite increases. On the other hand, the balancing of austenite-forming and ferrite-forming elements in the steel, could lead to a different temperature for δ-ferrite formation.

Figure 7 shows the phase diagrams of three basic compositions of Grade 91, with different Cr contents: 8.5, 9.0 and 9.5-wt%. By varying the Cr content, a strong ferrite stabiliser, while maintaining the content of all other elements, the calculated temperatures for δ-ferrite formation significantly change.

The chromium has a significant effect on the formation of δ-ferrite. Similar effects have been ascribed to W, Mo, V, Nb, Ti and Al. All these elements are ferrite-forming elements, which are able to move the δ-forming temperature with different effectiveness. On the opposite, Ni, Co, Mn, Cu, C and N are austenite-forming elements in steel.

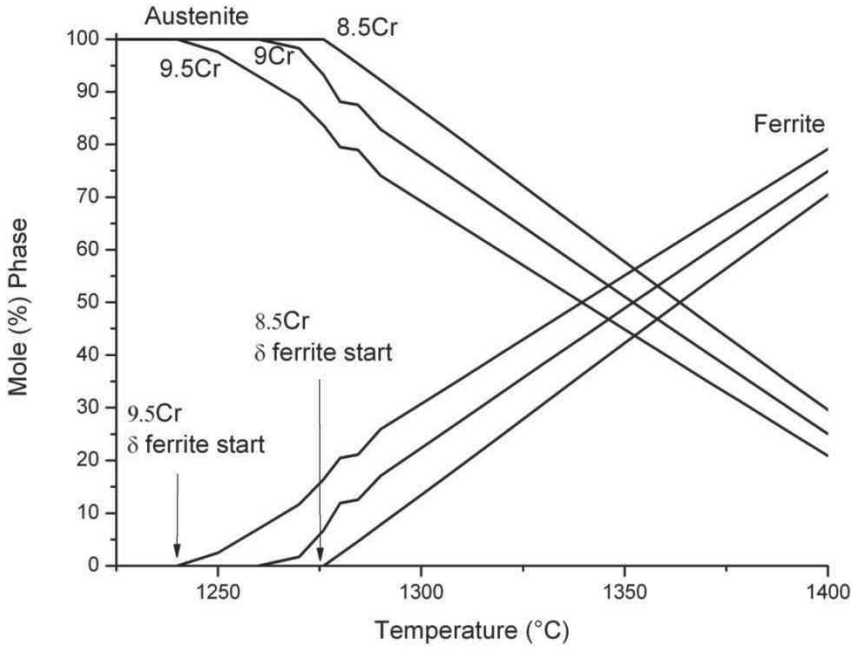

Figure 7 – Phase diagrams of three basic compositions of Grade 91, each with different Cr content (wt%): a) 8.5, b) 9.0, c) 9.5 (calculations performed by means of JMatPro© software).

The equivalent content of austenite-forming and ferrite-forming elements can be measured by means of Ni-equivalent and Cr-equivalent values, respectively.

These quantities can be calculated by the chemical composition of the steel, as follows [47]:

$$Cr_{equivalent} = Cr + 2Si + 1.5Mo + 5V + 5.5Al + 1.75Nb + 1.5Ti + 0.75W \text{ (wt\%)} \quad (1)$$

$$Ni_{equivalent} = Ni + Co + 0.5Mn + 0.3Cu + 25N + 30C \text{ (wt\%)} \quad (2)$$

Using these equivalents several diagrams have been given with the purpose to predict the amount of forming δ-ferrite in 9-12%Cr steels after normalising heat treatment; the most used and popular among them is the Schaeffler diagram, shown in Figure 8.
Although primarily intended for use in welding, equations (1) and (2) are semi-empirical and the Schaeffler diagram has limited validity, this approach is very useful from a practical point of view, in order to qualitatively measure the tendency of the steel to form δ-ferrite during austenitisation.

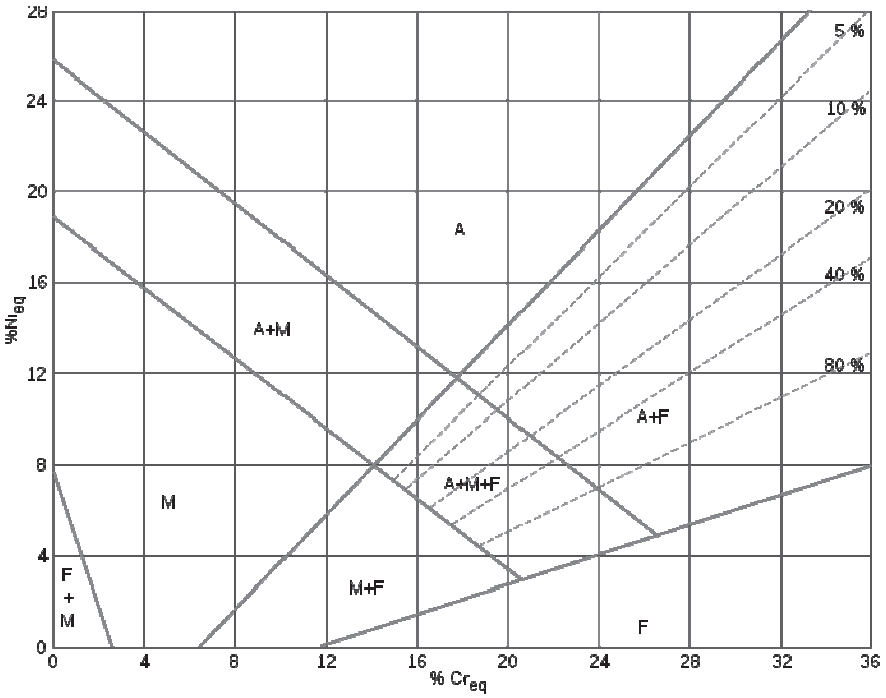

Figure 8 – Schaeffler diagram. M: martensite, F: ferrite, A: austenite [47].

Since the desired microstructure of 9-12%Cr steels is a predominant martensitic microstructure, with very small volume fraction of δ-ferrite, some considerations can be done:

- C is the cheapest austenite former, but only a small amount can be added, as it lowers the toughness and the weldability;
- N can also be used as austenite former, but excessive N amount may be required to reduce δ-ferrite, thus leading to a risk for developing N_2 filled pores;
- Mn, Ni and Cu have been used in small quantities to prevent delta ferrite formation, but their main drawback is that they lower the A_1 equilibrium temperature;
- Co has been recently shown to be an excellent austenite former as it does not have any known drawbacks, other than that it is quite expensive.

Since the modern design concepts tend to promote the use of a high content of tungsten up to 6-wt%, together with the 9-12%Cr content, high contents of cobalt have to be used to avoid δ-ferrite formation.

2.3.3 Martensite

The desired microstructure after normalising consists predominantly of martensite. This is a distorted crystal of the ferritic *bcc* structure, which is obtained when austenite is rapidly cooled and carbon remains in supersaturated solid solution.

In order to achieve maximum creep resistance from the 9-12%Cr steels, it is essential to transform the largest amount of austenite into martensite on cooling to room temperature (without traces of retained austenite).

Normally air cooling of 9-12%Cr steels is sufficient for a complete martensitic transformation, because the high amount of chromium retards the diffusion of carbon, thus preventing the formation of other phases, i.e. α-ferrite, perlite, precipitation of carbides.

The continuous cooling transformation (CCT) diagrams provide a significant contribution to the understanding of the transformation behaviour of the 9-12%Cr steels.

These diagrams provide important information about the transformation temperatures of the steel, A_{C1} and A_{C3}, M_s and M_f, as well as the hardness of the material at different cooling rates.

The 9-12%Cr steels are very hardenable and martensitic transformation takes place even at slow cooling rates. For components of large wall thickness or diameter, a small volume fraction of α-ferrite could locally transform where the slowest cooling rate occurs. Nevertheless, a limited amount of α-ferrite (≤2%) is considered acceptable with no

influence on material properties.

An example of a CCT diagram for a 9%Cr steel (Grade 92) is shown in Figure 9. In the range of martensitic transformation, the achieved hardness falls with decreasing the cooling rate from the austenitizing temperature.

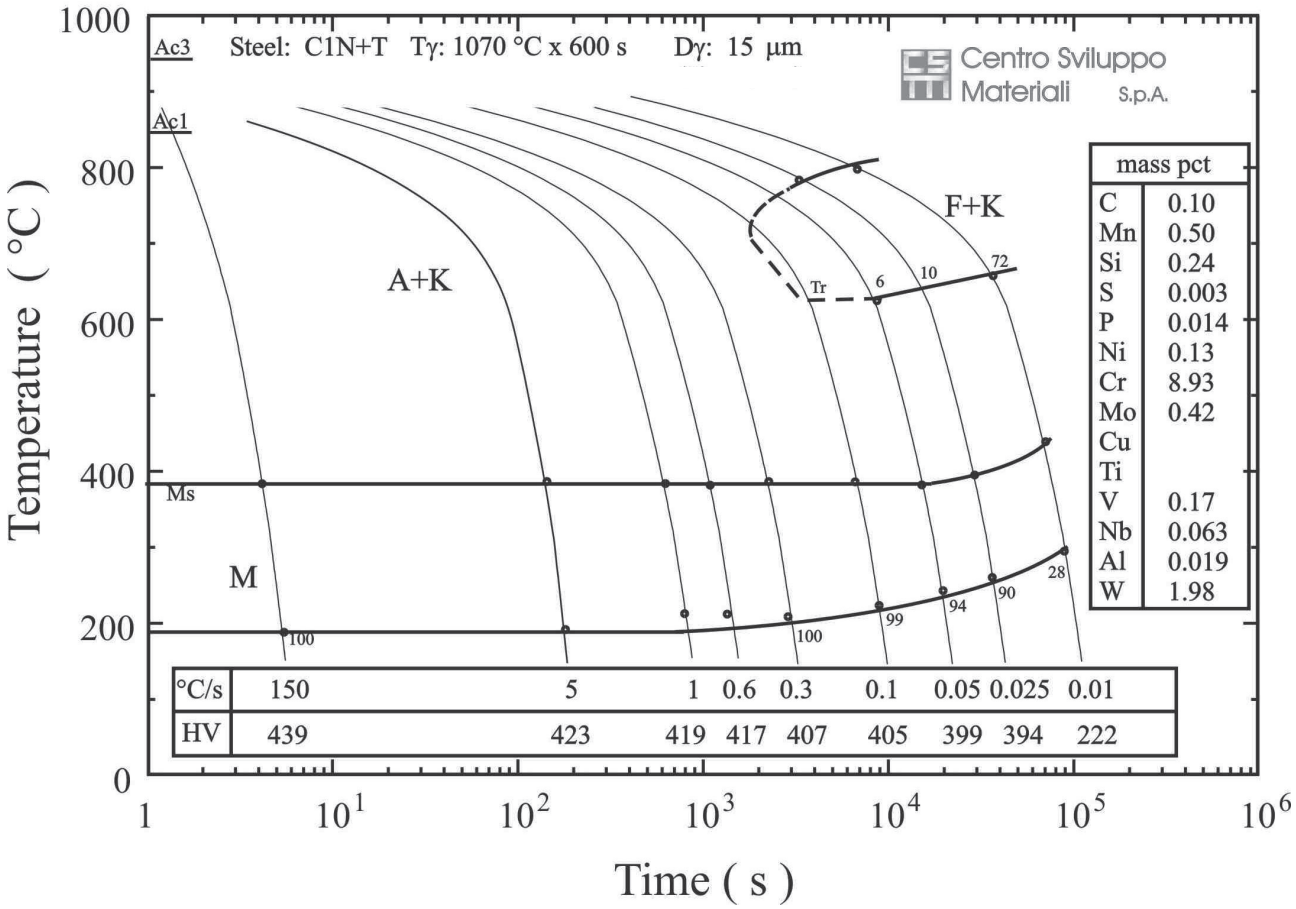

Figure 9 – CCT diagram of Grade P92.

Attention must be paid to the transformation temperatures, A_1 and A_3. These are the temperatures at which ferrite matrix starts (A_1) and finishes (A_3) the transformation into austenite. The transformation temperatures can be calculated by thermodynamic software such as Thermocalc© [48] and JMatPro© [49], and can be determined by dilatometry during heating (C) or during cooling (A_{r1} and A_{r3}). The cooling and heating rates largely effect the

measurements of transforming temperatures (A_{c1}, A_{c3}, A_{r1}, A_{r3}): the slower the cooling or heating rate is, the closer the measurements are to the equilibrium values (A_1, A_3).

The addition of alloying elements has the effect of increasing the value of transformation temperatures. The following semi-empirical formula is useful for a quick calculus [50]:

$$A_{C1}\ (℃) = 25Mo + 50V - 30Ni - 25Mn - 5Co + 25Si + 30Al \quad (3)$$

Regarding the transformation temperatures M_s and M_f at which the austenite starts and finishes its transformation into martensite during cooling, for a 0.1%C and 12%Cr steel the M_s is around 300℃ and the M_f lies in the 100-150℃ range. Most of the alloying elements reduce the M_s and M_f temperatures.

The following equation is used to estimate the effect of alloying elements (wt%) on M_s [50]:

$$M_s\ (℃) = 550℃ - 450C - 33Mn - 20Cr - 17Ni - 10W - 20V - 10Cu - 11Nb - 11Si + 15Co \quad (4)$$

Since the M_s transformation temperature could be even lower than 100℃, it is very important that during the cooling process, after austenitisation, the material is taken approximately down to room temperature. This is a fundamental procedure to avoid the formation of retained austenite, which could lead to very poor mechanical properties even when present in limited quantities.
The only element that raises the M_s temperature is cobalt, which is also an austenite former, making it important in high alloyed steels.

If normalising is performed at the proper temperature (1040℃-1080℃) and if the material is cooled down to room temperature, then the normalised sample of 9-12%Cr steel should consist of untempered martensite only, with average hardness $400HV_{10}$ (depending on the cooling rate as shown in CCT diagram of Figure 9).
Figure 10 shows the typical microstructure of ASTM Grade P92 after normalising.

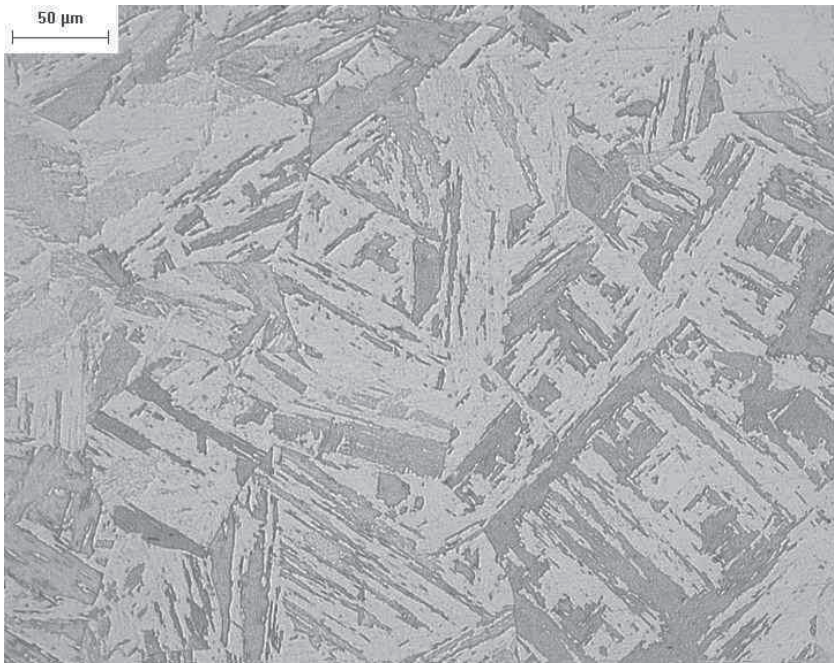

Figure 10 – Grade P92 microstructure after normalising (1070℃ x 1h).

2.3.4 Tempering

The tempering treatment is performed with the purpose to soften the material, since the hardness of as-normalised component is too high for material workability, i.e. cold-bending. Indeed the untempered martensite is hard and brittle.

Secondly, precipitation of carbides and nitrides which promote the high temperature resistance takes place during tempering. The initial normalising has already dissolved most elements, so they are available for precipitating during tempering. The tempering is usually performed in the range 730℃-800℃ [18], an d it can be followed by furnace or air cooling. It is mandatory that the tempering of martensite is carried out below the A_1 temperature in order to avoid a redevelopment of austenite and then brittle martensite after cooling. Since some elements, especially Ni and Mn, can significantly lower the A_1 temperature, the formation of austenite could occur during tempering; this dangerous practice which often occurs if not enough attention is paid to the problem. The average temperature of 9-12%Cr steels after tempering is about 220-230HV. Figures 11 and 12 show the typical microstructure of 9-12%Cr steels after tempering by Light Microscope (LM) and Scanning Electron Microscope (SEM): the visible precipitates along grain boundaries and along martensite laths are mainly Cr-carbides ($M_{23}C_6$ type). The following paragraphs detail the precipitate reactions and the precipitate types involved in the

strengthening of 9-12%Cr steels.

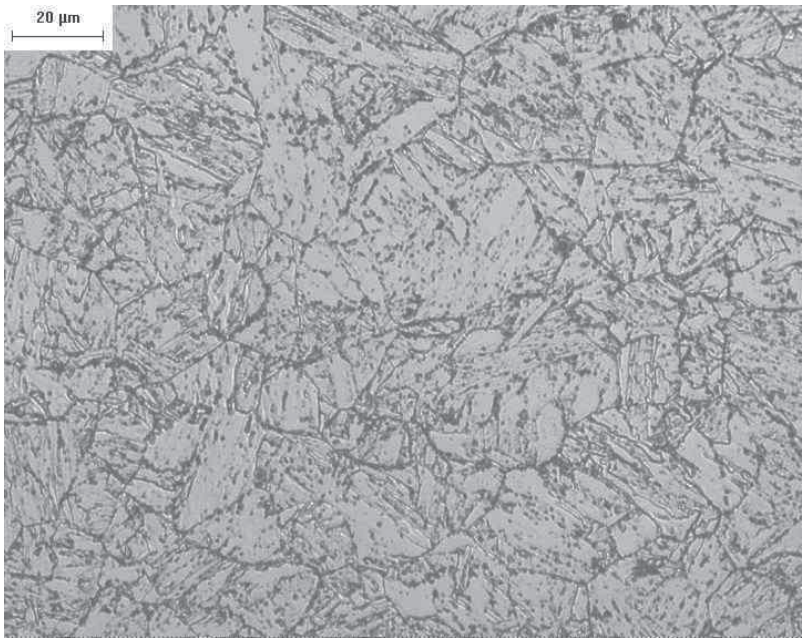

Figure 11 – Microstructure of P92 after tempering by LM (1070℃ x 1h; 780℃ x 2h).

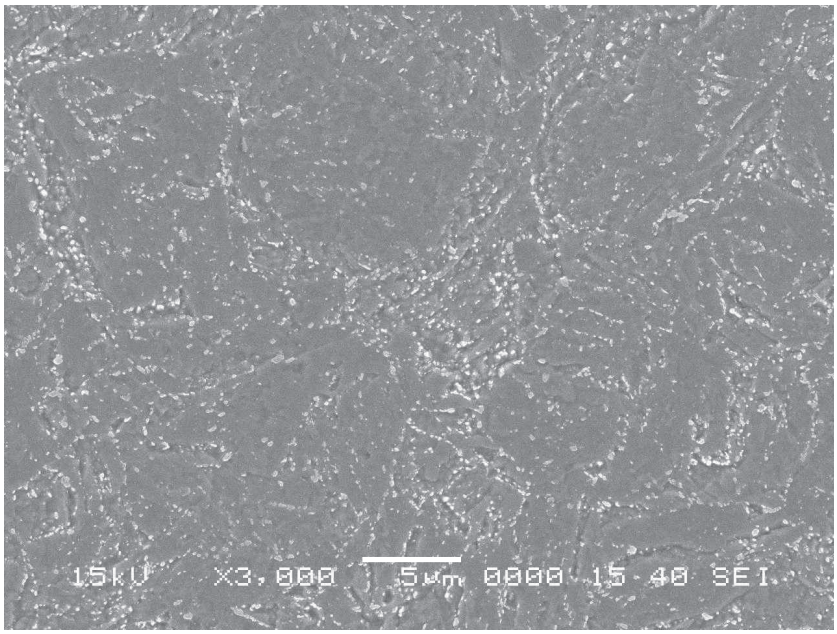

Figure 12 – Microstructure of P92 after tempering by SEM.

2.3.5. Strengthening Mechanisms

The fundamental knowledge of the strengthening mechanisms is a prerequisite for successful application and further development of high chromium steels.

Creep resistant steels containing 9-12% Cr have a predominant tempered martensite microstructure, high initial dislocation density, containing a wide range of precipitates, located within the grain, along grain boundaries and along martensite laths.
Thus the ways in which the 9-12%Cr steels are strengthened are basically: 1) solid solution strengthening, 2) dislocation hardening, 3) precipitation strengthening.
A brief description of the characteristics of the strengthening mechanisms is given below.

2.3.5.1 Solid Solution Strengthening

Substitutional solute atoms with larger atomic sizes than the atoms of solvent iron are effective solute strengtheners. Molybdenum and tungsten are the best solid solute strengtheners of 9-12%Cr steels. Even if the beneficial effect from the addition of Mo and W in terms of solute strengthening is theoretically true, it is very difficult to measure the contribution to creep resistance given by this mechanism, also because the solid solution hardening is always superimposed an all other creep strengthening mechanisms [26].

2.3.5.2 Dislocation hardening

Dislocation hardening given by [9] [51]:

$$\sigma_\rho = 0.5\, M\, G\, b\, (\rho_f)^{1/2} \qquad (5)$$

where ρ_f is the free dislocation density in the matrix, M is the Taylor factor (=3), G is the shear modulus, b is the Burgers vector. Tempered martensitic 9-12Cr steels usually contain a high density of dislocations in the matrix even after tempering, usually in the range 1-10 × 10^{14} m^{-2}. The density of dislocations produced by martensitic transformation during cooling after austenitisation can be controlled by changing the tempering temperature. Dislocation hardening is useful for creep strengthening in the short term, but it is not effective for increasing long-term creep strength, especially at elevated temperatures.

2.3.5.3 Precipitation hardening

During tempering of martensite, carbides, nitrides and carbonitrides precipitate along grain boundaries and martensite laths and inside the grains.

In commercial 9-12%Cr steels the precipitation sequence after tempering in the temperature range 730℃-800℃ is the following:

$$[\ \text{MATRIX}\ ] \rightarrow [\ M_{23}C_6 + M_2X\ ] \rightarrow [\ M_{23}C_6 + MX] \quad (6)$$

where *M* stands for metallic atoms (mainly Cr, V, Nb) and *X* stands for N or C.
Thus if tempering is performed at proper temperature and times, the precipitation sequence is completed and the final microstructure consists mainly of Cr-carbides, $Cr_{23}C_6$ type, located predominately at grain boundaries and martensite laths, as well as V- and Nb-nitrides, carbides and carbonitrides mainly located inside the grain.
When tempering treatment is performed at low temperature (730℃ or below) the M_2X can be often found in the some amounts; this means that the precipitation sequence was not completed and the M_2X had not sufficient time to decompose into more stable MX.

Figures 13-a and 13-b show the typical microstructure of E911 after tempering by TEM [52]. Table 3 summarises the typical precipitation in 9-12%Cr steels in terms of precipitate types and average equivalent diameters after normalising and tempering [52].

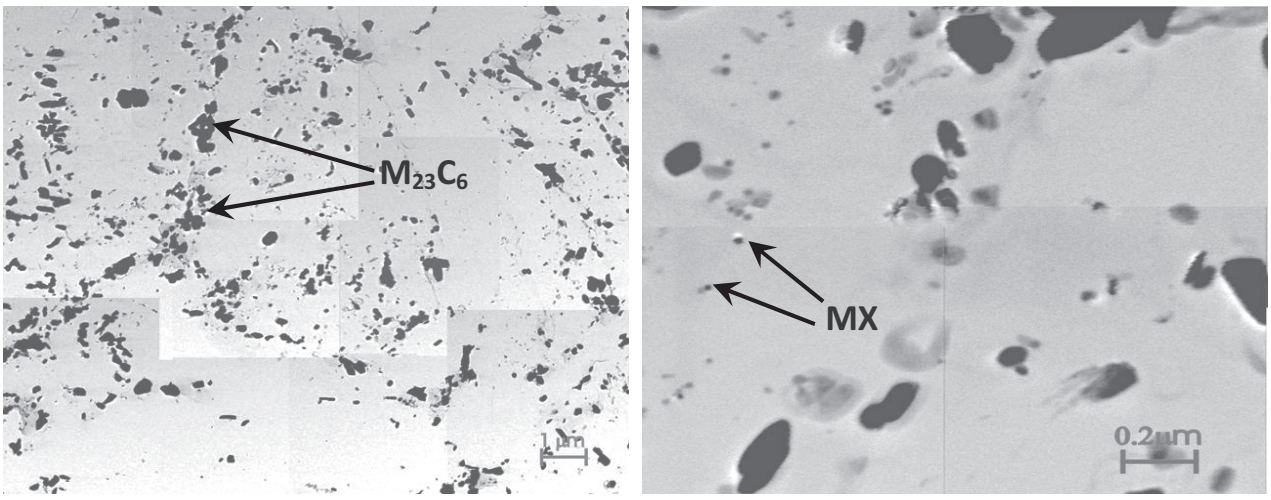

(a) (b)

Figure 13 – TEM images of extraction replicas of E911 as-treated pipe: a) $M_{23}C_6$ carbides located at subgrains; b) fine MX carbonitrides [52].

Table 3 – Precipitation in advanced 9%-12%Cr steels after normalizing and tempering. N: normalizing; T: tempering [52].

	9%Cr steels			12%Cr steels		
	P92	P911	P91	HCM12	X20	VM12
Treatment	1070℃+780℃	1060℃+760℃	1070℃+780℃	N+T	N+T	N+T
Average Equivalent Diameter (nm)						
MX	45	50	48	53	50	47
$M_{23}C_6$	125	130	140	131	143	140

Precipitation of second phases is one of the most important strengthening mechanisms in creep resistant steels. A dispersion of fine precipitates is responsible for stabilising the free dislocation in the matrix and sub-grain structures, thus during the creep regime a threshold stress is required for the dislocations to pass a precipitate (i.e. by Orowan mechanism, local climb mechanisms, general climb mechanisms, see Figure 14).

For the estimation of the effect of precipitates on creep resistance, the following equation can be used for calculating the threshold stress from particles on dislocations according to Orowan mechanism [53]:

$$\sigma_{or} = 0.84\, M\, G\, b/\, \lambda \qquad (7)$$

where λ is the mean interparticle spacing.

The mean interparticle spacing λ is calculated by [26] [54]

$$\lambda = 0.5\, (N_V \cdot d)^{-0.5} - d(2/3)^{0.5} \qquad (8)$$

where N_V is the number of particles per unit volume and d is the mean particle diameter.

It is evident that when the particles are fine and homogeneously distributed in the matrix, thus the λ value is small, the precipitation strengthening effect increases; conversely, when particles coarsen and the finest particles dissolve, this causes an increase in λ values and hence a decrease in Orowan stress.

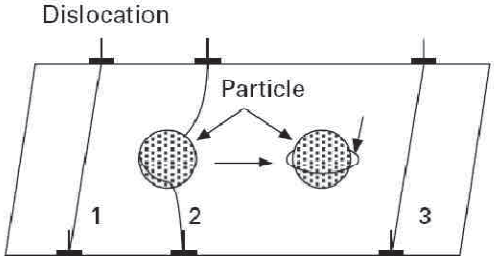

Figure 14 – Schematic drawings of a dislocation passing particles by Orowan mechanism [9].

Thus the precipitation strengthening of 9-12%Cr steels is mainly enhanced by small and homogeneous by distributed precipitates.

When assessing how the dispersion of the second phases affects the creep properties of the steel, it must take into account not only the status of precipitates obtained after heat treatment ($M_{23}C_6$ and MX if the heat treatment has been properly performed), but also the changes in the dispersion caused by coarsening of existing particles as well as by the precipitation and dissolution of secondary phases during creep regime.

Precipitates formed in 9-12%Cr steels can be divided into two groups:

- The first group contains all carbides and nitrides obtained after the normalising and tempering heat treatment: mainly M_2X, $M_{23}C_6$, MX.
- The second group consists of precipitates which nucleate during creep service: Laves phase and Z-phase.

In the following sections a brief description of the precipitates and their characteristics and effects on creep resistance is given.

2.3.6 Phases after normalising and tempering

$M_{23}C_6$ type

This is a Cr-rich carbide, capable of containing many other metallic elements than chromium (i.e. Mo, W, V) [52]. The structure of $M_{23}C_6$ is *fcc* and its lattice parameter was found to be dependent of the carbide composition: *a* value varies from 1.054 nm for $Fe_{21}W_2C_6$ carbide to 1.066 nm for the $Cr_{23}C_6$ carbide [55].

This precipitate is common to all 9-12%Cr steels and mainly forms along grain boundaries and martensite laths. Referring to precipitates chain reaction, it forms after either M_7C_3 or M_2X; it is often the equilibrium carbide in 9-12%Cr and it is predominant after tempering.

Like all other precipitates, $M_{23}C_6$ carbides tend to coarse during creep service, causing a deterioration in creep resistance. The addition of W can reduce this tendency, as shown in Figure 15 [21].

It has been recently demonstrated that boron has a beneficial effect on the stability of Cr-carbides, forming $M_{23}(C,B)_6$, reducing their coarsening rate [56].

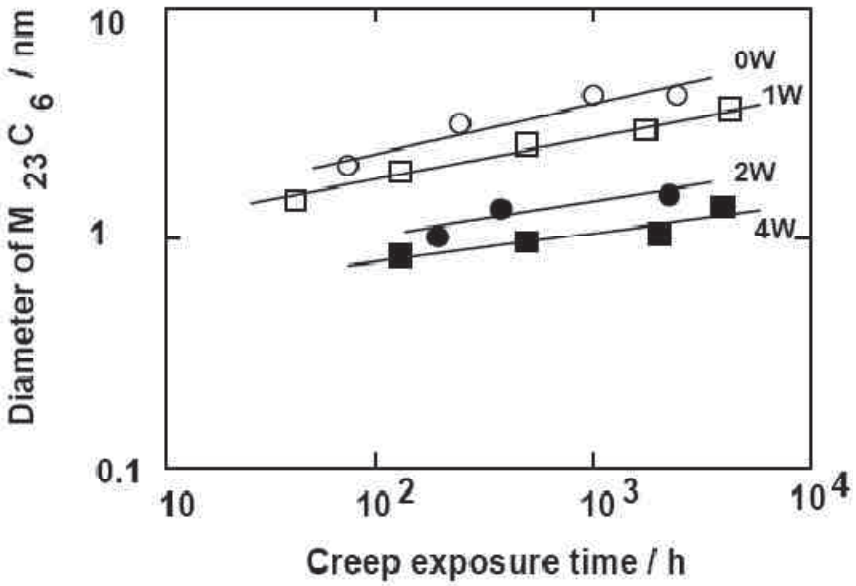

Figure 15 – Effect of W on a coarsening rate of $M_{23}C_6$ carbides during creep of 9Cr-W steel at 600℃ [21].

MX type

These occur as small, spherical precipitates, containing V, Nb, Ta and Ti [52]. MX precipitates can be observed after the normalising heat treatment, where they remain undissolved during austenitisation (i.e. NbX has very high thermal stability up to 1200℃).

The presence of NbX aids in refinement of prior austenite grains during normalising.

After tempering a fine dispersion of MX particles is obtained within the sub-grains, enhancing the creep resistance.

Generally, commercial 9-12%Cr steels contain Nb and V, thus two types of MX particles are formed: V-rich and Nb-rich carbonitrides. Both have a *fcc* structure and their lattice parameter is a function of the chemical composition, since both V and Nb are always mixed in the same MX-type particle. Pure VN has a lattice parameter a = 0.414 nm; pure NbN has a lattice parameter a = 0.439 nm [55].

The V and Nb content are well balanced to obtain maximum beneficial effect; Figure 16 shows the optimum combination of V and Nb to achieve the highest creep resistance in a 12%Cr steel [57] at 600℃ after 10,000 hours.

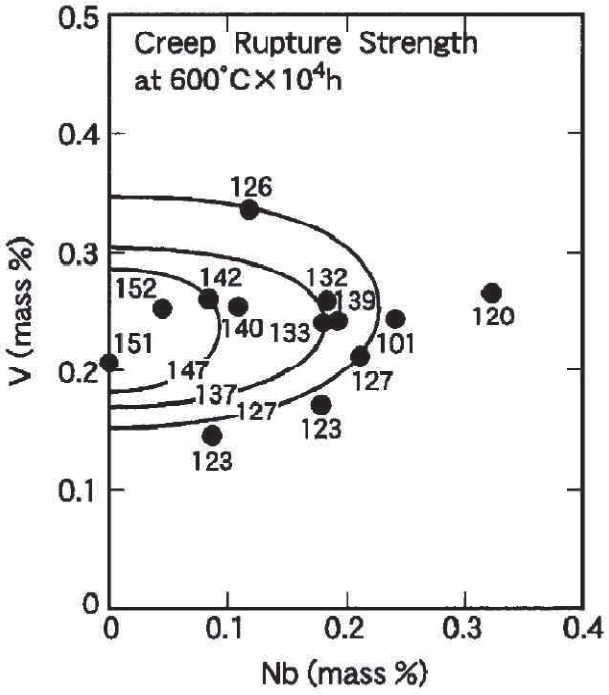

Figure 16 – Combined effect of V and Nb on creep resistance of 12%Cr steels [57].

M_2X type

This precipitate consists mainly of Cr, V, Fe, C and N. It has a hexagonal structure with lattice parameter a = 0.476 nm and c = 0.443 nm for $Cr_2(C,N)$ [55]. This phase is present as main precipitate in 9-12%Cr steels when tempered at low temperature (730℃ and below). The precipitation of M_2X is generally unwanted as it interferes with the precipitation of fine V- and Nb-carbonitrides. M_2X was found mainly along grain boundaries and martensite laths, and it grows usually as large particles.

2.3.7 Phases developing during creep regime

After tempering at 730℃-780℃, the 9-12%Cr compone nts are put in creep service for several thousands of hours at a lower temperature, usually in the range 550℃-650℃.

Since the microstructure was fixed at the tempering temperature, a new phase equilibrium will be established (slowly) and new precipitation reactions occur.

Laves Phase

The general composition of Laves phase is $(Fe,Cr)_2M$, where the M atoms can be W and/or Mo both. This is an intermetallic phase with an hexagonal crystal structure and lattice parameters approximately a=0.47 nm and c=0.77 nm for W- and Mo-based Laves phase [55]. The Mo-based Laves phase precipitates at temperatures below 650℃, while W-based Laves phase usually precipitates at temperatures up to approximately 750℃.

Thus Laves phase is not found after tempering of 9-12%Cr steels, while it gradually precipitates during creep service. During its precipitation, Laves-phase partially removes Mo and W from the matrix, thereby in principle causing a decrease of the content of solid solution strengthening elements in the matrix. For this reason Laves phase has been regarded as an unwanted phase for many years, because of its supposed detrimental effect on the strength of 9-12%Cr steels [54]. However, recent calculations have shown that the contribution from solid solution strengthening to the strength in terms of maximum friction stress from solid solution for Fe-4Mo-at% system, which corresponds to approximately 2-at% W, is about 3 MPa at 600℃ [26] . Therefore Laves phase is not likely to cause significant losses in creep strength of 9-12%Cr steels; quite the opposite, precipitation of Laves phase brings about precipitation strengthening, especially at short term times, when the particles are small [52].

Modified Z-phase, Cr(V,Nb)N

The CrNbN Z-phase is a complex nitride which forms in niobium stabilised austenitic steels, containing a relatively high amount of nitrogen. Z-phase was discovered in 1950 [58], with its structure being fully determined in 1972 [59]: the commonly accepted structure of Z-phase is a tetragonal unit cell (*space group P4/nmm*), with a=0.304 nm and c=0.739 nm cell parameters.

The unit cell is obtained by the ordering of Cr, Nb and N atoms, the formula being $Cr_2Nb_2N_2$ per unit cell, see Figure 17. In addition to the main elements, minor concentrations of Fe and Mo have also been identified.

Z-phase generally forms on grain boundaries, very rapidly, but also on twin boundaries and within the matrix, where it is associated with dislocations. When Z-phase forms, it is usually as a fine dispersion of particles, which makes it a beneficial precipitate when good

creep properties are required. The morphology has been reported to be either cuboidal or rodlike. *Sourmail* has given an excellent review on the CrNbN Z-phase in austenitic steels in [60].

In 1971, the stability of Z-phase in the ternary systems CrTaN, CrNbN and CrVN has been studied [61]; at that time, researchers identified the tantalum and niobium Z-phase, but they didn't manage to find any vanadium-based Z-phase.

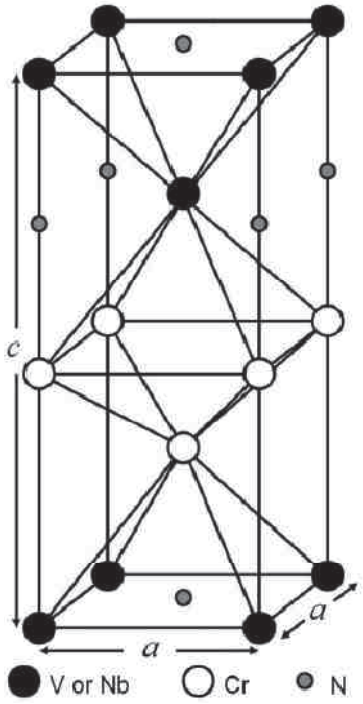

Figure 17 – Tetragonal structure of Z-phase, CrNbN: lattice parameters of Z-phase are c=0.739 nm and a=0.304 nm [59].

It has been recently found that the precipitation of Z-phase occurs in 9-12%Cr advanced ferritic steels after high temperature exposure in the range 600℃-700℃ [4] [17].

The Z-phase precipitates as a modified version of the nitride typically found in austenitic steels. It is assumed that the formation of the Z-phase causes a decrease in the creep strength especially in 12%Cr steels, since Z-phase formation consumes MX carbonitrides, which are important creep strengtheners. In addition Z-phase precipitates as large particles which do not contribute to creep strengthening [4], see Figure 18.

A thermodynamical model specialised for 9-12%Cr steels [64] predicts that Z-phase is the most stable nitride in the creep service temperature range 600℃-700℃ and, accordingly,

at equilibrium it will fully replace the finely dispersed MX nitrides which precipitate during normalising and tempering heat treatment. In the advanced 12%Cr steels, Z-phase precipitation occurs much faster than in 9%Cr steels and large colonies of Z-phase are observed in samples exposed for a few thousand hours at 650℃.

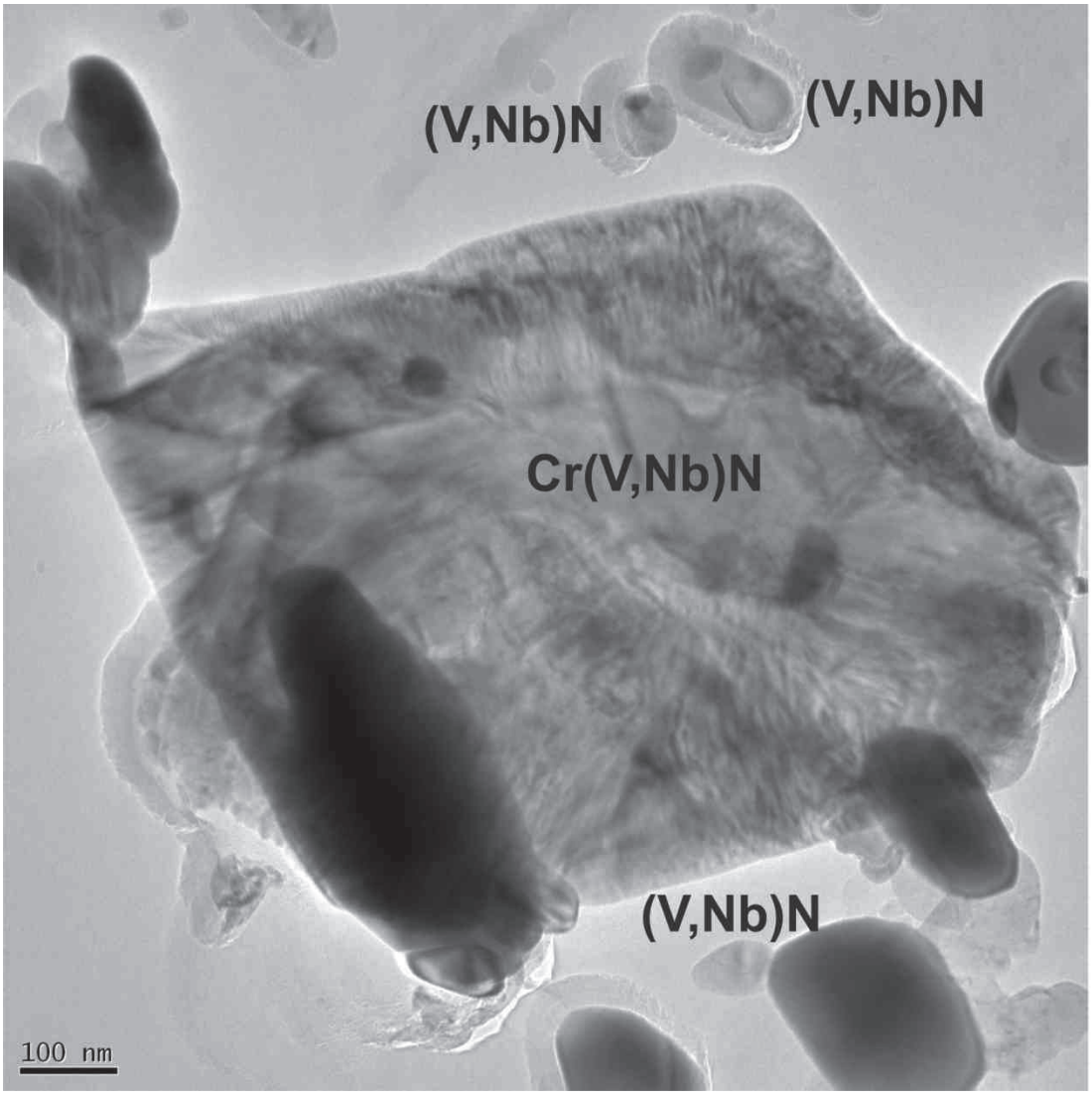

Figure 18 – Modified Z-phase and MX particles in a Grade 92 after 57,715 h at 650℃.

It was concluded that the chromium content has a major influence on the driving force for Z-phase formation, and thus on the precipitation rate, which explains why 12%Cr steels suffer from fast and abundant formation of Z-phase, while this occurs much more slowly in 9%Cr steels [4], see Table 4.

Table 4 – Average metallic composition of Z-phases found in several 9-12Cr steels: Nb/V ratio varied significantly from particles to particle, at% [4].

Steel Type	Observed Z-phase	Cr (at%)	Fe (at%)	V (at%)	Nb (at%)
P91	Very Low	Not enough particles observed for statistics			
X20	Low	40	6	54	/
E991	Low	46	4	27	23
P92	Low	48	5	33	14
P122	Medium	45	5	33	17
AXM	Medium	43	5	44	8
FN5	Medium	47	6	38	9
TB12M	High	47	5	37	11
T122	High	46	5	42	7
NF12	High	47	5	37	10

Recently, a more complex crystal structure of the modified Z-phase was proposed: electron diffraction showed the presence of cubic *fcc* diffraction patterns, similar to those found in MX precipitates, though with a slightly lower lattice parameter, a=0.405 nm [62]. This cubic structure was found to coexist with the tetragonal structure in the Z-phase. The proposed hybrid crystal structure is shown in Figure 19.

Furthermore, investigations showed that the cubic structure was predominant in 9-12%Cr samples which had been exposed for relatively short times, while the tetragonal diffraction patterns became clearer in more aged samples [63].

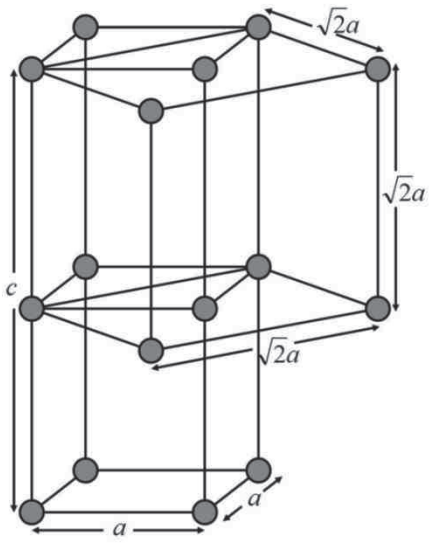

Figure 19 – Proposed hybrid structure of modified Z-phase, where cubic and tetragonal crystal structures coexist [62].

It was reported also that, after creep exposure, Z-phase develops preferentially along prior austenite grain boundaries, along martensite lath boundaries or boundaries along delta ferrite grains. It was also shown that the main metallic composition of the Z-phase does not depend on the precipitation site [65].

At the starting of the present Ph.D. project, the mechanism of formation of Z-phase was not completely clear yet. More recently several high-Cr MX particles were identified in T122 steel aged for about 10,000 hours at 660℃ [7] : these particles showed smooth Cr and V gradients within the particles. The particles were called *hybrid MX/Z particles* and they are believed to be the nucleation stage of final Z-phase particles. Hybrid particles have been thoroughly investigated in the appended papers of this thesis.

Together with its mechanism of formation, there are still many things which are unknown about the Z-phase, the rate at which MX is replaced, such as the time-temperature regions of formation, the formation of MX/Z hybrid particles. A thorough investigation of Z-phase behaviour is the main topic of this Ph.D.

2.3.8 Degradation Mechanisms

The basic knowledge of microstructural evolution of 9-12%Cr steels during high temperature exposure, as well as the understanding of their strengthening and degradation mechanisms is a fundamental prerequisite for successful development of ferritic steels with high creep resistance.

The intention of this paragraph is to survey the available data on structural changes occurring during creep.

Creep resistance of 9-12%Cr steels is a direct effect of their microstructural status; a change in the precipitates will be reflected in a change of the material's creep strength. Since the microstructure of the as-treated material could be far different from that found after several thousands of hours in service, these changes make it difficult to predict the creep behaviour of 9-12%Cr steels over 200,000 hours by short and mid-term creep tests only. When assessing the creep rupture strength of advanced 9-12%Cr steels, changes of microstructure during creep must always be taken into account.

The following degradation mechanisms can be identified in the 9-12%Cr steels:

- Coarsening of precipitates;
- Nucleation, precipitation and coarsening of Laves phase;

- Formation of the modified Z-phase at the expense of MX nitrides, especially in 12%Cr steels;
- Recovery of martensite.

2.3.8.1 Coarsening of precipitates

The $M_{23}C_6$ carbide is one of the most important secondary phases in the 9-12%Cr steels. Therefore, great attention has been paid to the coarsening of this phase during high temperature exposure.

Coarsening is the last stage of the precipitation of a secondary phase and must be preceded by nucleation and growth of particles. In contrast with the growth stage, no new particles precipitate during coarsening, but larger particles grow at the expense of the smaller ones. The coarsening process, known as the Ostwald ripening process, results in a decrease in the number of particles and increases of the mean particle size, while the total amount of the secondary phase (volume fraction) remains almost constant. The driving force for this process is the difference of solubility and concentration of alloying elements around the fine and large precipitates [66].

The theoretical basis of Ostwald ripening was worked out by Wagner, Lifshitz and Slyozov, who derived the formula [66]:

$$d^3 - d_0^3 = K_d \cdot t \qquad (9)$$

where d and d_0 are particle diameters after the exposure time t and at the beginning of coarsening respectively, K_d is the temperature dependent coarsening constant.

Ostwald ripening theory was successfully applied in case of many systems: coarsening of precipitates in rod and platelet shape as well as coarsening on grain boundaries [67].

The most frequently used time exponent is 3 (time law $t^{1/3}$). As far as the coarsening of $M_{23}C_6$ carbides is concerned, the time exponent 3 results adequate [68].

The strength and creep properties of 9-12%Cr steels depends significantly on the amount, size and dispersion of $M_{23}C_6$ carbides.

If the coarsening process is slowed, this results in a delay in the loss of creep rupture strength. Boron additions to 9-12%Cr steels may stabilise the Cr-carbides, thus positively affect the creep resistance [56].

Dimension of MX carbonitrides have been reported by many authors to be almost constant during creep service, even after very long high temperature exposure.
Typical values of coarsening rate constant K_d of $M_{23}C_6$ and MX particles of 9-12%Cr steels are shown in Table 5 [69].

Table 5 – Calculated coarsening rate constants K_d for $M_{23}C_6$ and MX particles at 600℃ and 650℃ for Grades 91 and 92 [69].

Precipitate	Steel	Coarsening Rate Constant K_d [m^3 s^{-1}] at 600℃	Coarsening Rate Constant K_d [m^3 s^{-1}] at 650℃
$M_{23}C_6$	P91	$2.88\ 10^{-29}$	$25.3\ 10^{-29}$
	P92	$1.24\ 10^{-29}$	$1.37\ 10^{-29}$
MX	P91	$1.73\ 10^{-32}$	/
	P92	$2.33\ 10^{-32}$	$9.15\ 10^{-32}$

2.3.8.2 Precipitation of Laves phase: $Fe_2(W,Mo)$

During creep service, Laves phase becomes the largest precipitate in 9-12%Cr steels; after relatively short times Laves phase grows up to average micrometric dimensions, thus showing a high growth and coarsening rate.
The Mo-based Laves phase (in Grades 91 and X20) reaches a larger average size than the W-based Laves phase (in Grades 92, 122 and VM12): after 100,000h at 600℃ Fe_2Mo particles of P91 reach 400 nm average diameter, with a large standard deviation of the distribution (about 350 nm) [70]. The W-based Laves phase is more stable against coarsening and average diameter of Fe_2W of P92 was measured as 240 nm after 60,000h at 600℃ and 400 nm after 30,000h at 650℃ [69]. Ty pical values of coarsening rate constants K_d of Laves phase in Grade 92 are shown in Table 6.

Table 6 – Calculated coarsening rate constants for Laves phase particles at 600℃ and 650℃ for Grade 92 [69].

Precipitate	Steel	Coarsening Rate Constant K_d [m^3 s^{-1}] at 600℃	Coarsening Rate Constant K_d [m^3 s^{-1}] at 650℃
$Fe_2(W,Mo)$	P92	$3.5 \cdot 10^{-29}$	$15 \cdot 10^{-29}$

2.3.8.3 Formation of Modified Z-Phase

The formation of Z-phase is responsible for the recent failures of the advanced 12%Cr ferritic steels: the intentions were to combine superior oxidation/corrosion resistance given by 12%Cr amount with high creep resistance typical of 9%Cr ferritic steels, such as Grade 92, thus developing new steels for 650℃ applicatio ns.

However, the transformation of V- and Nb-nitrides into the thermodynamically more stable modified Z-phase was unforeseen and this led to an unexpected drop of creep resistance within a few thousand hours at 650℃.

Currently, the formation of Z-phase broke all promising expectations originally put into 12%Cr steels, such as P122, VM12, NF12, cancelling about twenty years of R&D activities for obtaining ferritic steels for 650℃. Figure 20 shows the drop of creep resistance observed in 12%Cr steels. This left Grade 92 as the best performing creep resistant steel among advanced ferritic steels [1].

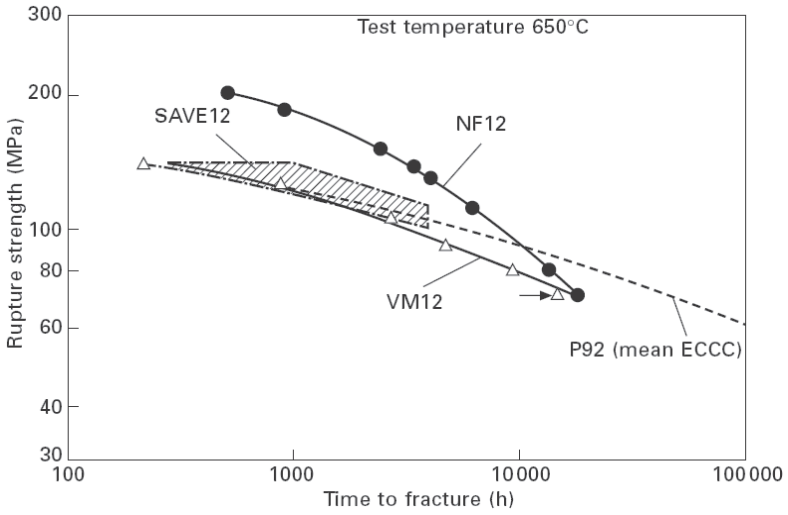

Figure 20 – Creep rupture strength of 12%Cr steels: NF12, SAVE12 and VM12 as a function of test time at 650℃ in comparison to the behaviour of 9%Cr steel P92 [1].

2.3.8.4 Recovery of Martensite

The recovery of martensite preferentially occurs near prior austenite grain boundaries during creep service and this promotes preferential and localised creep deformation, resulting in a premature creep rupture. Recovery of microstructure is caused by carbides forming and coarsening, removing solutes and dissolving smaller precipitates in the surrounding region. This loss of pinning precipitates allows the recovery process [8].

The formation of Z-phase at the expense of MX particles promotes this preferential recovery. Figure 21 shows a grain boundary of a P91 where recovery has occurred after creep test 600℃/100MPa/34,141h [8].

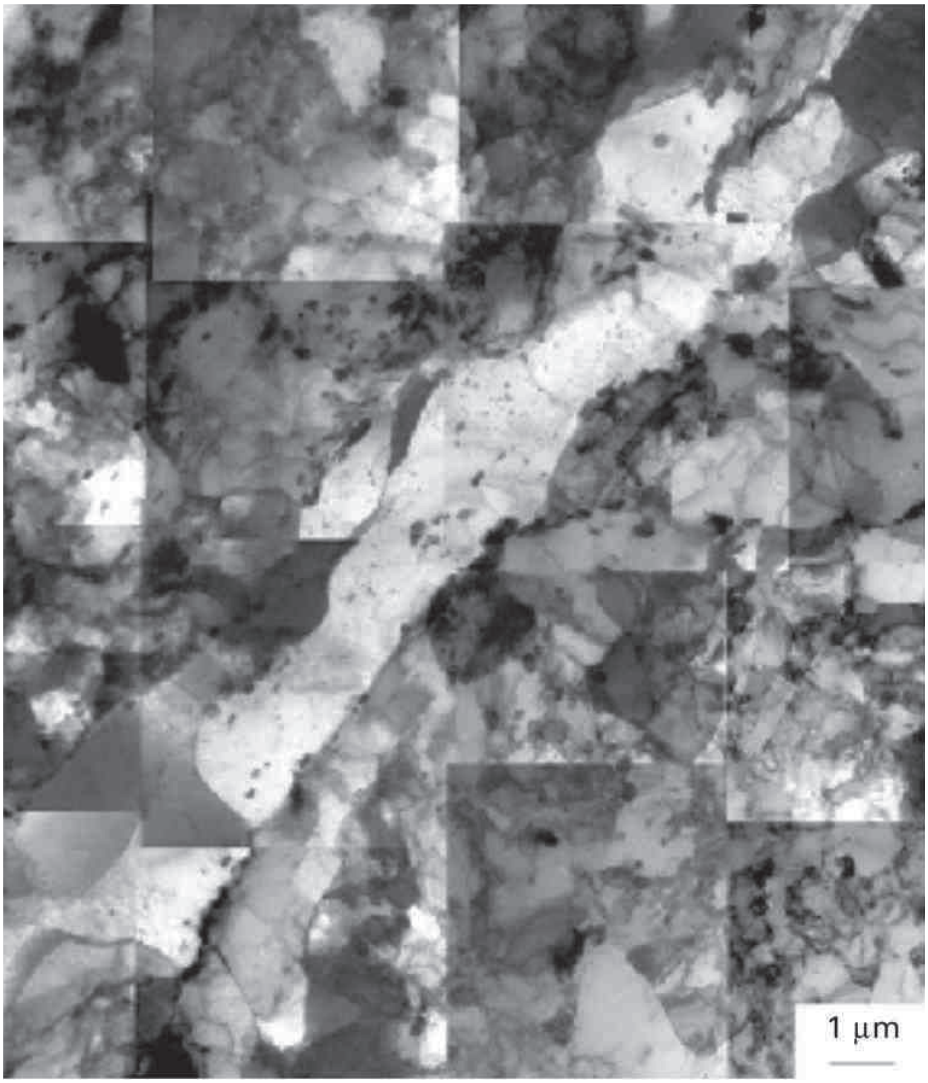

Figure 21 – TEM micrograph of P91 steel after creep rupture testing at 600℃/100MPa/34,141h [8].

CHAPTER 3

MATERIALS

This chapter gives a summary of the steels studied in this Ph.D. project.

3.1 Model alloys: 12CrV(Nb)N steels

Two 12%Cr model alloys were manufactured at Centro Sviluppo Materiali SpA (Rome, Italy), respectively coded M1 (12CrVNbN) and M2 (12CrVN). Their chemical compositions are shown in Table 7.

Table 7 – Chemical composition of investigated materials, (wt%).

	C	Mn	P	S	Si	Cr	Mo	V	N	Ni	Al	Nb	Ti
M1	0.0048	0.32	/	/	0.40	11.85	/	0.18	0.061	1.29	/	0.08	/
M2	0.0017	0.31	/	/	0.35	11.57	/	0.23	0.088	1.27	/	/	/

Two 80kg ingots were produced by Vacuum Induction Melting (VIM). The ingots were hot rolled to 20 mm thick plates, and subsequently normalized at 1050℃ for 1h, followed by air cooling. Thereafter the slabs were tempered at 750℃ for 2h, followed by air cooling to obtain a morphology of tempered martensite.

The model alloys were designed to investigate especially the formation of modified Z-phase, Cr(V,Nb)N, during high temperature exposure. Their chemical compositions were tailored on the basis of the thermodynamic model proposed in [64]: 12-wt% Cr to promote fast Z-phase formation; 1.3-wt% Ni to guarantee the martensitic microstructure after normalising; Nb and V in amounts similar to industrial 9-12%Cr steels; N in a large amount to promote the fast formation of nitrides. A very low carbon content was chosen to avoid carbide formation of $Cr_{23}C_6$ or NbC types; tungsten and molybdenum were excluded to avoid the formation of Laves phase, $Fe_2(Mo,W)$, during ageing. As such the model alloys were perfectly suited for studying the decomposition of the nitrides and the development of Z-phase.

The M1 model (12CrVNbN) alloy was produced to investigate the combined effect of Nb- and V-nitrides on the formation of Z-phase.

The M2 model alloy (12CrVN: Nb-free alloy) was chosen for understanding the role of V-nitride only in the formation of Z-phase: the atomic content of [Nb] + [V] in M1 alloy was

substituted by the atomic content of [V] only in model alloy M2.

Both microstructures of the normalized and tempered materials consist entirely of tempered martensite, with average hardness values of 235 HV_{10} and 237 HV_{10}, respectively for M1 and M2 alloy. After normalizing and tempering, samples of dimensions 100mm x 20mm x 15mm from both materials were aged at 650℃ for up to 10,000 h in laboratory furnaces flushed with air.

3.2 Industrial 9-12%Cr steels

Samples of several 9-12%Cr industrial steels were investigated after normalising and tempering and after long-term ageings.

The chemical composition of the investigated samples according to their reference Specifications is shown in Table 8. Table 9 summarises the ageing conditions (temperature / time) of the investigated samples.

It is worth to remark that during the Ph.D. project it was possible to study samples of commercial Grade 91 pipe after 100,000 creep hours at 550℃ and 600℃.

Table 8 – Chemical composition of investigated steels, according with Specifications. Table does not report requirements for minor elements: P, S, Si, Zr, Ti, Al, Ni.

Grade	Standard Code Source	Chemical Composition (wt%)										
		C	Mn	Cr	Mo	V	N	Nb	W	B	Cu	Co
P91	ASTM 335	0.08 - 0.12	0.30 - 0.60	8.0 - 9.5	0.85 - 1.05	0.18 - 0.25	0.030 - 0.070	0.06 - 0.10	/	/	/	/
E911	ASTM 335	0.09 - 0.13	0.30 - 0.60	8.5 - 9.5	0.90 - 1.10	0.18 - 0.25	0.040 - 0.090	0.06 - 0.10	0.90 - 1.10	0.0003 - 0.006	/	/
P92	ASTM 335	0.07 - 0.13	0.30 - 0.60	8.5 - 9.5	0.30 - 0.60	0.15 - 0.25	0.03 - 0.07	0.04 - 0.09	1.5 - 2.0	0.001 - 0.006	/	/
VM12	V&M	0.1 - 0.14	0.15 - 0.45	11 - 12	0.2 - 0.4	0.2 - 0.3	0.03 - 0.07	0.03 - 0.08	1.3 - 1.7	0.003 - 0.006	0.25 max	1.4 - 1.8
FB2	COST Steel	0.14	0.82	9.1	1.5	0.20	0.015	0.046	/	0.001	/	1.23
T122	ASTM 235	0.07 - 0.14	0.70 max	10.0 - 11.5	0.25 - 0.60	0.15 - 0.30	0.04 - 0.10	0.04 - 0.10	1.50 - 2.50	0.0005 - 0.0050	0.30 - 1.70	/
X20	DIN 17175	017 - 0.23	1.00 max	10.0 - 12.5	0.8 - 1.2	0.25 - 0.35	/	/	/	/	/	/

Table 9 – Ageing conditions (temperature / time) of the investigated samples.

Steel	Exposure Condition		Cr content (wt%)
	Temperature (℃)	Time (h)	
P91	550	110,000	8.5
	600	58,439	8.7
	600	104,000	8.5
	650	10,000	8.3
	650	53,318	8.5
E911	575	64,000	9.2
	625	55,591	9.2
	650	10,354	9.2
	650	55,691	9.2
P92	600	33,051	9.3
	600	60,628	9.3
	650	57,715	9.3
T122	660	12,000	11.0
FB2	600	39,328	9.1
	625	36,986	9.1
VM12	650	6,000	11.5
X20	600	150,000	11.5

3.3 Laboratory 12%Cr Steels

Two crept samples of 12Cr Nb-free laboratory steels were investigated during Ph.D. project. The samples belong to heats 52Cs and 46Cs, whose chemical composition is reported in Table 10. The materials were produced in the framework of COST 536 project [73] [74]; the heats were melted by the forgemaster Saarschmiede; the heat treatments were carried out by IfW Darmstadt and consisted of normalising (1150℃/0.5h/AC) and tempering (750℃/2h/AC). Crept samples of heat 52Cs and 46Cs broke respectively after 18,605 and 11,669 hours at 650℃.

Table 10 – Chemical composition of the 12Cr Nb-free steels (mass%).

Heat Code	C	Si	Mn	Cr	W	Co	Cu	V	N	B
52Cs	0.16	0.38	0.32	11.8	4.07	5.50	-	0.39	0.049	0.0066
46Cs	0.14	0.40	0.29	11.9	3.97	4.44	1.0	0.22	0.066	0.0068

CHAPTER 4

EXPERIMENTAL METHODS

This chapter gives a summary of the experimental methods adopted for investigations of selected samples as well as the used instruments.
The experiments have been carried out at DTU and CSM laboratories. Occasionally instruments belonging to European scientific network (i.e. Universities and International Institutes) have been used.

4.1 Light Microscopy

Samples were observed by reflected Light Microscopy (LM) available at CSM: Leica, model Reichert MeF3A, equipped with digital camera and ImageProPlus© software for image processing, enhancement, and analysis.
Samples were etched with Vilella's reagent (1% picric acid and 5% hydrochloric acid in ethanol).
Reflected Light Microscopy was used to identify the microstructure of the material in as-rolled, normalised and tempered conditions (i.e. to assess the presence of martensite, α- and δ-ferrite) as well as to identify the macro-precipitates along grain boundaries and martensite laths (i.e. primary NbN, TiN, and coarse $M_{23}C_6$ and Laves phases).

4.2 Hardness Measurements

Hardness measurements were performed by automatic hardness tester at CSM, Future Tech model FM-700, adopting Vickers penetrator, with loads ranging from 1 g to 30 kg.

4.3 Scanning Electron Microscope

Scanning Electron Microscope (SEM) investigations were carried out at CSM using a JEOL 5900, with a tungsten filament, equipped with Oxford Instruments Inca Link ISIS Energy Dispersive Spectroscopy (EDS) unit and a software for Automatic Image Analysis (AIA). All investigated metallographic samples were etched with Vilella's reagent.
SEM was used to characterise the microstructure of the samples (i.e. identification of δ-ferrite grains) and to determine the morphology, volume fraction, size distribution and composition of large precipitates (>200 nm).

Measurements of Laves phase on long-term aged samples were carried out by SEM. As Laves phase is a Mo-based or W-based particle, it can be easily identified by Back Scattered Electron (BSE) images. BSE images were processed adopting an AIA procedure, coupling particle size with chemical composition. During SEM session, several hundred random particles from 50 random frames at 3000X magnification were identified (standard procedure), over a large scattered area. A cut-off of particles with mean diameter less than 200 nm and a [Mo]+[W] content less than 5 wt% was imposed.

4.4 Transmission Electron Microscopy

A Field Emission Gun Transmission Electron Microscope (FEG-TEM), JEOL 3000F, operated at 300kV and equipped with an Oxford Instruments EDS unit and a Gatan Imaging Filtered (GIF) Electron Energy Loss Spectroscopy (EELS) was used at DTU.

A 200kV Scanning/Transmission Electron Microscope (STEM), JEOL 200CX, equipped with an EDS Noran Instruments was used at CSM.

Occasionally, a FEG-TEM, FEI TITAN 80-300, operated at 300kV, was applied at the demonstration room of FEI Company.

TEM observations were carried out on carbon extraction replicas as well as on thin foils. The replicas were prepared by chemical etching with Vilella's reagent.

TEM was adopted to determine the morphology, chemical composition and equivalent diameter of phases on extraction replicas.

Typically, several particles of same the class (i.e. MX, $M_{23}C_6$, Laves types) were analysed in order to determine reliable values of average diameter and average chemical composition; only particles above 10 nm and sufficiently far from each other to avoid overlapping were analysed for measuring average size and average composition of phase-type.

Occasionally EDS linescan analysis was conducted on selected particles with varying chemical composition (smooth Cr and V gradient), where the EDS step measurement was 2 nm.

A limited number of analyses was conducted by EF-TEM (from both extraction replicas and thin foils) to assess the local chemistry of the precipitates; thus it was possible to distinguish nitride and carbide particles by measuring element maps (i.e. Cr, V, Nb, C, N) as well as to qualitatively measure the variation of chemical composition within the same particle.

A Selected Area Diffraction (SAD) analysis was performed on a limited number of particles, in order to couple crystal structure with the chemical composition obtained through EDS.

Some thin foils were studied for measurements of the average dislocation density and the average sub-grain size; these measurements were performed with a standard and well-established procedure based on the intercept method applied on thin foils [71].

4.5 X-Ray Powder Diffraction

X-Ray powder Diffraction (XRD) was used for determination of the precipitated phases present in the material. XRD was performed with a Siemens D500 X-ray diffractometer equipped with Co radiation at CSM. The adopted step size was 0.2° in 2 θ and the counting time was 34 s per step. In order to avoid interference from matrix reflections the precipitates were extracted from the bulk by electrolysis in an acidic solution of 5% HCl in 95% ethanol, which dissolves the matrix. The solution thus obtained was filtered through a 20 nm Millipore filter to capture the powder. The dissolution of samples for XRD investigation involved at least 10 g of each sample, providing the statistical background for quantitative assessment of the fractions of the phases present.

By comparing the diffractograms of aged samples from the same material, it was possible to qualitatively follow the microstructural evolution of the steel during thermal exposure. Generally the diffractograms are normalised to a peak which is believed to be (almost) unchangeable during high temperature service. Figure 22 shows two diffractograms of X20 steel, in as-tempered condition (bottom) and after 150,000 hours at 600℃ (top). The appearance of new peaks corresponding to Laves phase and Z-phase is clearly visible by a direct comparison.

Phase weight fractions present in M1 (12CrVNbN) and M2 (12CrVN) samples were quantified by reconstruction of the diffractograms by a Rietveld-like algorithm, taking the volume fractions of the various nitrides as a fitting parameter and taking into consideration a modified Pearson VII peak shape and a correction of the X-ray absorption.

A representative example of a fitted diffractogram is shown in Figure 23. The evolution of the calculated weight fractions of the phases was obtained by assuming that, since the nitrides have a very low solubility in body-centred cubic (*bcc*) iron, the residual amount of nitrogen in solid solution is negligible so that nitrogen can be considered completely bound to the precipitates.

The detailed procedure is reported in the appended paper: *Quantitative X-ray diffraction analysis of the development of Z-phase in a 12% Cr Nb V N steel*, accepted in Material Science and Technology and currently in print. The paper is reported in this thesis.

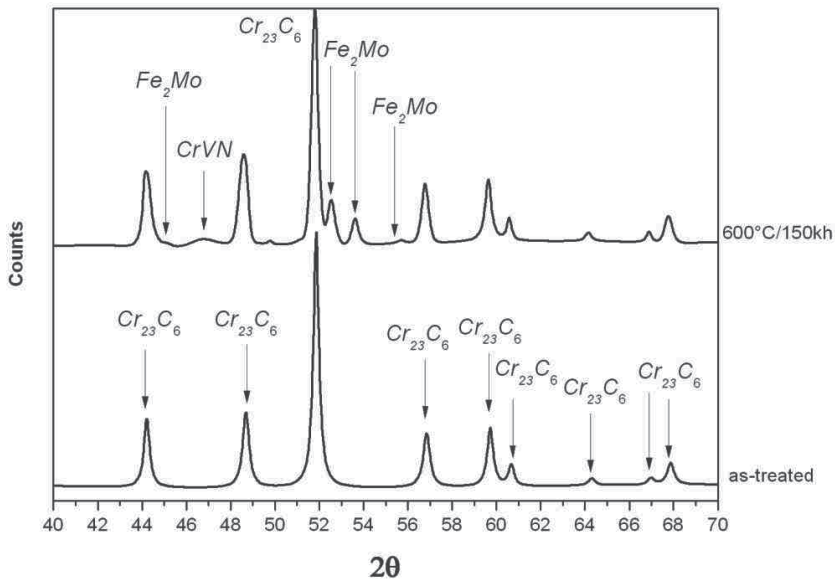

Figure 22 – XRD diffractometers of X20 steel in as-treated condition and after 150,000h at 600℃. Both diffractograms were normalised to $Cr_{23}C_6$ tallest peak.

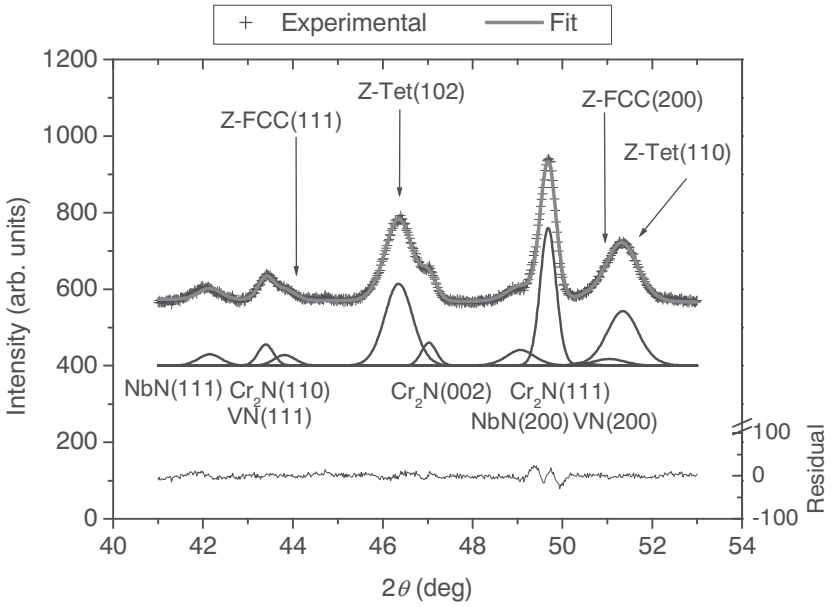

Figure 23 - X-ray diffraction spectrum (Co-Kα incident radiation) of the M1 (12CrVNbN steel) sample aged for 3000 h at 650℃ and calculat ed spectrum after Rietveld refinement (solid line) superimposed to the measured data points (uppermost line), theoretical diffraction peaks of the phases (middle) and fitting residuals (lowermost line).

CHAPTER 5

RESULTS

5.1 Results reported in the appended papers

This paragraph gives a short summary of the papers appended to this thesis, where main results are reported. The reader is encouraged to read the papers for the full details, in the proposed sequence.

5.1.1 PAPER I - Conversion of MX Nitrides to Z-Phase in a Martensitic 12% Cr Steel

Paper published in Acta Materialia 58 (2010) pp. 669-679.

This paper describes the experimental results on model alloy M1, 12CrVNbN, especially designed for studying the role of Nb- and V-nitrides in the formation of modified Z-phase, Cr(V,Nb)N.

An ingot of 12CrVNbN model alloy was produced by Vacuum Induction Melting; then it was hot rolled into a 20 mm thick plate and this was normalised and tempered. The model alloy was especially designed to precipitate Z-phase as fast as possible and only contains nitrides. Samples of as-treated material were aged at 600℃, 650℃ and 700℃ up to 10,000 hours.

Transmission Electron Microscopy and X-Ray powder Diffraction analysis of extracted particles were used to follow the behaviour of Z-phase during ageing.

The model alloy develops Z-phase very fast: first Z-phase particles were identified after 300 hours at 650℃ only and within 10,000 hours at 650℃ all V- and Nb-nitrides transform into Z-phase.

The development of Z-phase was investigated by examining hybrid MX/Z-phase particles found at several temperatures and ageing time; they are high Cr MX, neither final Z-phases, nor original MX. Hybrids are characterised by smooth Cr and V gradients within the particle from the original MX (poor Cr area) to forming Z-phase (rich Cr area). It is believed that such hybrid particles represent the nucleation stage of Cr(V,Nb)N particles.

The MX particles were converted into modified Z-phase via the uptake of Cr from the matrix. The chemical transformation from (V,Nb)N to Cr(V,Nb)N is assumed to be followed by crystallographic transformation of the crystal structure from cubic to tetragonal.

Studies of the precipitation rate of Z-phase shows it is fastest at 650℃, and that it precipitates faster at grain boundaries compared to the interior of the grains.

5.1.2 PAPER II - Quantitative X-Ray Diffraction Analysis of the Development of Z-Phase in a 12% Cr-Nb-V-N Steel

Paper accepted for publication in Materials Science and Technology and currently in print.
This paper describes the calculation procedure for the quantitative analysis of X-ray diffractograms obtained during investigation of model alloy M1, 12CrVNbN steel.

The aim of the present work is to develop a procedure far quantitative assessment of the evolution of the Z-phase nitrides in a model alloy M1, 12CrVNbN steel.
The procedure consists of electrolytic extraction of the precipitates from the metallic matrix and quantitative X-ray diffraction determination of the volume fraction of second phases based on the Rietveld approach.
The procedure accounts for the chemical composition of the phases involved, being (V,Nb)N, (Nb,V)N, Cr_2N and tetragonal and cubic Z-phase, which significantly affects the absolute intensity of the diffraction peaks, and by correcting the results of the Rietveld refinement by the not negligible absorption contributions in the extracted precipitates. The determination of the average chemical composition of the phases involved is provided by TEM analysis techniques.
The evolution of the total mass fraction of Z-phase was described in terms of a Johnson-Mehl-Avrami-Kolmogorov analysis. The kinetic exponent, providing the best fit is very close to unity, indicating that the formation mechanism of Z-phase is not associated with a conventional process of nucleation, but that rather at a gradual diffusion-controlled transformation of the pre-existing V- and Nb-nitrides.
The results of this work indicate that Z-phase formation is actually a transformation and growth of (V,Nb)N and (Nb,V)N into Z-phase by an exchange of substitutional elements, particularly Cr, with the surrounding matrix. This implies that all nuclei are available and have an appreciable size at the start of the transformation.

5.1.3 PAPER III - Microstructural Evolution of ASTM P91 after 100,000 hours exposure at 550℃ and 600℃

Paper submitted to 9th Liège Conference on Materials for Advanced Power Engineering, September 27th –29th, 2010, Liège, Belgium.

In this paper long term aged samples of ASTM P91 were investigated. Mechanism of Z-phase formation, throughout hybrid MX/Z particles, was confirmed in P91 samples too, aged over 100,000 hours at 600℃.

Some ASTM P91 samples were investigated after creep testing at 550℃ and 600℃ for over 100,000h hours. X-Ray Diffraction, Scanning and Transmission Electron Microscopy were used to assess the microstructural evolution of the material in terms of precipitation, growth and coarsening of precipitates during high temperature exposure; mean equivalent diameter and average chemical composition of MX, $M_{23}C_6$ and Laves precipitates were assessed through the analysis of a large number of particles. Growth and coarsening kinetics were determined at 600℃ up to 100,000 hou rs: Laves particles reach an average diameter of about 450 nm and $M_{23}C_6$ mean size stays below 200 nm; the dimension of MX carbonitrides remains almost constant during exposure and stays below 50 nm.

Also the presence of modified Z-phase, Cr(Nb,V)N, has been investigated. Only few Z-phase precipitates and even fewer hybrid MX/Z particles were found in the sample exposed at 600℃ for 100kh.

Two main degradation mechanisms of microstructure were distinguished: 1) the coarsening of $M_{23}C_6$ carbides; 2) nucleation, growth and coarsening of Laves phase.

Z-phase formation cannot be listed among the degradation mechanisms of the microstructure until 100,000 hours at 600℃, as ver y few particles of this nitride were found. However, the general Cr enrichment of MX particles suggests that the conversion to Z-phase is occurring, albeit slowly.

The presence of fine and diffuse MX carbonitrides even after 100,000 hours at 600℃ is the strongest evidence of the high stability of Grade 91 even after long-term thermal exposure.

5.1.4 PAPER IV – On the Role of Nb in Z-Phase Formation in Model 12% Cr Steels

Paper submitted to Scripta Materialia.

This paper describes the experimental results on model alloy M2, 12CrVN, especially designed for studying the role of V-nitrides only in the formation of modified Nb-free Z-phase, CrVN.

An ingot of 12CrVN model alloy was produced by Vacuum Induction Melting; then it was hot rolled into a 20 mm thick plate and this was normalised and tempered.

Subsequently, samples of the as-treated material were aged at 650℃ up to 10,000 hours.

The alloy was especially designed to investigate the role of niobium in the development of Z-phase. Aged samples were investigated by TEM and XRD. Compared with model alloy M1, 12CrVNbN steel, the formation of Z-phase is much delayed in model alloy M2, 12CrVN steel; in fact after 10,000 hours at 650℃ no final Z-phase was identified in alloy M2. Only a few hybrid VN/Z particles were identified in the most aged sample (650℃/10,000h); the hybrids showed the typical Cr and V smooth gradient within the particle. The comparison between model alloys M1 and M2 showed the key-role of niobium in the formation of Z-phase: Nb-free steel showed a much slower formation rate of Z-phase. Thus one way of delaying the Z-phase formation in 12%Cr steels could be by avoiding Nb in the steel (*Nb-free alloying concept*).

5.2 Results in Manuscript

This paragraph reports some results obtained during the Ph.D. project, which are not ready for publication yet, but they are worth mentioning.

5.2.1 Investigations of Z-Phase in 9-12%Cr Industrial Steels

A general overview of the Z-phase behaviour in 9-12%Cr commercial steels has been performed, giving application to the knowledge developed on model alloys M1 and M2, including identification of hybrid MX/Z particles.

Z-phase was recognised in aged samples of Grades 91, 92, 911, FB2, VM12, X20, 122 steels in the temperature range 600℃-650℃ up to 1 00,000 hours. Z-phase particles were identified by the following compositional criterion: Fe(wt%)+Cr(wt%) ≈ V(wt%)+Nb(wt%).

Table 11 summarises the average chemical compositions of identified Z-particles in the investigated 9-12%Cr steels and the number of particles found.

Chromium and iron content of Z-phase is very uniform among the investigated samples, with limited variations: 41≤Cr(wt%)≤51 and 3≤Fe(wt%)≤9; average vanadium an niobium content in Z-phase can sensibly vary among steels: vanadium generally remains around 35% (wt%), while niobium around 15% (wt%).

The Z-phase formation mechanism by Cr diffusion from the matrix into the original MN particles was described, focusing on the role of the mid-stage hybrid particles; they are neither original MN nitrides, nor final Z-phase particles, but hybrids are forming Z-phase, under metastable conditions. Hybrid MN/Z-particles were identified in Grades 91, 92 and X20 aged samples.

Table 11 – Average chemical composition of Z-phase particles identified in the crept samples of 9-12%Cr steels.

Steel	Exposure Condition		Cr content (wt%)	No. particles	Z-phase average composition (wt%)			
	Temperature (℃)	Time (h)			Cr	Fe	V	Nb
P91	550	110,000	8.5	0	*Not found*			
	600	58,439	8.7	0	*Not found*			
	600	104,000	8.5	7	48	3	27	22
	650	10,000	8.3	0	*Not found*			
	650	53,318	8.5	3	43	9	26	22
E911	575	64,000	9.2	0	*Not found*			
	625	55,591	9.2	4	51	6	33	10
	650	10,354	9.2	2	43	4	34	19
	650	55,691	9.2	7	49	4	35	12
P92	600	33,051	9.3	2	43	9	29	19
	600	60,628	9.3	11	51	9	22	18
	650	57,715	9.3	11	45	5	33	17
T122	660	12,000	11.0	12	51	6	30	13
FB2	600	39,328	9.1	3	45	6	28	21
	625	36,986	9.1	2	36	3	37	24
VM12	650	6,000	11.5	6	45	4	34	17
X20	600	150,000	11.5	3	41	5	54	0

Figure 24 shows a typical Z-phase in a P92 crept sample after 57,715 at 650℃, with corresponding EDS measurements in Table 12. Figure 25 shows a hybrid MX/Z-phase particle identified in the same P92 sample, with corresponding EDS measurements in Table 13.

Results of TEM investigations on P92 650℃/58kh sam ple were confirmed by XRD analysis also: Figure 26 shows the diffractogram of the sample, where the Z-phase peak is small, but evident.

Figure 27 shows a typical Z-phase in a VM12 aged sample after 6,000 at 650℃; EDS measurements in Table 14.

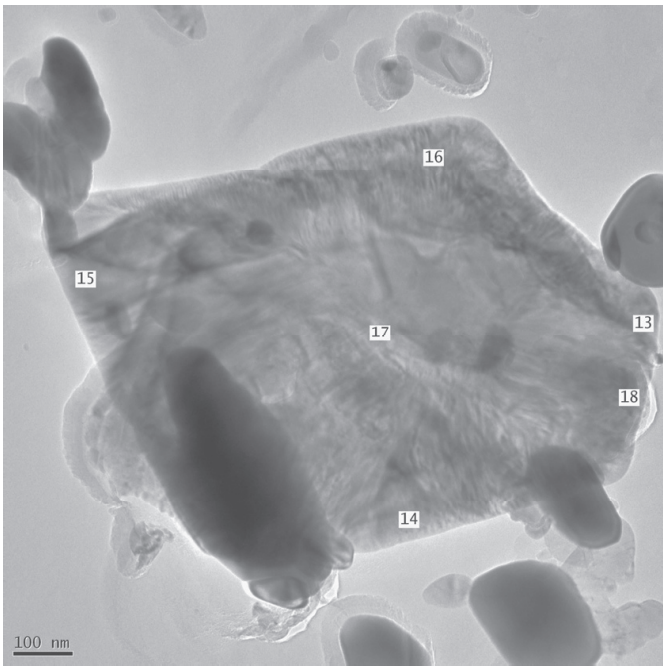

Figure 24 – Z-phase in P92 aged sample: 650℃/57,71 5h.

Table 12 - EDS analysis from sites in Figure 24.

	Cr wt%	Fe wt%	V wt%	Nb wt%
Sp.13	47	4	26	23
Sp.14	47	4	25	24
Sp.15	48	4	26	22
Sp.16	44	5	27	24
Sp.17	43	6	36	15
Sp.18	37	3	41	19

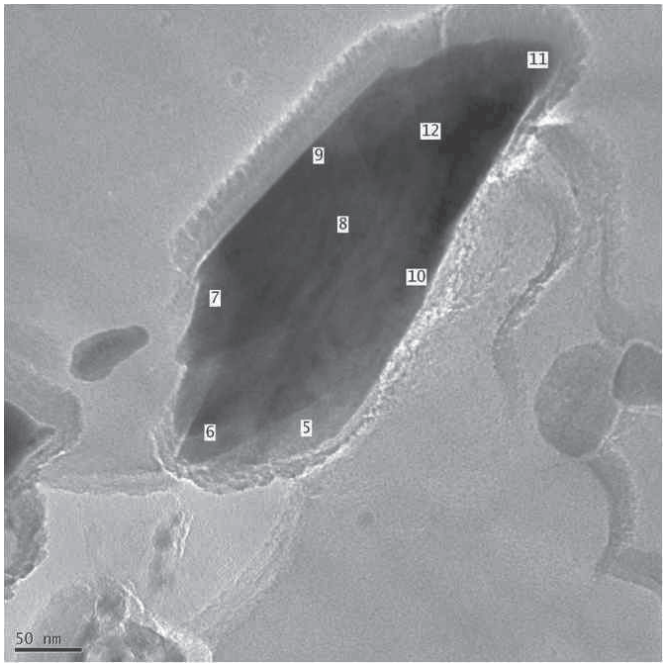

Figure 25 – Hybrid particle in Grade 92 aged sample after 57,515h at 650℃.

Table 13 - EDS analysis from sites in Figure 25.

	Cr wt%	Fe wt%	V wt%	Nb wt%
Sp.5	27	48	3	22
Sp.6	32	43	9	16
Sp.7	29	43	5	23
Sp.8	26	46	4	24
Sp.9	33	45	4	18
Sp.10	30	42	4	24
Sp.11	44	33	2	21
Sp.12	54	28	3	15

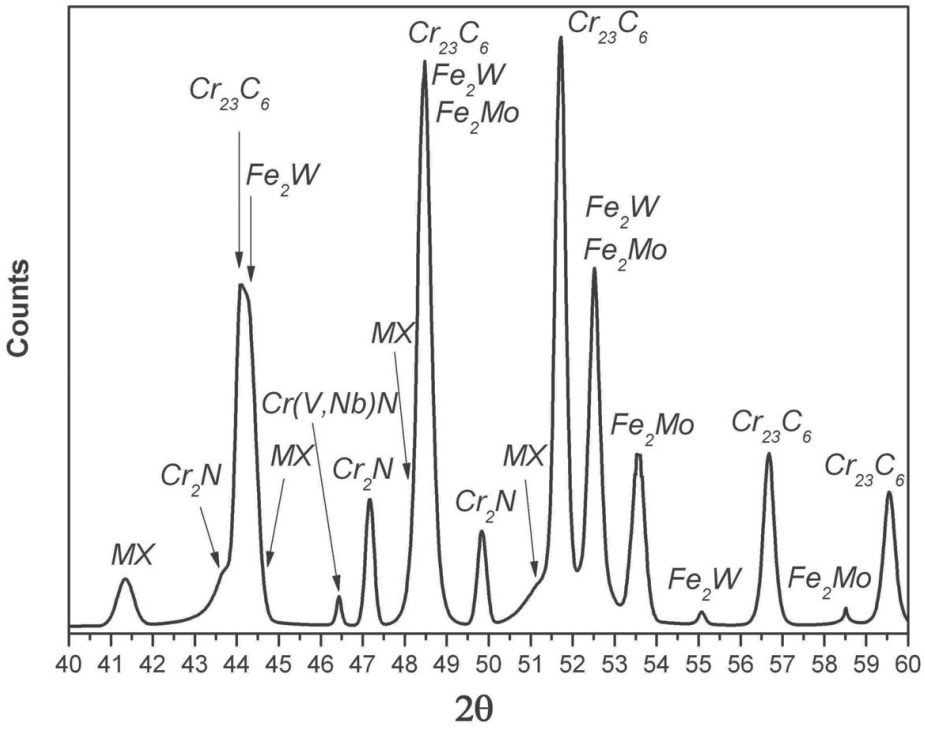

Figure 26 – XRD diffractogram of P92 aged sample after 57,715h at 650℃.

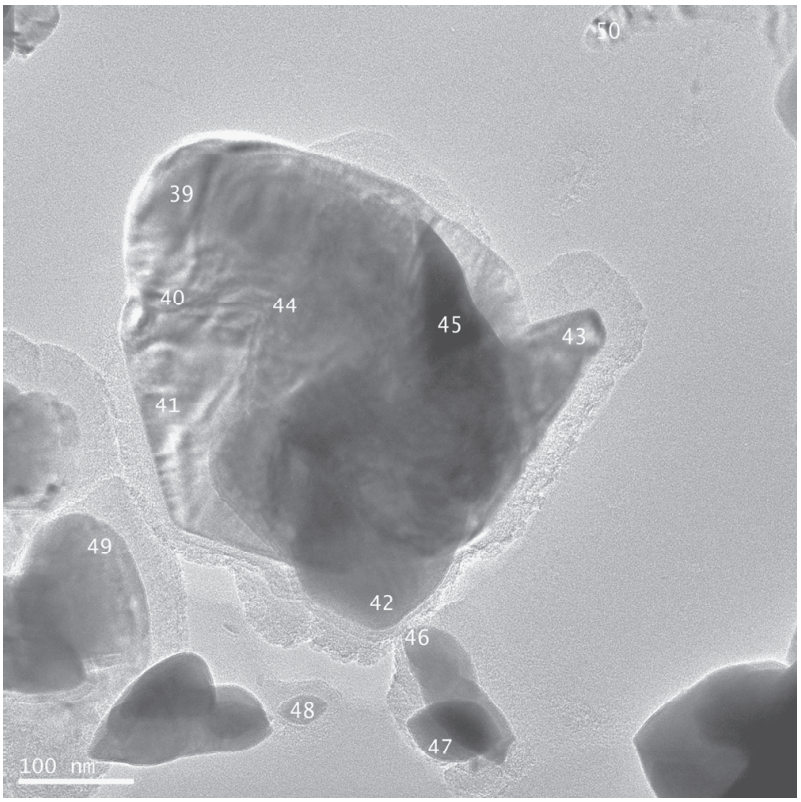

Figure 27 – Z-phase in a VM12 aged sample: 6,000h at 650℃.

Table 14 - EDS analysis from sites in Figure 27.

	Cr wt%	Fe wt%	V wt%	Nb wt%
Sp.40	45	5	35	15
Sp.41	41	5	38	16
Sp.43	43	4	34	19
Sp.44	44	4	35	18
Sp.45	42	4	38	16
Sp.48	18	1	67	14

5.2.2 Behaviour of Z-Phase in 12%Cr Nb-free Steels

Two crept samples from 12%Cr Nb-free heats, 46Cs and 52Cs heats, were investigated by TEM in order to obtain new evidence if *Nb-free alloying concept* works in industrial-like steels, outside model alloys.

CSM and DTU received a couple of crept samples of two 12Cr Nb-free steels from Dr. K.-H. Mayer (ALSTOM Energie GmbH), produced and tested in the framework of COST 536 project [73], see Table 10.

Few V-based Z-phases, CrVN, were found in the 46Cs and 52Cs crept samples after 11kh and 19kh at 650℃, respectively; the observed Z-pha se particles were so few that it was not possible to obtain a reliable statistical assessment of the particles.

Figure 27 shows a TEM frame with some VN particles and one Z-phase (Z-phase is at site 66; the particle is probably viewed from its side). Some $Cr_{23}C_6$ (at sites 71, 72 and 73) and a couple of Laves phases are present, too. Table 15 shows the atomic content of metallic atoms of particles shown in Figure 28.

Many VN particles were identified in both samples.

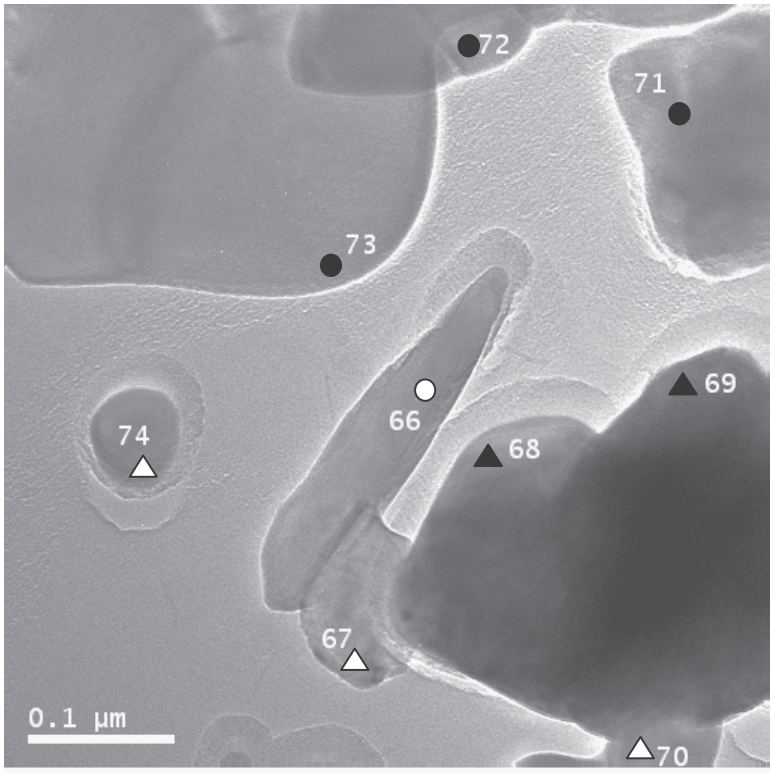

Figure 28 – CrVN Z-phase (site 66) in 46Cs crept sample.

EDS Spectrum	V	Cr	Fe	W
Sp. 66	41	55	2	2
Sp. 67	88	7	4	1
Sp. 68	3	15	54	28
Sp. 69	5	23	41	31
Sp. 70	84	7	2	7
Sp. 71	4	82	9	5
Sp. 72	7	78	12	3
Sp. 73	3	71	18	8
Sp. 74	77	12	7	4

Table 15 – EDS chemical analysis (at%) of particles shown in Figure 28.

CHAPTER 6

DISCUSSION OF RESULTS

The discussion of the results can follow the proposed scheme below:

1. **Basic study** of Z-phase precipitation in M1 and M2 model alloys;
2. **Application to industrial** 9-12%Cr steels;
3. **Alloying Concept** for delaying Z-phase formation.

6.1 Basic Study of Z-Phase Precipitation in M1 and M2 Model Alloys.

The production of M1 and M2 alloys, respectively 12CrVNbN and 12CrVN steels, gave the opportunity to observe nitrides behaviour only, during high temperature exposure, without disturbing presence of carbides (i.e. $Cr_{23}C_6$, NbC) and Laves phase (i.e. $Fe_2(W,Mo)$).

The TEM observations and XRD interpretations were relatively simple due to only nitrides being present in the material: Cr_2N, V-rich and Nb-rich MN nitrides and modified Z-phase, Cr(V,Nb)N.

It has been possible to isolate the forming Z-phases from the beginning and it was concluded that Z-phase particles do not nucleate on existing (V,Nb)N – as it was believed at the start of the Ph.D. project – instead Z-phase forms by means of existing MX particle, through a Cr diffusion from the matrix into the particle. Thus original MX particles gradually transform into final Z-phase. Hybrids were found in both M1 and M2 alloys.

The M1 alloy, 12CrVNbN steel, developed Z-phase within 300 hours at 650℃. On the other hand, the M2 alloy, 12CrVN, developed only a few hybrid particles after 10,000 hours at 650℃. After 10,000 hours at 650℃ all V- and Nb-nitrides of M1 model alloy have transformed into final Z-phase; in M2 model alloy, no final Z-phase was found in the aged sample after 10,000 hours at 650℃, thus revealing a key-role of the niobium in the formation of Z-phase.

Indeed in M1 model alloy, V and Nb are always mixed in the same MX particles, either as (V,Nb)N or as (Nb,V)N, forming complex nitrides; hence niobium always participates in the MX→Z transformation.

Instead the M2 model alloy is Nb-free, hence the original MX particles are vanadium nitrides, with some Cr dissolved.

An hypothesis to explain this Nb effect is put forward: Nb expands the VN lattice and thereby enhances the VN/α interfacial energy. Dissolving Cr into the (V,Nb)N, the lattice reduces and thus the interfacial energy, particularly with Z-phase at the rim (see hybrids).
This suggests that niobium plays a fundamental role in accelerating the transformation of MX into Z-phase.

6.2 Application to industrial 9-12%Cr Steels.

The results obtained from model alloys M1 and M2 were confirmed by similar results obtained from samples of 9-12%Cr commercial steels after several thousands of hours of exposure in the temperature range 600℃-650℃.
The formation mechanism of Z-phase by means of Cr diffusion into existing MX nitrides throughout hybrid MX/Z particles was confirmed, as several hybrids were identified in X20 sample after 150,000 hours at 600℃, P92 sample aft er 50,000 hours at 650℃ and P91 sample after 100,000 hours at 600℃.

6.3 Alloying Concept for Delaying Z-Phase Formation.

The comparison between M1 (12CrVNbN) and M2 (12CrVN) steels reveals the fundamental role of Nb in the development of Z-phase: the Nb-free alloy did not form Z-phase after 10,000 hours at 650℃, but only a few hybrid VN/CrVN particles were identified in the aged sample. This means that the absence of Nb in M2 model alloy delays the formation of Z-phase of, at least, a hundred times with respect of M1 model alloy (where Z-phase appeared after 300 hours at 650℃ on ly).
The Nb effect on Z-phase formation rate is consistent with observations from a 12CrMoV steel (X20 steel, with 12%Cr but no Nb), where only few Z-phase particles, CrVN, were identified after exposure for 150,000 hours at 600°C [4]. Even after such extended exposure, very few CrVN particles were observed. The slow Z-phase formation in Nb-free X20 steel suggests that Nb has a similar effect on Z-phase precipitation in commercial steels as in the model alloys.
TEM investigations of COST 12Cr Nb-free samples (Table 10) revealed that most V-nitrides are still present and stable after several thousands of hours of thermal exposure at 650℃. On the other hand, Z-phase, CrVN, is rare in both samples.

Hence, the presence of Nb seems to largely accelerate the formation of Z-phase in 12%Cr steels. This *Nb-free alloying concept* could be used in developing of new creep resistant 12%Cr ferritic steels with retarded Z-phase formation.

The new class of Nb-free steels could move by the following alloying principles:

- 12%Cr content (wt%) to improve oxidation resistance of the steel.
- Balancing of V, N, B, W, Mo, Cr content to promote precipitation strengthening after the tempering heat treatment by $M_{23}(C,B)_6$, MX and $Fe_2(Mo,W)$
- Balancing of Co content (and other austenite former elements) to generate a ferritic-martensitic microstructure after the normalising heat treatment
- Nb-free, in order to delay the formation of Z-phase at the expense of VN. This is the most important change in alloy chemistry, which should extend the creep life of 12%Cr steels.

CHAPTER 7

CONCLUSIONS

At the beginning of this Ph.D. project much was not completely clear about modified Z-phase in 9-12%Cr steels. Of course, Z-phase has been already identified and studied in commercial steels as well as evidence of the existence of hybrid MX/Z particles and their key-role in Z-phase formation were found.

Nevertheless, there were some *obscure areas* in the understanding of the Z-phase behaviour: the time-temperature regions for Z-phase formation were uncertain; it was not clear whether Z-phase nucleates and whether MX nitrides dissolve or transform; also the formation of hybrid MX/Z-phase particles was a mechanism yet to be understood.

The basic idea of producing two 12%Cr model alloys in this Ph.D. project was to have material samples where the mechanism of Z-phase formation could be isolated, without the disturbing contribution of carbides, Laves phase and other particles which are not nitrides. Thus the role of vanadium and niobium nitrides during the formation of Z-phase was clarified.

This approach was a success, since the study of the two model alloys revealed mechanisms that would not been possible to identify and isolate in industrial 9-12%Cr, crowded of other precipitates (i.e. carbides and intermetallic phases) together with the desired nitrides. Thanks to model alloys the mechanism of formation of modified Cr(V,Nb)N Z-phase was revealed, the MX/Z-phase hybrid particles were analysis in details and the key-role of Nb as Z-phase accelerator was discovered.

But the results mentioned above were not left confined in the model alloy systems only, but all results were applied to industrial 9-12%Cr steels too. Aged samples of commercial steels revealed the same mechanisms of Z-phase formation which were stated for model alloys. Also, the fist hybrid MX/Z-phase in a P91 sample aged for 104,000 hours at 600℃ was identified during the Ph.D. project.

CHAPTER 8

OUTLOOK

During the three years of this Ph.D. project, many initial doubts about Z-phase behaviour in 9-12%Cr steels were solved, however following the natural continuous process of developing knowledge, the answers to our questions led to new unexplained phenomena.
Indeed, it was demonstrated that the Nb accelerates the conversion of complex (V,Nb)N nitrides to Z-phase.
In future, the Nb effect on Z-phase formation could be applied for developing new Nb-free creep high-resistance steels, coupling the superior oxidation resistance, given by 12%Cr content, with the creep resistance of high-alloyed ferritic/martensitic steels, stabilised by retarded conversion of VN to CrVN.

CHAPTER 9

REFERENCES

[1] K. -H. Mayer, F. Masuyama, *The Development of Creep-Resistant Steels*. T.U. Kern, R. Viswanathan, F. Abe editors, *Creep-resistant steels*, Woodhead Publishing Limited, 2008, § 2, pp. 15-77.

[2] R. L. Klueh, *Elevated-Temperature Ferritic and Martensitic Steels and their Application to Future Nuclear Reactors*, Oak Ridge National Laboratoy, 2004, ORNL/TM-2004/176.

[3] J. Gabrel, W. Bendick, *Assessment of Creep Rupture Strength for the New Martensitic 9%Cr Steels E911 and T/P92*, Proceedings of the Creep & Fracture in High Temperature Components - Design & Life Assessment Issues, September 12-14, 2005, London (UK).

[4] H. K. Danielsen, J. Hald, *Behaviour of Z phase in 9-12%Cr* steels, Energy Materials 1 (2006) pp. 49-57, doi: 10.1179/174892306X99732.

[5] M. Yoshizawa, M. Igarashi, K. Moriguchi, A. Iseda, H. G Armaki, K. Maruyama, *Effect of Precipitates on Long-Term Creep Deformation Properties of P92 and P122 type Advanced Ferritic Steels for USC Power Plants*, Materials Science and Engineering A 510-511 (2009) pp. 162-168, doi:10.1016/j.msea.2008.05.055.

[6] A. Golpayegani, H-.O. Andren , H.K. Danielsen, J. Hald, *A study on Z-phase Nucleation in Martensitic Chromium Steels*, Materials Science and Engineering A 489 (2008) pp. 310-318, doi:10.1016/ j.msea.2007.12.022.

[7] H. K. Danielsen, J. Hald, *On the Nucleation and Dissolution Process of Z-Phase Cr(V,Nb)N in Martensitic 12%Cr Steels*, Materials Science and Engineering A 205 (2009) pp. 169-177, doi:10.1016/ j.msea.2008.11.019.

[8] F. Abe, *Strengthening Mechanisms in Steel for Creep and Creep Rupture*. T.U. Kern, R. Viswanathan, F. Abe editors, *Creep-resistant steels*, Woodhead Publishing Limited, 2008, § 6, pp. 279-304.

[9] F. Abe, *Precipitate Design for Creep Strengthening of 9% Cr Tempered Martensitic Steel for Ultra-Supercritical Power Plants*, Sci. Technol. Adv. Mater. 9 (2008) pp. 1-15. doi:10.1088/1468-6996/9/1/013002.

[10] J. Hald, H. K. Danielsen, *Z-Phase Strengthened Martensitic 9-12%Cr Steels*, 3rd Symposium on Heat Resistant Steels and Alloy for High Efficiency USC Power Plants, June 2-4, 2009 Tsukuba (JP).

[11] J. Hald, H. K. Danielsen, *Martensitic Creep Resistant Steels Strengthened by Z-Phase*, Patent WO 2008/106978 A1 12 9 2008.

[12] J. Hald, *Status of the Martensitic Creep Resistant 9-12%Cr Steels*, Proceedings of the Creep & Fracture in High Temperature Components - Design & Life Assessment Issues, April 21-23, 2009, Zurich (CH).

[13] W. Bendick, L. Cipolla, J. Gabrel, J. Hald, *New ECCC Assessment of Creep Rupture Strength for Steel Grade X10CrMoVNb9-1 (Grade 91)*, Proceedings of the Creep & Fracture in High Temperature Components - Design & Life Assessment Issues, April 21-23, 2009, Zurich (CH).

[14] WG3A, ECCC Data Sheet, Steel Grade 91 (X10CrMoVNbN9-1), edition 2009.

[15] WG3A, ECCC Data Sheet, Steel ASTM Grade E911 (X11CrMoWVNb9-1-1), edition 2005.

[16] WG3A, ECCC Data Sheet, Steel ASTM Grade 92, edition 2005.

[17] H. K. Danielsen, J. Hald, *Influence of Z-phase on Long-Term Creep Stability of Martensitic 9 to 12 % Cr Steels.* Vol. VGB PowerTech 5/2009, pp. 68-73.

[18] ASTM Standard A 335/A, *Standard Specification for Seamless Ferritic Alloy-Steel Pipe for High-Temperature Service*, 2006.

[19] P. J. Ennis, Y. Wouters, W. J. Quadakkers, *Steam Oxidation and its Potential Effects on Creep Strength of Power Station Materials*, Materials and Corrosion 56 (2005) pp.890-896.

[20] F. Abe, S. Nakazawa, Materials Science and Technology 8 (1992) pp.1063-1069.

[21] M. Murugananth, *Design of Welding Alloys Creep and Toughness*, Ph.D. Dissertation, Department of Materials Science and Metallurgy, University of Cambridge, November 2002.

[22] http://www.thomas-sourmail.org/stainless/index.html

[23] K. J. Irvine, D. J. Crowe, F. B. Pickering, JISI 195 (1960) p386.

[24] **T**. Fujita, K. Asakura, *Effects of Carbon on Creep-rupture Strength and Toughness of High Cr-Mo Heat Resisting Steels Containing V and Nb*, Transactions of the Iron and Steel Institute of Japan 26 (1986) pp.1073-1079.

[25] F. Abe, M. Igarashi, N. Fujitsuna, K. Kimura, S. Muneki, Proceeding of 6th Leige Conference on Materials for Advance Power Engineering, October 1998, pp. 259-268.

[26] L. Korcakova, *Microstructure Evolution in High Strength Steel for Power Plant Application: Microscopy and Modelling*, Ph.D. Dissertation, Department of Manufacturing Engineering and Management, Technical University of Denmark, 2002.
[27] F. Masuyama, ISIJ International 41 (2001) pp.612-625.
[28] A. Iseda, Y, Sawaragi, S. Kato, F. Masuyama, Creep: Characterisation, Damage and Life Assessment Progeedings of the fifth International Conference on Creep of Materials, 1992, Lake Buena Vista, Florida (USA).
[29] V. Vodarek, S. Strang, Int. Conf. on Microstructural Stability of Creep Resistant Alloys for High Temperature Plant Application, 1997, Sheffiled (UK).
[30] T. Tsuchiyama, Y. Futamura, A. Takaki, *Creep and Fracture of Engineering Materials and Structures, Key Engineering Materials,* Volume 171-174, pp.411-418.
[31] M. Igarashi, Y. Sawaragi, ICOPE'97, Vol.2, pp. 107-112, Tokyo, 1997.
[32] K. J. Irivine, D. J. Crowe, F B. Pickering, Journal of Iron and Steel Institute, 1960, pp.386-405.
[33] K. Hidaka, Y. Fukui, S. Nakamura, R. Kaneko, Y. Tanaka, T. Fujita, *Proceeding of Advanced Heat Resistant Steels for Power Generation*, pp.418-429*,* San Sebastain, Spain, 1998.
[34] L. Helis, Y. Toda, T. Hara, H. Miyazaki, F. Abe, *Effect of Cobalt on The Microstructure of Tempered Martensitic 9Cr Steel for Ultra-Supercritical Power Plants*, Materials Science and Engineering A 510-511 (2009) pp.88-94.
[35] R. L. Klueh, D. J. Alexander, M. A. Sokolov, *Effect of Chromium, Tungsten, Tantalum, and Boron on Mechanical Properties of 5-9Cr-WVTaB Steels*, Journal of Nuclear Materials 304 (2002) pp.139-152.
[36] R.L. Klueh, N. Hashimoto, M.A.Sokolov, *Effect of Heat Treatment and Tantalum on Microstructure and Mechanical Properties of Fe-9Cr-2W-0.25V Steel*, Journal of ASTM International 1 (2004), ISSN: 1546-962X.
[37] H. K. Danielsen, J. Hald,*Tantalum-Containing Z-Phase in 12%Cr Martensitic Steels*, Scripta Materialia 60 (2008) pp. 811-813.
[38] K. Sakuraya, H. Okada, F. Abe, *BN Type Inclusions Formed in High Cr Ferritic Heat Resistant Steel*, Energy Materials 1 (2006) 3.
[39] N. Fujitsuna, M. Igarashi, F. Abe, Key Engineering Materials, 171-174 (2000) pp.469-476.

[40] S. Brett, *In-Service Type IV Cracking in a Modified 9Cr (Grade 91) Header*, Proceedings of the Creep & Fracture in High Temperature Components - Design & Life Assessment Issues, September 12-14, 2005, London (UK), pp.563-572.

[41] S. Brett, *Service Experience with a Retrofit Modified 9Cr (Grade 91) Steel Header*, Advances in Materials Technology for Fossil Power Plants - Proceedings from the 5th International Conference, 2008, pp. 590-600.

[42] F. W. Noble, B.A. Senior, B.L. Eyre, *The Effect of Phosphorus on the Ductility of 9Cr-1Mo Steels*, Acta Metallurgica Et Materialia, 38 (1990) pp.709-717.

[43] C. J. Middleton, *Reheat Cavity Nucleation and Nucleation Control in Bainitic Creep-Resisting Low-Alloy Steels: Roles of Manganese Sulphide, Residual, and Sulphur-Stabilizing Elements*, Metal Science 15 (1981) pp.154-167.

[44] J. Pilling, N. Ridley, D. J. Gooch, *The Effect of Titanium on Creep Strength in 2.25%Cr-1%Mo Steels*, Metallurgical Transactions A, 14A (1983) pp.1443-1449.

[45] T. Fujita, N. Takahashi, *Effects of Individual Addition of Alloying Elements on the Microstructure and Creep Rupture Strength of 12% Chromium Heat Resisting Steels*, Trans Iron Steel Inst Jpn 18 (1978) pp.702-711.

[46] D. G. Cole, *Design of Heat Resistant Steels for Small Power Plants*, University of Cambridge, 2000, Department of Material Science and Metallurgy.

[47] J. R. Davis, *Stainless steels,* ASM Speciality Handbook, 1994, ISBN: 0-87170-503-6.

[48] http://www.thermocalc.com/

[49] http://www.sentesoftware.co.uk/jmatpro.aspx

[50] F. B. Pickering, Microstructural Development and Stability in High Chromium Ferritic Power Plant Steels, A. Strang editor, 1996, Cambridge, pp 1-30.

[51] K. Maruyama, K. Sawada K., J. Koike, ISIJ Int. 41 (2001) 641.

[52] L. Cipolla, A. Di Gianfrancesco, D. Venditti, G. Cumino, S. Caminada, *Microstructural Evolution during Long Term Creep Tests of 9%Cr Steel Grades*, Proceedings of the ASME Pressure Vessels and Piping Conference - 8th International Conference on Creep and Fatigue at Elevated Temperatures - CREEP8, July 22-26, 2007, San Antonio, Texas (USA).

[53] R. O. Scattergood, D. J. Bacon, *The Orowan Mechanism in Anisotropic Crystals*, Philosophical Magazine 31 (1975) pp.179-198.

[54] W. Blum, G. Gotz, Steel Research 70 (1999) pp.72-74.

[55] Atlas of Precipitates in Steels, *Arbeitskreis Elektronemmikroskopie des Werkstoffausschusses des Vereins Deutscher Eisenhuttenleute (ed.)*, *VerlaStahleisen mbH, Dusseldorf, 1983.*

[56] A. Di Gianfrancesco, L. Cipolla, D. Venditti, S.Neri, M. Calderini, *Creep Behaviour and microstructural stability of FB2 (CrMoCoB) Steel Trial*, Proceeding of 3rd Symposium on Heat Resistant Steels and Alloys for High Efficiency USC Power Plants 2009, June 2-4, 2009, Tsukuba (JP).

[57] F. Masuyama, *History of Power Plants and Progress in Heat Resistant Steels*, ISIJ International 41 (2001) pp.612-625.

[58] W. O. Binder, Symposium on Sigma-Phase, 1950 p.146, Cleveland, OH, ASTM.

[59] D. H. Jack, K. H. Jack, J. Iron Steel Inst. 210 (1972) pp.790-792.

[60] T. Sourmail, Mater. Sci. Technol. 17 (2001) 17 pp.1-14.

[61] P. Ettmayer, P, Monatsh, Chem. 102 (1971) 102 pp.858-863.

[62] H.K.Danielsen, J.Hald, *On the Crystal Structure of Z-phase Cr(V,Nb)N*, Met. and Mat. Trans. A 37A (2006) pp.2633-2640.

[63] L. Cipolla, H. K. Danielsen, D. Venditti, P. E. Di Nunzio, J. Hald, M. A. J. Somers, *Conversion of MX to Z-phase in a 12%Cr* steel, Acta Materialia 58 (2010) 669-679.

[64] H. K. Danielsen, J. Hald, *A Thermodynamical Model of Z-Phase Cr(V,Nb)N*, Calphad: Computer Coupling of Phase Diagrams and Thermochemistry 31 (2007) pp.505-514.

[65] K. Sawada, H. Kushima, K. Kimura, *Z-phase Formation during Creep and Aging in 9-12% Cr Heat Resistant Steels*, ISIJ International 46 (2006) pp.769-775.

[66] W. Ostwald, Lehrbuch der Allgemeinen Chemie, vol. 2, part 1, 1896, Leipzig, Germany.

[67] V. Foldyna, *Microstructural Stability of Ferritic 9-12% Chromium Steels*, COST Report No. COST-94-0076-CZ(DG 12CSMC).

[68] K. Dijdueld, *Creep of Low Alloy and Modified Chromium Steels*, Hutnícka Aktuality, Technickè aktuality VITKOVIC, No.1, 1988.

[69] L. Korcakova, J. Hald, *Precipitate Stability in Creep Resistant Ferritic Steels: Experimental Investigations and Modelling*, ISIJ international 43 (2002) pp.420-427.

[70] C. Panait, W. Bendick, A. Fushsmann, A.-F. Gourgues-Lorenzon, J. Besson, *Study of the Microstructure of the Grade 91 Steel after more than 100,000h of Creep Exposure at 600℃* , Proceedings of the Creep & Fracture in High Temperature Components - Design & Life Assessment Issues, April 21-23, 2009, Zurich (CH).

[71] P. Hirsch, A. Howie, R. Nicholson, W. Pashley, M.J. Whelan, *Electron Microscopy of Thin Crystals*, second edition, Krieger Publishing Company, Malabar, Florida, 1977.
[72] L. Cipolla, A. Di Gianfrancesco, D. Venditti, G. Cumino, S. Caminada, *Microstructural Evolution during Long Term Creep Tests of 9%Cr Steel Grades*, Proceedings of CREEP8, Eighth International Conference on Creep and Fatigue at Elevated Temperatures, July 22-26, 2007, San Antonio, Texas (USA).
[73] ACCEPT, Alloy development for Critical Components of Environmental friendly Power planT, http://www.cost.esf.org/domains_actions/mpns/Actions/ACCEPT.
[74] K.-H. Mayer, A. Scholz, Y. Wang, *Investigations of Ferritic/Martensitic Super Heat Resistant 11-12%Cr Steels for 650℃ Power Plants* , Mat.-wiss. u. Werkstofftech 37 (2006) pp.10.

CHAPTER 10

ACKNOWLEDGEMENT

During my Ph.D. thesis I have worked with a great number of people whose contribution in assorted ways to the research and the making of this thesis deserved special mention. It is a pleasure to convey my gratitude to them all in my humble acknowledgment.

I am heartily thankful to my supervisor, Prof. Marcel A.J. Somers (DTU), for his supervision, advice, and guidance from the very early stage of this research as well as giving me extraordinary experiences throughout the work. Above all and the most needed, he provided me unflinching encouragement and support in various ways.

I gratefully acknowledge Prof. John Hald (DONG/DTU) for his advice, supervision, and crucial contribution, which made him a backbone of this research and so to this thesis. His involvement with his originality has triggered and nourished my intellectual maturity that I will benefit from, for a long time to come. John, I am grateful in every possible way and hope to keep up our collaboration in the future.

Many thanks go in particular to Hilmar K. Danielsen, Ph.D (DTU). I am much indebted to him for his valuable advice in science discussion and supervision in each part of the project. Furthermore, I thank Hilmar for using his precious time to read this thesis and many paper revisions and giving me critical comments.

I have also benefited by advice and guidance and friendship from my colleague Dario Venditti (CSM) who always kindly grants me his time even for answering some of my unintelligent questions about transmission electron microscopy. He has been the best fellow traveller during my frequent trips from Rome to Copenhagen. We enjoyed many beers together!

I am very grateful to my colleague Paolo Emilio di Nunzio (CSM) for the stimulating science discussion we had day-by-day over the last three years.

Thanks are due to my colleagues Augusto Di Gianfrancesco (CSM) and Paolo Folgarait, PhD (CSM); they largely contributed to the birth of this research project.

I am also grateful to CSM Management, especially to Mauro Pontremoli, CEO, who always believed in the project and always authorised the research activities from CSM side.

It is also a pleasure to pay tribute to my research collaborators: Marcello Ballone (CSM), Silvia Tiberi Vipraio (CSM) and Flemming B. Grumsen (DTU). I would like to thank all of

them for their priceless assistance.
This wonderful three-years experience would not have been possible without the steadfast encouragement of my lovable and patient wife Valentina, who always found the right words to strengthen my will.

PAPER I

Available online at www.sciencedirect.com
ScienceDirect
Acta Materialia 58 (2010) 669–679
Acta MATERIALIA
www.elsevier.com/locate/actamat

Conversion of MX nitrides to *Z*-phase in a martensitic 12% Cr steel

Leonardo Cipolla [a,b,*], Hilmar K. Danielsen [b], Dario Venditti [a], Paolo Emilio Di Nunzio [a], John Hald [b,c], Marcel A.J. Somers [b]

[a] *Centro Sviluppo Materiali SpA, Rome, Italy*
[b] *Department of Mechanical Engineering, Technical University of Denmark, DTU, Lyngby, Denmark*
[c] *DONG Energy, Fredericia, Denmark*

Received 9 July 2009; received in revised form 20 September 2009; accepted 21 September 2009
Available online 14 October 2009

This page was left blank on purpose

Available online at www.sciencedirect.com
ScienceDirect
Acta Materialia 58 (2010) 669–679
Acta MATERIALIA
www.elsevier.com/locate/actamat

Conversion of MX nitrides to *Z*-phase in a martensitic 12% Cr steel

Leonardo Cipolla [a,b,*], Hilmar K. Danielsen [b], Dario Venditti [a], Paolo Emilio Di Nunzio [a], John Hald [b,c], Marcel A.J. Somers [b]

[a] *Centro Sviluppo Materiali SpA, Rome, Italy*
[b] *Department of Mechanical Engineering, Technical University of Denmark, DTU, Lyngby, Denmark*
[c] *DONG Energy, Fredericia, Denmark*

Received 9 July 2009; received in revised form 20 September 2009; accepted 21 September 2009
Available online 14 October 2009

Abstract

A 12% Cr model steel was designed with the purpose of studying the nucleation and growth of modified *Z*-phase, Cr(V,Nb)N. The model alloy develops *Z*-phase after relatively short ageing times and contains only nitrides of Cr, V and Nb. Interferences from the presence of carbides and the development of Laves phase were avoided by keeping the C, W and Mo contents as low as possible. Transmission electron microscopy and X-ray diffraction analysis of extracted particles were used to follow the evolutions of phase composition, phase morphology and phase fraction, particularly of the precipitation of *Z*-phase, during ageing at 600, 650 and 700 °C for up to 10^3 h. The development of *Z*-phase appears to be accomplished by the diffusion of Cr atoms into (V,Nb)N particles and their subsequent conversion into cubic or tetragonal *Z*-phase. Studies at various temperatures indicate that *Z*-phase development proceeds fastest at 650 °C and that *Z*-phase forms faster at prior austenite grain boundaries.

Keywords: TEM; XRD; Heat resistant steels; Nitrides; Phase transformation kinetics

1. Introduction

In the last two decades the pressure and temperature service conditions of components for advanced power plants have increased, imposing more severe requirements on the strength, corrosion resistance and creep properties of high-temperature steels. To comply with these requirements, advanced 9–12% Cr martensitic steels were developed and are now extensively applied in new high-efficiency ultra super critical (USC) power plants. These steels are generally furnished after a normalizing and a tempering heat treatment, with the final microstructure consisting of fully tempered martensite.

During high-temperature service, 9–12% Cr steels show a gradual degradation of their properties due to the evolution of the microstructure. In order to improve their creep resistance, this microstructural evolution should be retarded. Attempts to stabilize the microstructure involve the precipitation of finely dispersed MX carbonitride (M = metal; X = N,C) particles. Furthermore, mainly Cr-based $M_{23}C_6$ carbides, located preferentially along prior austenite grain boundaries and martensite laths, contribute to improved creep strength [1]. In general, small variations in the alloying element content can lead to substantial changes in the creep strength of these steels [2,3].

Recently, it was found [4–6] that the modified *Z*-phase, a complex nitride Cr(V,Nb)N, develops in 9–12% Cr steels during long-term exposure in the temperature range 600–700 °C. The development of *Z*-phase has been held responsible for a detrimental effect on the creep strength, since it is associated with the consumption of the finely dispersed small nitrides, (V,Nb)N, which are considered to make the most important contribution to the creep resistance. Unfortunately, *Z*-phase develops as large particles, and thus cannot compensate for the loss in creep strength as a consequence of the dissolution of MX. A thermodynamic

* Corresponding author. Address: Centro Sviluppo Materiali SpA, Rome, Italy.
E-mail address: l.cipolla@c-s-m.it (L. Cipolla).

1359-6454/$36.00 © 2009 Acta Materialia Inc. Published by Elsevier Ltd. All rights reserved.
doi:10.1016/j.actamat.2009.09.045

model for *Z*-phase has recently been proposed based on literature and complementary experimental data [7]. The model predicts that *Z*-phase is the most stable nitride in 9–12% Cr steels in the creep service temperature range 600–700 °C, and accordingly will attempt to fully replace the finely dispersed MX nitrides, which precipitate during normalizing and tempering heat treatment. It was concluded that the Cr content has a major influence on the driving force for *Z*-phase formation, which explains why advanced 12% Cr steels suffer from abundant formation of *Z*-phase, while 9% Cr steels do not [5,6,8]. It was also reported that, after creep exposure, *Z*-phase had developed preferentially along prior austenite grain boundaries, along martensite lath boundaries or boundaries along delta ferrite grains. It was also shown that the main metallic composition of *Z*-phase does not depend on the precipitation site [9].

The *Z*-phase which forms in 9–12% Cr martensitic steels is primarily a CrV-based nitride, but also contains limited quantities of Nb and Fe, and is usually termed modified *Z*-phase. The crystal structure of modified *Z*-phase has generally been described as tetragonal, with $a = 0.286$ nm and $c = 0.739$ nm [10], as shown in Fig. 1a.

Extensive electron diffraction on various exposed 9–12% Cr steels has recently revealed a more complex crystal structure of modified *Z*-phase. NaCl-type cubic diffraction patterns, similar to those found in MX precipitates, albeit with a slightly lower lattice parameter, $a = 0.405$ nm, were identified [11]. This cubic structure was found to coexist with the tetragonal structure in the *Z*-phase. The proposed hybrid crystal structure is shown in Fig. 1b. Furthermore, investigations showed that the cubic structure was predominant in 9–12% Cr samples which had been aged for relatively short times (of the order of 10,000 h at 600 °C), while the tetragonal diffraction patterns become more pronounced upon prolonged ageing [12]. The cubic *Z*-phase structure is regarded as an intermediate metastable crystal structure and is expected to be completely replaced by the tetragonal structure, although this process may well take hundreds of thousands of hours.

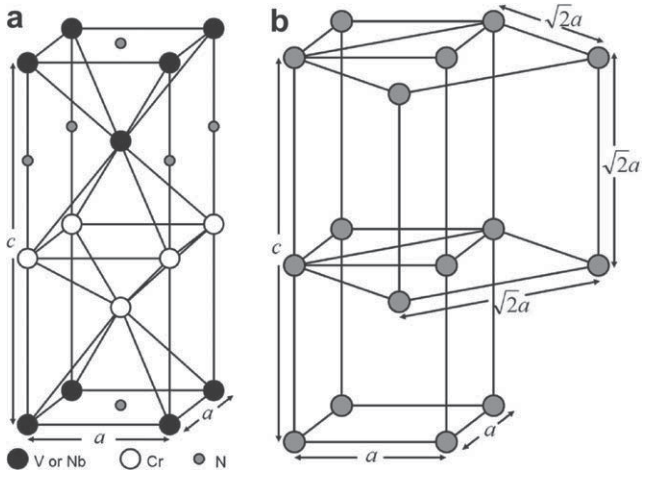

Fig. 1. (a) Tetragonal crystal structure generally associated with *Z*-phase [10]; (b) proposed hybrid crystal structure of modified *Z*-phase [11], in which cubic and tetragonal crystal structures coexist.

The present work seeks to clarify the nucleation mechanism, the main metallic composition, the size distribution and the time–temperature regions of *Z*-phase formation in a model 12% Cr steel. In particular, the present work focuses on how V- and Nb-nitrides are converted into more thermodynamically stable *Z*-phase during long-term high-temperature exposure.

2. Materials and methods

An 80 kg ingot model alloy was produced by vacuum induction melting (VIM); the chemical composition as determined by X-ray fluorescence spectroscopy is given in Table 1. The ingot was hot rolled to a 20 mm thick plate, and subsequently normalized at 1050 °C for 1 h, followed by air cooling. Thereafter the slab was tempered at 750 °C for 2 h, followed by air cooling to obtain the morphology of tempered martensite.

The model alloy was specifically designed to rapidly precipitate the modified *Z*-phase, Cr(V,Nb)N, during high-temperature exposure. Its chemical composition was tailored on the basis of the thermodynamic model proposed in Ref. [7]: 12 wt.% Cr to promote fast *Z*-phase formation; 1.3 wt.% Ni to guarantee the martensitic microstructure after normalizing; Nb, V and N in amounts similar to industrial 9–12% Cr creep steels. A very low C content of 45 ppm was chosen as to avoid carbide formation of $Cr_{23}C_6$ or NbC types; W and Mo were excluded to avoid the formation of Laves phase, $Fe_2(Mo,W)$, during ageing. As such, the model alloy was perfectly suited for studying the decomposition of the nitrides and the development of *Z*-phase. The microstructure of the normalized and tempered material consists entirely of tempered martensite, with an average hardness of 235 HV_{10}. After normalizing and tempering, samples of dimensions 100 mm × 20 mm × 15 mm were aged at 600, 650 and 700 °C for up to 10,000 h in laboratory furnaces flushed with air.

X-ray powder diffraction (XRD) was used for determination of the precipitated phases present. XRD was performed with a Siemens D500 X-ray diffractometer equipped with Co radiation. The step size was 0.2° in 2θ and the counting time was 34 s per step. In order to avoid interference from matrix reflections the precipitates were extracted from the bulk by electrolysis in an acidic solution of 5% HCl in 95% ethanol, which dissolves the matrix. The

Table 1
Chemical composition (in wt.%) of model alloy as determined by X-ray fluorescence spectroscopy.

C	Cr	Ni	Nb	V	N
0.0048	11.85	1.29	0.076	0.183	0.061
Si	Mn	P	S	Fe	
0.40	0.32	<0.005	<0.003	Bal.	

solution thus obtained was filtered through a 20 nm Millipore filter to capture the powder. The dissolution of samples for XRD investigation involved at least 10 g of each sample, providing the statistical background for quantitative assessment of the fractions of the phases present.

The morphology and composition of the precipitates in the as-treated and aged samples were investigated by field emission gun transmission electron microscopy (FEG-TEM), using a JEOL 3000F microscope, operated at 300 kV and equipped for energy dispersive spectroscopy (EDS, Oxford Instruments Inca Link ISIS) and electron energy loss spectroscopy (EELS, Gatan Imaging Filtered). Statistical measurements were acquired by scanning/transmission electron microscope (STEM) using a JEOL 200CX at 200 kV, equipped for EDS (Noran Instruments).

All TEM observations were carried out on carbon extraction replicas. The replicas were prepared by a chemical etch with Vilella's reagent (1% picric acid and 5% hydrochloric acid in ethanol) [13,14].

3. Results

3.1. XRD

After normalizing and tempering, the precipitates in the model alloy consisted only of the nitrides M_2X ($(Cr,V)_2N$) and MX ((V,Nb)N). Two populations of MX nitrides were identified: V-rich and Nb-rich. The diffractogram of extracted precipitates from the as-treated sample showed no indication of *Z*-phase particles (Fig. 2).

Both VN and NbN have a NaCl-type crystal structure (face-centered cubic (fcc) lattice of metal atoms), with lattice parameters of 0.413 nm and 0.439 nm, respectively. Since a significant dissolution occurs of Nb in VN and of V in NbN, the actual compositions of the nitrides are rather (V,Nb)N and (Nb,V)N. Accordingly, the lattice parameter of (V,Nb)N will be higher than 0.413 nm and that of (Nb,V)N will be lower than 0.439 nm. The Cr_2N particles have a hexagonal crystal structure, with lattice parameters $a = 0.481$ nm and $c = 0.448$ nm. Although significant amounts of V can be dissolved into the Cr_2N, this will not greatly affect the lattice parameter, as V and Cr atoms have almost the same size.

Comparison among powder diffractograms (Co K_α radiation) of as-treated and aged samples at 650 °C is shown in Fig. 2. All diffractograms were normalized with respect to the highest intensity peak of Cr_2N for graphical representation, as the Cr_2N quantity only changes slightly with time. Qualitatively, the XRD results show a gradual reduction in the NbN and VN peak intensities with increasing ageing times: after 10,000 h at 650 °C the (Nb,V)N peaks (~48.8° 2θ and ~42° 2θ) and the (V,Nb)N peak (~50.4° 2θ) disappeared. The (V,Nb)N peak at ~43.3° 2θ overlaps with an Cr_2N peak. The intensity reduction of (Nb,V)N and (V,Nb)N peaks corresponded to the appearance of three new peaks, which were identified as belonging to modified *Z*-phase, Cr(V,Nb)N. As the main *Z*-phase peak (~46.3° 2θ; tetragonal *Z*-phase) is clearly visible after only 300 h, this alloy manifested a very fast rate of Z-precipitation as compared to other 9–12% Cr steels, where *Z*-phase development is usually first observed after several thousands of hours at 650 °C [9,10]. The diffractograms were quantified by reconstruction of the spectra by a Rietveld-like algorithm, taking the volume fractions of the various nitrides as a fitting parameter and taking into consideration a modified Pearson VII peak shape and a correction of the X-ray absorption [15].

A representative example of a fitted diffractogram is shown in Fig. 3. The evolution of the calculated weight fractions of the phases with increasing time at 650 °C was obtained by assuming that, since the nitrides have a very low solubility in body-centered cubic (bcc) iron, the residual amount of nitrogen in solid solution is negligible so that nitrogen can be considered completely bound to the precipitates. The results of the calculation are reported in Table 2.

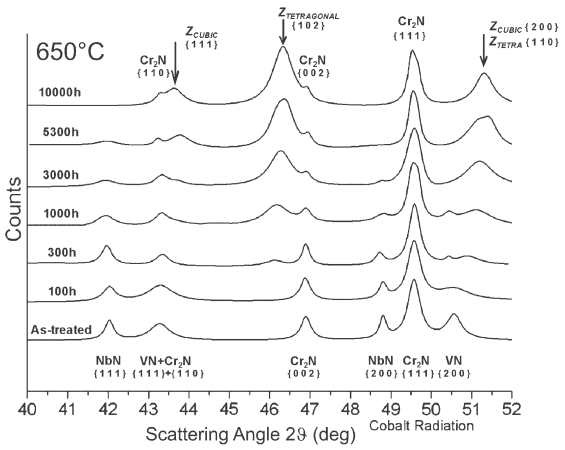

Fig. 2. X-ray diffractograms (Co K_α incident radiation) of aged samples at 650 °C.

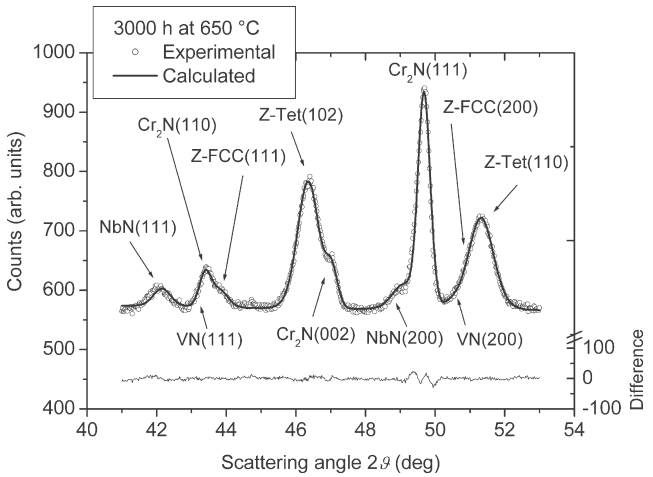

Fig. 3. X-ray diffraction diffractogram (Co K_α incident radiation) of the sample aged for 3000 h at 650 °C and calculated diffractogram after Rietveld refinement. The difference between the measured and the calculated diffractogram is displayed in the bottom of the frame.

Table 2
Evolution of the absolute weight fraction of the precipitate phases in the steel as a function of the ageing time at 650 °C, as determined from XRD analysis [15].

Ageing time (h)	Cr_2N	NbN	VN	Z_{fcc}	Z_{tetra}	Z_{total}
0	4.22×10^{-3}	3.78×10^{-4}	2.70×10^{-4}	0	0	0
100	3.50×10^{-3}	6.46×10^{-4}	5.00×10^{-4}	0	0	0
300	3.87×10^{-3}	4.38×10^{-4}	3.05×10^{-4}	1.86×10^{-4}	4.92×10^{-5}	2.36×10^{-4}
1000	3.54×10^{-3}	3.45×10^{-4}	1.84×10^{-4}	1.75×10^{-4}	7.56×10^{-4}	9.32×10^{-4}
3000	3.22×10^{-3}	2.02×10^{-4}	2.15×10^{-5}	3.01×10^{-4}	1.47×10^{-3}	1.77×10^{-3}
5300	2.78×10^{-3}	1.31×10^{-4}	1.50×10^{-5}	3.73×10^{-4}	2.00×10^{-3}	2.37×10^{-3}
10000	2.78×10^{-3}	8.18×10^{-5}	2.35×10^{-5}	5.39×10^{-4}	1.89×10^{-3}	2.43×10^{-3}

and Fig. 4. A detailed description of the procedure followed is provided elsewhere [15]. Clearly, the weight fractions of (V,Nb)N and (Nb,V)N decrease with time; both are reduced to practically zero after 10,000 h ageing. Cubic *Z*-phase is formed earlier and in larger quantities than tetragonal *Z*-phase; this latter is characterized by high formation rate and overcomes cubic *Z*-phase precipitation after 1000 h ageing.

Fig. 5 shows diffractograms from samples aged for 3000 h at 600, 650 and 700 °C. The largest weight fraction of *Z*-phase peak was determined in the sample aged at 650 °C (see Table 3). This suggests that the fastest *Z*-phase formation in 12% Cr model alloy occurs at 650 °C. These results are consistent with time–temperature–precipitation (TTP) maps for *Z*-phase formation in 9–12% Cr commercial steels [16], which show the fastest precipitation at 650 °C.

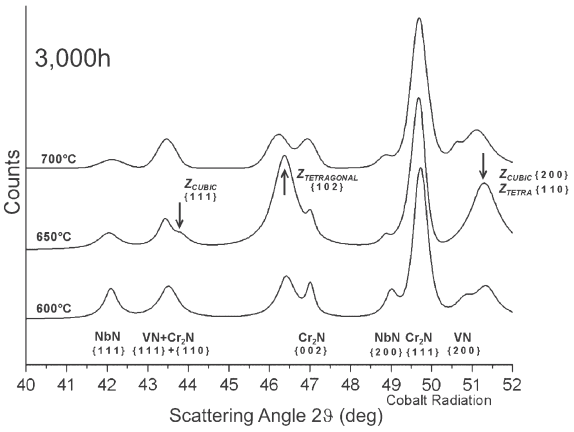

Fig. 5. X-ray diffractograms (Co K_α incident radiation) of aged samples after 3000 h at 600, 650 and 700 °C.

3.2. TEM investigations

All extraction replicas were investigated with TEM using EDS for further identification of the particles found in XRD. The precipitate distribution in the as-treated sample is shown in Fig. 6: Cr_2N is mainly precipitated along prior austenite grain boundaries and martensite lath boundaries, while V-rich and Nb-rich nitrides are distributed throughout the microstructure. No *Z*-phase was found in the as-treated sample, which is consistent with the XRD results.

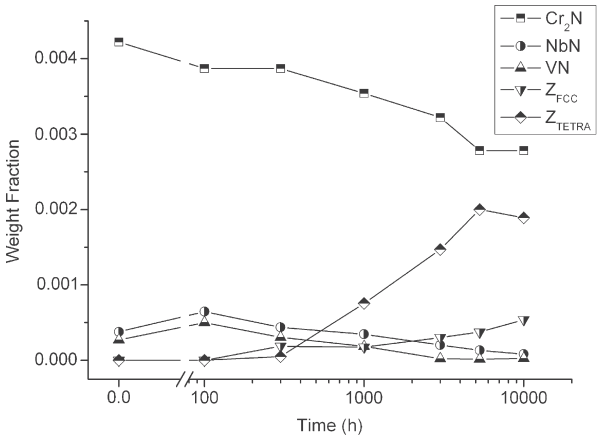

Fig. 4. Evolution of the weight fraction of phases as a function of the time at 650 C.

The mean chemical compositions (in at.% of all the metal atoms in the nitrides, i.e. N atoms are not taken into consideration) of Cr_2N, V-rich and Nb-rich nitrides as well as *Z*-phases of as-treated and aged samples are given in Table 4. For each sample more than 100 particles were analyzed with EDS: only particles sufficiently distant from each other (at least 50 nm) were analyzed in order to avoid overlap. The analyzed particles were at least 10 nm in diameter in order to get reliable measurements over a relatively large particle volume.

On the basis of the composition analysis, two populations of MX nitrides were distinguished: Nb-rich nitrides, (Nb,V)N, with $[Nb] \geqslant [V]$, and V-rich nitrides, (V,Nb)N, with $[V] > [Nb]$; for both kinds of nitrides $[V] + [Nb] \geqslant 70$ at.%. Cr_2N nitrides are characterized by the following compositional criterion: $[Fe] + [Cr] \geqslant 70$ at.%. *Z*-phases are characterized in aged samples by the following compositional criterion: $[Fe] + [Cr] \approx [V] + [Nb]$, where $40 < [Fe] + [Cr] \leqslant 70$ at.% [6,9]. The phase types were confirmed by selected-area electron diffraction (SAED) analysis carried out on random particles.

In all aged samples, except for the 10,000 h sample, Nb- and V-rich nitrides with an average $[Fe] + [Cr]$ of 30–40 at.%. were observed. These particles can neither be classified as complex (V,Nb)N nor as proper Cr(V,Nb)N. In Table 4 this class of precipitates is therefore indicated as $30 \leqslant [Cr] \leqslant 40$ at.%.

Table 3
Absolute weight fraction of phases after annealing for 3000 h at 600, 650 and 700 °C, as determined from XRD analysis [15].

Temperature(°C)	Weight fraction				
	Cr_2N	NbN	VN	Z_{fcc}	Z_{tetra}
600	4.06×10^{-3}	3.00×10^{-4}	7.33×10^{-5}	1.67×10^{-4}	4.49×10^{-4}
650	3.22×10^{-3}	2.02×10^{-4}	2.15×10^{-5}	3.01×10^{-4}	1.47×10^{-3}
700	3.44×10^{-3}	2.94×10^{-4}	2.26×10^{-4}	2.97×10^{-4}	7.52×10^{-4}

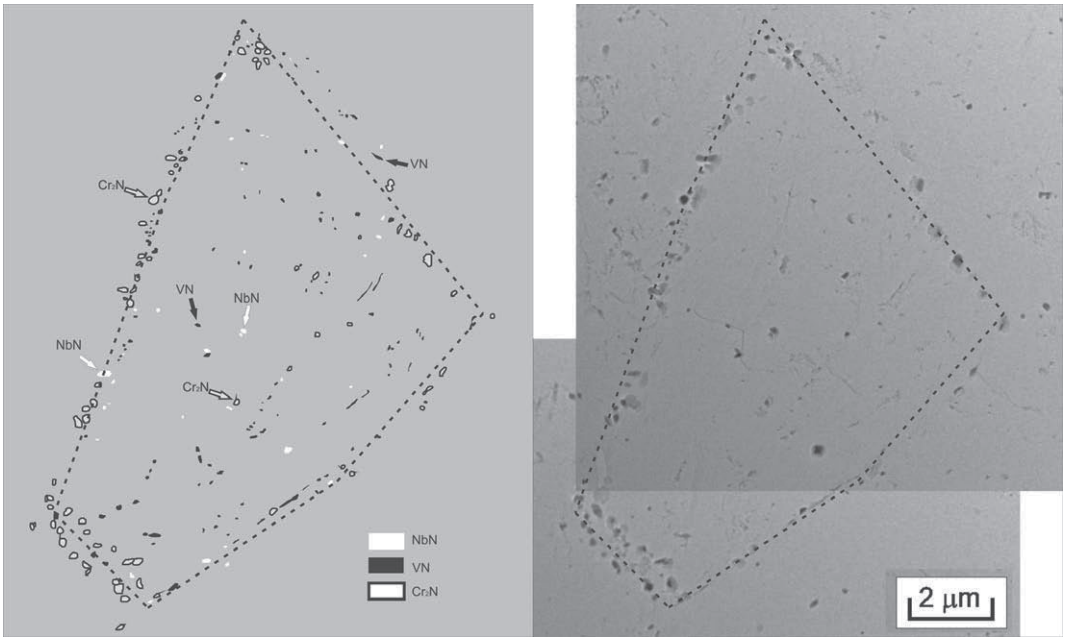

Fig. 6. Distribution of particles using EDS of the as-treated sample: grey, Cr_2N; black, V-rich nitride; white, Nb-rich nitride. Dotted lines indicate the location of the grain boundaries.

The chemical evolution of the analyzed particles in as-treated and annealed samples is depicted in the quasi-ternary (Cr + Fe)–V–Nb diagrams in Fig. 7a–f (data from Table 4). The average chemical compositions of Cr(V,Nb)N, (V,Nb)N and (Nb,V)N particles changed gradually during temperature exposure. Clearly, the Cr content increases in the MX particles and an overall shift towards a *Z*-phase composition appears on prolonged ageing. The chemical compositions of the observed *Z*-phase are similar to those reported for *Z*-phase particles that have developed in commercial 9–12% Cr steels [6].

For the longer ageing times no (V,Nb)N particles were detected (Table 4. and Fig. 7e–f), while (Nb,V)N particles were still present. This observation is consistent with Fig. 4, where it is observed that (Nb,V)N is present up to longer ageing times than (V,Nb)N. Apparently, (Nb,V)N is more stable against dissolution than (V,Nb)N, which can be explained from the mechanism by which (Nb,V)N is converted into *Z*-phase (see Section 4.2 and Figs. 10 and 12).

The *Z*-phase particles were generally observed as isolated particles, but could also be observed in pairs and in contact with MX particles. The morphology of *Z*-phase particles was usually thin faceted plates – see Fig. 8 and Table 5. In the extraction replica most *Z*-phase particles look plate-like, i.e. the plane of the plate is parallel to the plane of the carbon replica (sites 1 and 2 in Fig. 8). When not aligned in such a way, the *Z*-phase may appear rod-like, as they are viewed from the side (sites 3 and 4 in Fig. 8).

In the sample aged for 3000 h at 650 °C, only little MX was left, while numerous *Z*-phase particles were identified. After 5300 h at 650 °C all V-rich MX particles had disappeared. After ageing for 10,000 h at 650 °C, the precipitate population consisted predominantly of *Z*-phase and Cr nitrides, as MX transformation into modified *Z*-phase is all but complete.

4. Discussion

4.1. Hybrid MX/Z particles

Nb- and V-rich nitrides classified as $30 < [Fe] + [Cr] < 40$ at.% were observed for all ageing times, except for 10,000 h (Table 4). These particles can be classified neither as complex (V,Nb)N nor as proper Cr(V,Nb)N. The occurrence of such Cr-rich MX particles has been reported for commercial steel grades such as P122 [17,18]. These Cr-rich MX particles were investigated further and were found to contain both MX and *Z*-phase regions (according to the composition analysis). Therefore, these particles are

Table 4
Mean chemical composition of *Z*-phase, Cr_2N, V-rich and Nb-rich nitrides of aged sample by EDS analysis after tempering and ageing (only particles larger than 10 nm were analyzed). The atomic percentages apply only to the metal atoms in the nitrides.

Sample	Particle type	Frequency (%)	Average chemical composition (at.%)			
			Cr	V	Nb	Fe
As-treated (189 particles)	(Nb,V)N	10	10	37	52	1
	(V,Nb)N	44	20	60	18	2
	$30 \leqslant [Fe] + [Cr] \leqslant 40$	0	No particles found			
	Cr(V,Nb)N	0	No particles found			
	Cr_2N	46	82	14	2	2
650 °C 300 h (111 particles)	(Nb,V)N	17	11	38	49	2
	(V,Nb)N	39	14	53	32	1
	$30 \leqslant [Fe] + [Cr] \leqslant 40$	4	34	40	24	2
	Cr(V,Nb)N	8	49	32	15	4
	Cr_2N	32	81	17	1	1
650 °C 1000 h (185 particles)	(Nb,V)N	5	14	35	49	2
	(V,Nb)N	18	22	54	22	2
	$30 \leqslant [Fe] + [Cr] \leqslant 40$	11	33	46	18	2
	Cr(V,Nb)N	57	52	30	15	3
	Cr_2N	9	80	18	1	1
650 °C 3000 h (148 particles)	(Nb,V)N	5	22	35	41	2
	(V,Nb)N	4	25	49	24	2
	$30 \leqslant [Fe] + [Cr] \leqslant 40$	2	32	44	22	2
	Cr(V,Nb)N	72	50	33	14	3
	Cr_2N	16	79	19	1	1
650 °C 5300 h (132 particles)	(Nb,V)N	5	10	36	53	1
	(V,Nb)N	2	12	45	41	2
	$30 \leqslant [Fe] + [Cr] \leqslant 40$	3	36	44	18	2
	Cr(V,Nb)N	83	53	33	10	4
	Cr_2N	7	79	19	1	1
650 °C 10,000 h (101 particles)	(Nb,V)N	2	16	35	48	1
	(V,Nb)N	0	No particles found			
	$30 \leqslant [Fe] + [Cr] \leqslant 40$	0	No particles found			
	Cr(V,Nb)N	89	54	32	10	4
	Cr_2N	9	79	19	1	1

referred to as hybrid particles. The spatial variation of the chemical composition within the hybrid particles was investigated using the EDS microprobe. Generally, composition profiles of hybrid particles showed a smooth transition from Cr-rich regions, with chemical composition close to *Z*-phase, towards Cr-poor regions, with compositions close to V-rich MX. Usually the *Z*-phase composition was observed at the rim of the particle, while the core consisted of MX. An example is given in Fig. 9a, which shows a symmetric hybrid particle found in the 650 °C/1000 h sample; the entire rim has a composition similar to *Z*-phase, while the core has a considerably lower Cr content. The concentration profile (Fig. 9b) shows a smooth transition from core to rim without any observable phase boundary. These observations are consistent with a straightforward chemical transformation of MX into *Z*-phase by the incorporation of Cr from the surroundings (see Section 4.2) which has previously been reported for commercial steels [18].

More complicated concentration profiles and morphologies of particles were also found, especially in relatively large particles. Such particles frequently had a Nb-rich core, with enhanced V content in the periphery, often as a shell encasing the core. Fig. 10 shows a case where a Nb-rich area of a MX particle is completely encased in a V-rich area. Two regions of *Z*-phase have formed on opposite sides of the MX particle. Such cases of *Z*-phase formation were only observed for MX particles with a Nb-rich core. For those relatively large particles it is unlikely that Cr diffuses from the surroundings into the centre (cf. the straightforward conversion of V-rich MX particles to *Z*-phase above).

4.2. Mechanisms of Z-phase formation

Investigation of the hybrid particles suggests that a possible path for the formation of *Z*-phase is a transformation of V-rich MX into *Z*-phase through Cr diffusion from the matrix into the nitride [18]. This mechanism is illustrated in Fig. 11. The transformation of (V,Nb)N into Cr(V,Nb)N by Cr diffusion would explain the hybrid crystal structure observed in several *Z*-phase particles in short-term aged samples. The (V,Nb)N precipitates have a cubic crystal structure, with lattice parameter 0.416 nm. Upon incorporation of Cr into the particles, the composition gradually changes to Cr(V,Nb)N, while the metal-to-nitrogen ratio changes from 1:1 to 2:1. The lattice remains cubic and the lattice parameter is reduced to 0.405 nm, as only half the interstitial sites are now

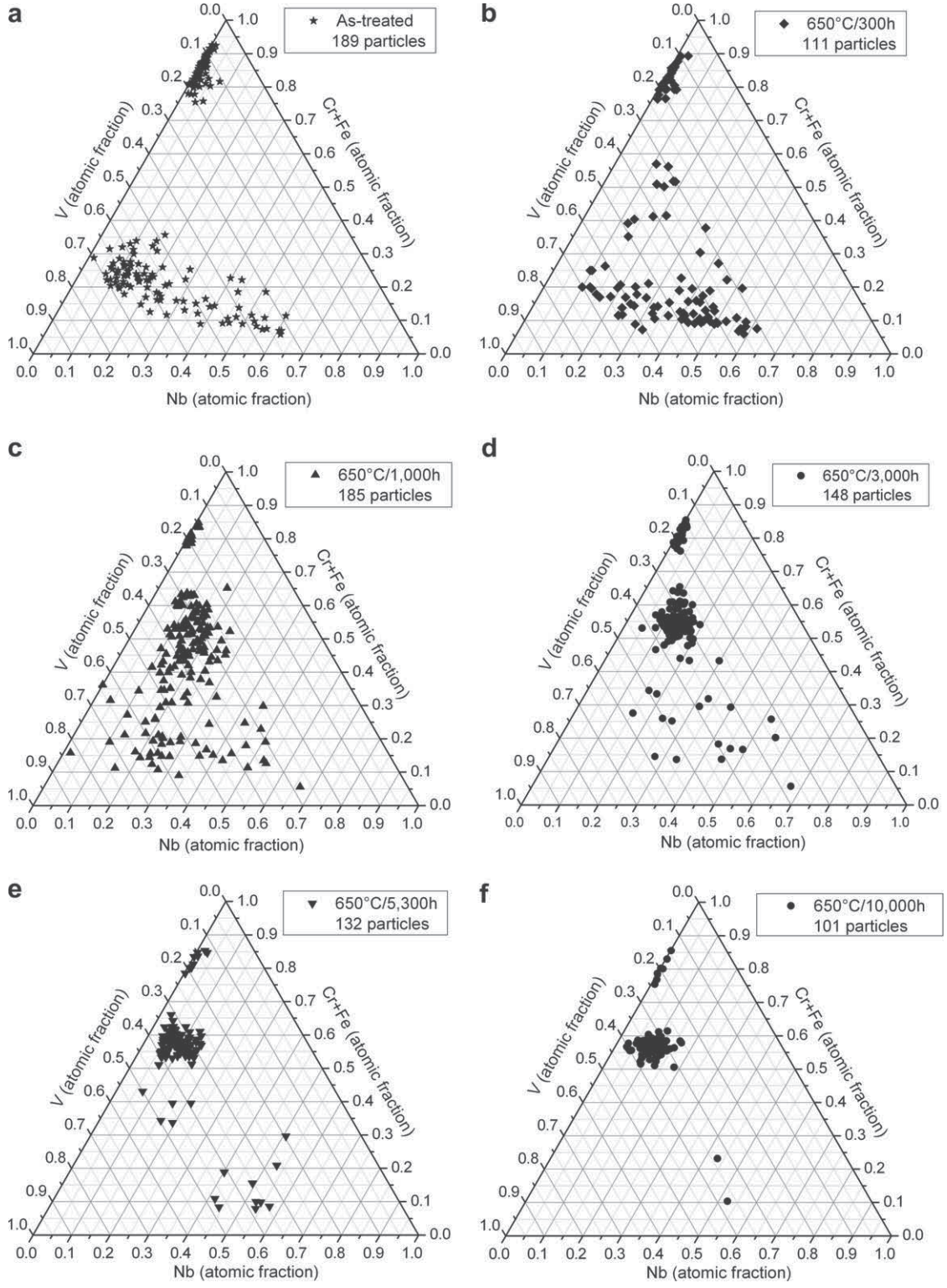

Fig. 7. Ternary diagrams of as-treated and aged samples at 650 °C from Table 4. (a) As-treated sample; (b) 300 h, (c) 1000 h, (d) 3000 h, (e) 5300 h, (f) 10,000 h samples. Atomic fractions relate to the metal atoms only.

occupied by N. It is speculated that on continued ageing the atoms in this metastable cubic *Z*-phase rearrange themselves into the ordered tetragonal lattice of the modified *Z*-phase (cf. Fig. 1).

A less straightforward mechanism initiates at (Nb,V)N particles and is illustrated in Fig. 12. Here, several Cr-rich areas form separately on larger MX particles with Nb-rich centres. The *Z*-phase tends to form on the opposite sides of

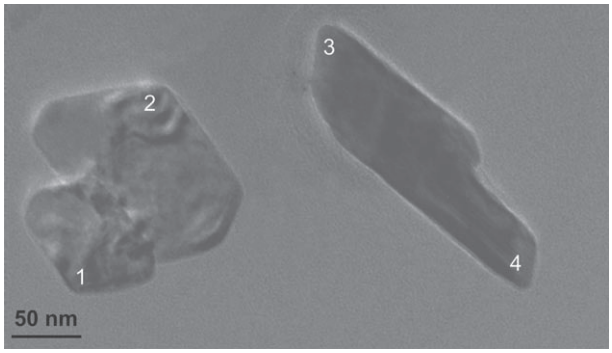

Fig. 8. *Z*-phase particles in the 700 °C/3000 h sample. Compositions at the indicated locations are given in Table 5.

the particle by incorporation of Cr from the matrix. After the development of Cr-rich regions of a certain size, the *Z*-phase grows by consumption of the V, Nb and N from the host precipitate (see arrows in Fig. 12), probably assisted by diffusion through the ferrite matrix rather than through the particle and consequently leading to dissolution of the "core", leaving several *Z*-phase particles, most often observed as parallel particles.

4.3. Kinetics of Z-phase development

According to the assumption on the complete precipitation of nitrogen in the model alloy, the evolution of the weight fraction of the *Z*-phase permits a detailed examination of the process kinetics of this phase. From the mass fraction of cubic and tetragonal *Z*-phase as a function of the ageing time at 650 °C, the overall mass fraction of the *Z*-phase ($Z_{CUBIC} + Z_{tetra}$) is readily obtained [15]. The total fraction of *Z*-phase was fitted by the Johnson–Mehl–Avrami–Kolmogorov (JMAK) kinetics equation to extract kinetic parameters, with particular reference to the exponent (n) [19–21]:

$$f_w(T,t) = f_w(T,t=\infty)[1 - \exp\{\ln(0.5)(t/t_{0.5})^n\}] \quad (1)$$

The following results were obtained at 650 °C: $f_w(T, t=\infty) = 0.0025$, $t_{0.5} = 1572$ h and $n = 1.09$. The evolution of the mass fraction of *Z*-phase and of the JMAK fitting at 650 °C is shown in Fig. 13.

In the present case, the value of $n = 1$–$1\frac{1}{2}$ is associated with a diffusion-controlled transformation with zero nucleation rate and growth of particles of appreciable size [22].

The results are consistent with the mechanism of *Z*-phase formation depicted in Section 4.2. Instead of the dissolution of MX nitrides and the subsequent nucleation of *Z*-phase, it was shown that *Z*-phase develops by a gradual transformation of (V,Nb)N under Cr uptake, i.e. particles growing to an appreciable size. During this transformation the diffusion of Cr from the matrix towards the transforming (V,Nb)N is likely to be rate determining.

Table 5
Chemical analysis of particles in Fig. 8 (atomic percentages apply only to the metal atoms in the nitrides).

	Cr (at.%)	V (at.%)	Nb (at.%)	Fe (at.%)
Site 1	36	44	13	7
Site 2	47	42	6	5
Site 3	55	36	4	5
Site 4	54	38	5	3

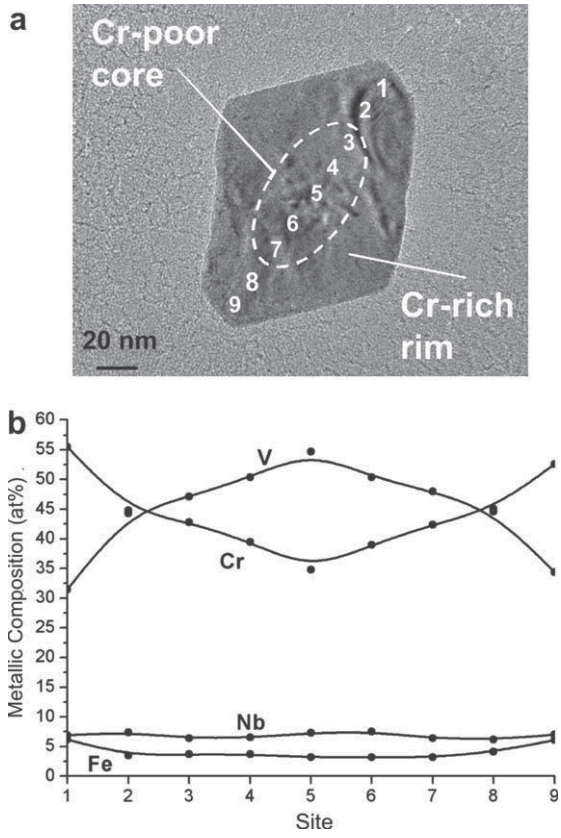

Fig. 9. (a) Hybrid particle developed after 1000 h at 650 °C; (b) smooth transition in the composition from core to rim.

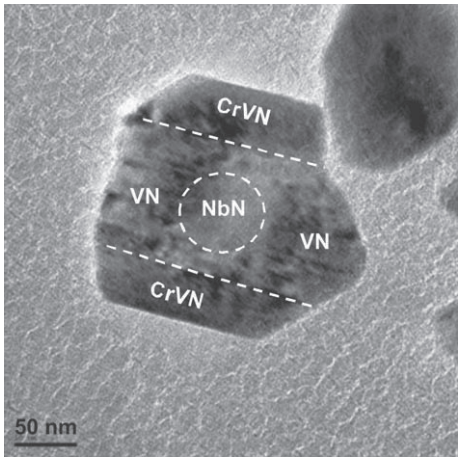

Fig. 10. A MX particle with Nb-core, encased in a V-rich area from 650 °C/3000 h aged sample. Two *Z*-phases have started to form simultaneously on opposite sides of the MX particle.

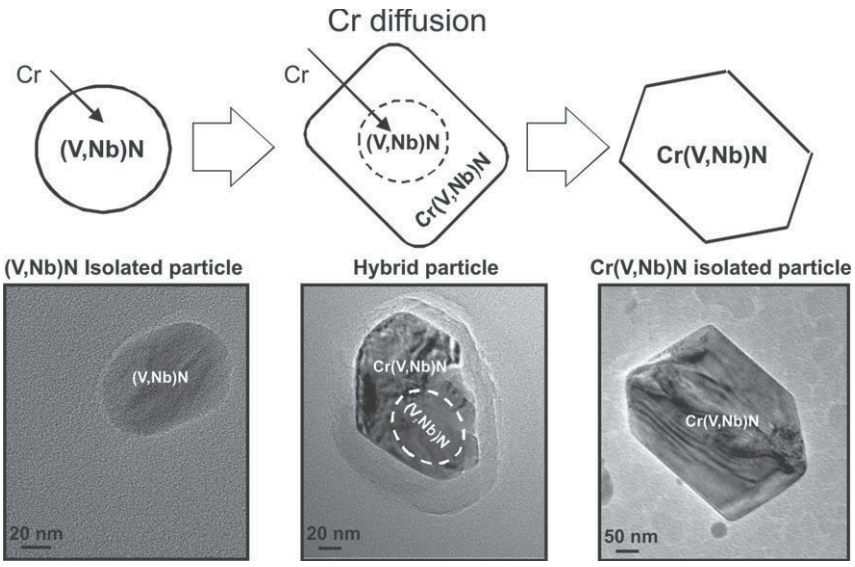

Fig. 11. Formation of a *Z*-phase particle by Cr diffusion from ferritic matrix. The pictures of the animation are taken by the following samples, starting from the left: as-treated material, 650 °C/300 h and 650 °C/3000 h samples.

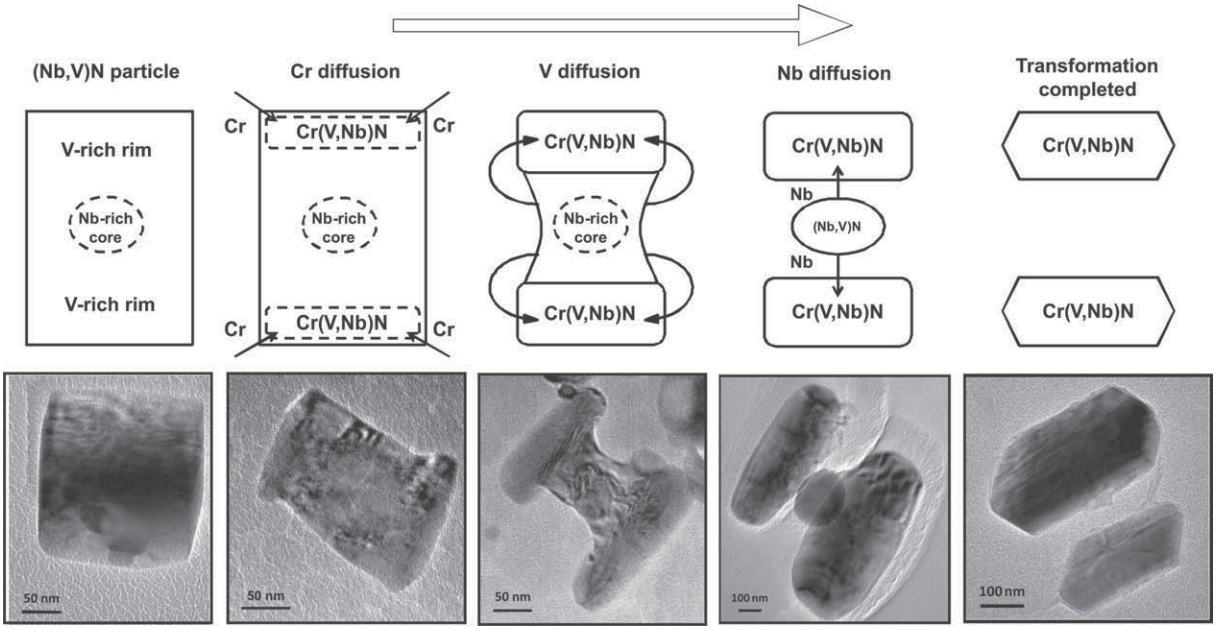

Fig. 12. Formation of two parallel *Z*-phases. The pictures of the animation are taken by the following samples, starting from the left: as-treated material, 650 °C/300 h, 650 °C/1000 h, 650 °C/1000 h and 650 °C/10,000 h samples.

4.4. Sites of Z-phase formation

Although *Z*-phase forms everywhere in the microstructure, TEM investigations indicate an earlier development along the prior austenite grain boundaries. The MX particles disappear sooner at the prior austenite grain boundaries as well as in the adjacent regions within the grain. In addition, the *Z*-phase particles are generally larger at the prior austenite grain boundaries. These observations are explained by faster diffusion of substitutional elements along prior austenite grain boundaries, leading to faster growth of *Z*-phase at the expense of MX located at or near the prior austenite grain boundaries.

The 650 °C/1000 h sample was investigated using EDS to determine the distribution of Cr_2N, MX, hybrid and *Z*-phase particles along prior austenite grain boundaries and inside the grains within a 140 μm^2 frame area, summarized in Table 6. A smaller area is shown in Fig. 14, where it is notable that there is a significant MX depletion adjacent to the prior austenite grain boundaries. Inside the

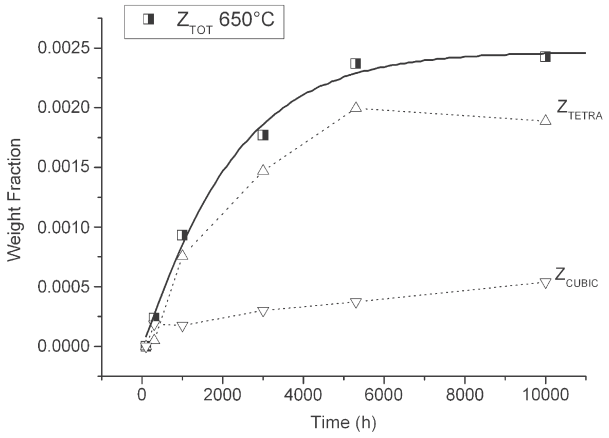

Fig. 13. Evolution of the weight fractions of cubic and tetragonal *Z*-phase (open triangles) at 650 °C and fit of the overall fraction of *Z*-phase (solid line) by Eq. (1) (JMAK).

Table 6
Summary of particle distributions within 140 μm^2 frame area from the sample aged for 1000 h at 650 °C; GB: grain boundary; IG: inside the grain.

Position	Cr_2N	MX	Hybrid	*Z*-phase
GB	57	8	5	73
IG	6	103	71	45

grain, many MX precipitates still remain, but *Z*-phase and hybrid particles (particles with between 30% and 40% [Fe] + [Cr] at.%) were also identified.

The formation of *Z*-phase particles along prior austenite grain boundaries is suggested to have a detrimental effect on the creep resistance of the steel as the MX depletion around prior austenite grain boundaries leads to a local reduction of the precipitate strengthening.

5. Conclusions

An investigation of the evolution of precipitate morphology, composition and phase fraction in a 12% Cr model alloy demonstrated that MX nitride particles are not thermodynamically stable during high-temperature exposure in 12% Cr steels, but are replaced by *Z*-phase particles.

The development of *Z*-phase was investigated by examining hybrid MX/*Z*-phase particles found at several temperatures and ageing times. The MX particles were converted into modified *Z*-phase via the uptake of Cr from the matrix. The chemical transformation from (V,Nb)N to Cr(V,Nb)N is assumed to be followed by crystallographic transformation of the crystal structure from cubic to tetragonal.

XRD and SAED both showed the presence of the cubic *Z*-phase crystal structure, which is believed to be a metastable intermediate structure in the transition from cubic MX to tetragonal *Z*-phase.

Investigations of the precipitation rate at 600, 650 and 700 °C, using XRD measurements, showed that *Z*-phase forms fastest at 650 °C.

Z-phase particles are preferentially located along prior austenite grain boundaries, leading to an earlier consump-

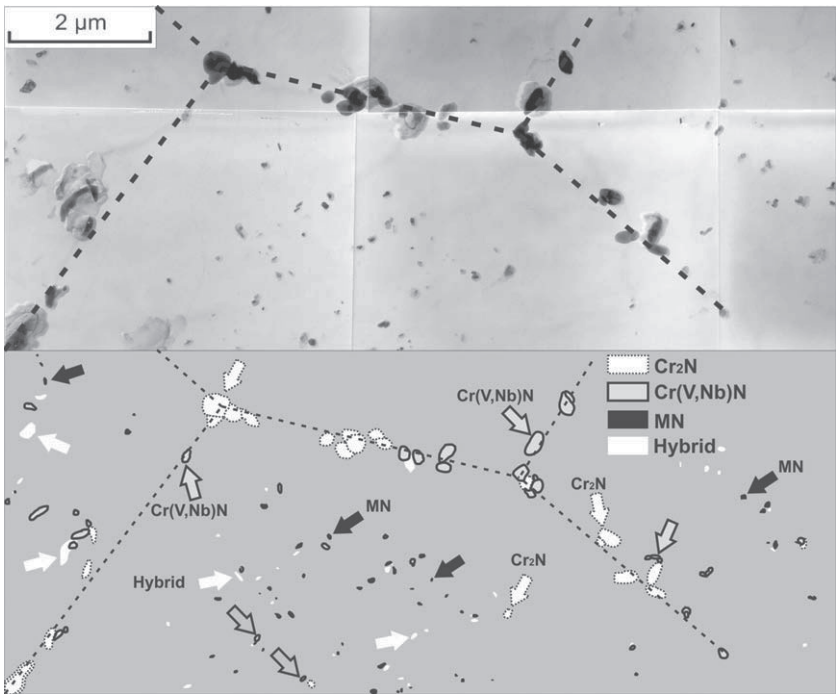

Fig. 14. Distribution of particles using EDS from 650 °C/1000 h aged sample: dotted white, Cr_2N; grey, *Z*-phase; white, hybrid MN/Z; black, MN lines indicate the location of the grain boundaries.

tion of (V,Nb)N in the regions adjacent to the prior austenite grain boundaries.

The transformation kinetics is representative for the growth of particles of appreciable size, which is consistent with a mechanism of gradual conversion of existing MX precipitates rather than nucleation of *Z*-phase, followed by dissolution of MX precipitates.

Acknowledgement

Augusto di Gianfrancesco and Silvia Tiberi Vipraio from Centro Sviluppo Materiali and Flemming Bjerg Grumsen from the Technical University of Denmark are thanked for their valuable work and suggestions. Marcello Ballone from Centro Sviluppo Materiali is thanked for excellent TEM sample preparation. Part of the project has been carried out under the European COST 536 ACCEPT action.

References

[1] Hald J. Steel Res Int 1996;67:369.
[2] Ennis PJ. Creep strengthening mechanisms in 9–12% chromium steels. In: Viswanathan R, Gandy D, Coleman K, editors. Proceedings of the 4th international conference on advances in materials technology for fossil power plants, 25–28 October 2004, Hilton Head Island, SC. Materials Park, OH: ASM International; 2005. p. 1146.
[3] Cipolla L, Di Gianfrancesco A, Venditti D, Cumino G, Caminada S. Microstructural evolution during long term creep tests of 9% Cr steel grades. In: Hasegawa K, Scarth DA, editors. Proceedings of the ASME pressure vessels and piping conference – 8th international conference on creep and fatigue at elevated temperatures – CREEP8, 22–26 July 2007, San Antonio, TX. New York: ASME; 2008. p. 445.
[4] Danielsen HK. Z-phase in 9–12% Cr steels. PhD thesis, Department of Manufacturing, Engineering and Management of Technical University of Denmark, Lyngby; 2006.
[5] Golpayegani A. Precipitate stability in creep resistant 9–12% chromium steels. PhD thesis, Department of applied physics, microscopy and microanalysis of Chalmers university of technology, Göteborg; 2006.
[6] Danielsen HK, Hald J. Energy Mater 2006;1:49.
[7] Danielsen HK, Hald J. Calphad 2007;31:505.
[8] Strang A, Vodarek V. Precipitation processes in martensitic 12CrMoVNb steels during high temperature creep. In: Strang A, Gooch DJ, editors. Microstructural development and stability in high chromium ferritic power plant steels, vol. 1. Maney: London; 1997. p. 31.
[9] Sawada K, Kushima H, Kimura K. ISIJ Int 2006;46:769.
[10] Strang A, Vodarek V. Mater Sci Technol 1996;12:552.
[11] Danielsen HK, Hald J, Grumsen FB, Somers MAJ. Metall Mater Trans A 2006;37A:2633.
[12] Vodarek V, Danielsen HK, Grumsen FB, Hald J, Strang A. Electron diffraction studies on (Nb,V)CrN particles in 12CrMoVNbN steels. In: Lecomte-Beckers J, Carton M, Schubert F, Ennis PJ, editors. Proceedings of the 8th Liège conference – materials for Advanced Power Engineering, 18–20 September 2006, Liège. Jülich: Forschungszentrum Jülich GmbH; 2006. p. 1251.
[13] Williams DB, Carter CB. Transmission electron microscopy – a textbook for materials science. Berlin: Springer Verlag; 2009.
[14] E407 – Standard practice for microetching metals and alloys. West Conshohocken, PA: ASTM International; 2007.
[15] Di Nunzio PE, Cipolla L, Tiberi Vipraio S, Martelli A, Somers MAJ. Quantitative X-ray diffraction analysis of the development of Z phase in a 12% CrNbVN steel. Mater Sci Technol, submitted for publication.
[16] Sawada K, Kushima H, Kimura K, Tabuchi M. ISIJ Int 2007;47:733.
[17] Yoshizawaa M, Igarashia M, Moriguchia K, Isedab A, Armakic HG, Maruyamac K. Mater Sci Eng A 2009;510–511:162.
[18] Danielsen HK, Hald J. Mater Sci Eng A 2009;205:169.
[19] Kolmogorov AN. Bull Acad Sci USSR Phys Ser 1937;1:355.
[20] Johnson WA, Mehl PA. Trans Am Inst Mining Metall Eng 1939;135:416.
[21] Avrami M. J Chem Phys 1939;7:1103.
[22] Christian JW. The theory of transformations in metals and alloys. Oxford: Pergamon Press; 2002.

This page was left blank on purpose

PAPER II

Maney Publishing
Research · Knowledge · Innovation

IOM3
The Institute of Materials, Minerals and Mining

ORIGINAL RESEARCH PAPER

Quantitative X-ray diffraction analysis of development of Z phase in 12%Cr–Nb–V–N steel

P. E. Di Nunzio*[1], L. Cipolla[1,2], S. Tiberi Vipraio[1], S. Martelli[1] and M. A. J. Somers[2]

Accepted for publication in Materials Science and Technology; currently in printing.

This page was left blank on purpose

Quantitative X-Ray Diffraction Analysis of the Development of Z-Phase in a 12%CrNbVN Steel

P.E. Di Nunzio [a*], L. Cipolla [a,b], S. Tiberi Vipraio [a], S. Martelli [a], M.A.J. Somers [c]

a) Centro Sviluppo Materiali Via di Castel Romano 100, I-00128 Rome, Italy

b) PhD student at Technical University of Denmark

c) Department of Mechanical Engineering, Technical University of Denmark, Lyngby, Denmark

**) Corresponding Author (p.dinunzio@c-s-m.it)*

Abstract

To study the evolution of nitrides (Nb, V)N, (V, Nb)N and Cr_2N, and in particular the formation of the Z-phase Cr(V, Nb)N, a model alloy with composition similar to that of 12% Cr steels for high temperature applications, microalloyed with Nb and V but with a very low carbon content, has been designed. A quantitative determination of the volume fractions of the extracted nitrides that had formed after ageing treatments at 650 °C up to 10000 hours was carried out by a X-ray diffraction procedure, based on the Rietveld approach.

The investigation of the Z-phase evolution by the JMAK kinetics at 650 °C and 700 °C revealed that, being the kinetic exponent very close to unity, the formation mechanism of this phase is not associated with a conventional process of nucleation but hints at a gradual diffusion-controlled transformation of the pre-existing V and Nb nitrides.

Keywords

X-ray diffraction, Rietveld method, Ageing, Kinetics, Z-phase

1. Introduction

The evolution of precipitates during thermal treatments in metals and alloys is usually carried out by electron microscopy techniques. On one hand this approach allows to collect topological, morphological, crystallographic, and accurate micro-analytical data but, on the other hand, it suffers from the absence of statistical averaging, which is mandatory for estimating the overall volume fraction of the precipitates and the partitioning among the various phases.

X-ray diffraction represents a valuable complementary analytical technique to microscopic data since, in principle, it permits to add quantitative information on all second phases provided that distinctive diffraction patterns can be collected. In bulk samples the strong matrix reflections obscure those

originating from the usually small amount of precipitates, thus hindering an accurate determination of their volume fraction. Therefore, a necessary condition for the analysis to be performed is that precipitates are separated from the parent phase. When precipitates and matrix have different electrochemical potentials, a suitable technique for isolating the particles is by means of electrochemical dissolution, under controlled electric potential conditions.

In this work, the evolution of second phases in a 12Cr-Nb-V-N model steel with a composition similar to that of 12% Cr steels for high temperature applications was studied by extracting the precipitates. In particular, the chemical composition of the alloy has been deliberately modified by reducing the carbon content to prevent the formation of carbides and to promote the formation of the modified Z-phase, a nitride containing Cr V and Nb, by adding nitrogen.

Recently, it was found [1–8] that the modified Z-phase develops in 9–12% Cr martensitic steels during long-term exposure in the temperature range 600–700 °C. Its development has been considered responsible for a detrimental effect on the creep strength, since it is associated with the consumption of the finely dispersed small nitrides, (V, Nb)N, which provide the most important contribution to the creep resistance.

The modified Z phase is primarily a CrV-based nitride with limited quantities of Nb and Fe and with a tetragonal crystal structure [1]. Extensive electron diffraction studies on various aged 9–12% Cr steels have revealed that the modified Z-phase can also exhibit a crystal structure characterized by a NaCl type cubic lattice similar to that of MX nitrides [3], coexisting with the tetragonal form. Further investigations have shown that the cubic structure is predominant in 9-12% Cr steels aged for relatively short times (of the order of 10000 h at 600 °C), while the tetragonal structure emerges upon longer ageing [9].

Specific attention has given to the mechanisms of diffusional transformation of vanadium and niobium nitrides into Z-phase during prolonged ageing treatments at temperatures in the range from 600 °C to 700 °C up to 10000 hours.

The specificity of the present X-ray evaluation procedure is that an *ad hoc* pattern fitting analysis based on the Rietveld algorithm was developed to meet the need of calculating the absolute scattered intensity of the diffraction peaks from phases which are not stoichiometric compounds, and where the actual chemical composition is adjusted by the mixing of isomorphous crystals of the alloying elements in the steel.

2. Experimental

A model alloy based on a 12% Cr Nb- and V-microalloyed steel generally employed in power plants was designed, the carbon content has been limited to about 45 parts per million in mass to promote the precipitation of nitrides only, avoiding the interference of carbides, most specifically of $Cr_{23}C_6$. Likewise, Mo

and W were left out of the model alloy to prevent the precipitation of Laves phases of the type $Fe_2(Mo, W)$. In this alloy only nitrides precipitate as second phases and in particular the formation of Z-phase, a nitride of general composition Cr(V, Nb)N, is greatly enhanced. The chemical composition of the alloy is given in Table 1.

A 80 kg ingot of the alloy, produced by a Vacuum Induction Melting furnace, was hot rolled to a 20 mm thick plate. Then the steel was normalized at 1050 °C for 1 hour and tempered at 750 °C for 2 hours and subsequently subjected to accelerated cooling to room temperature. Samples with an initial microstructure composed entirely of tempered martensite, were subjected to ageing treatments at 650 °C for 100 h, 300 h, 1000 h, 3000 h, 5300 h and 10000 h to study the evolution of the precipitates.

In order to extract the precipitates an anodic dissolution of the matrix was carried out in a solution of 5 vol.% hydrochloric acid in pure ethanol at room temperature at a potential of 15 V.

For each sample about 10 g of steel were dissolved in about 0.5 litres of electrolytic solution. Second phase particles were extracted from the solution by filtering through a Millipore Isopore™ VMTP (0.05 μm mesh size) polycarbonate filter. Thereafter, the precipitates were carefully washed with ethanol to clear from possible contaminations due to the original solution containing iron and chlorides. Finally, the filter was dried and the powder collected.

X-ray diffractograms of the powders were determined with a Siemens D500 diffractometer in Bragg-Brentano geometry, using Co-K_α radiation in the 2θ range from 41° to 53° at a step size of 0.02° and a counting time of 70 s per step.

Microstructural investigations were also performed by transmission electron microscopy (TEM-EDS) to identify the nature of the second phases and the evolution of their morphology and chemical composition as a function of temperature and annealing time. Details on this activity are outside the scope of the present work and will be reported elsewhere [10].

Five main second phases could be distinguished in the extracted powders. In the early stages the precipitate population is essentially composed of hexagonal Cr_2N, cubic Nb-rich and cubic V-rich nitrides. The cubic Nb-rich and V-rich nitrides are isomorphous but, since they are not pure, they will be represented by the chemical formulas (Nb, V)N and (V, Nb)N, respectively. On prolonged ageing, the Z-phase appears in two distinct crystal structures: tetragonal and fcc. The tetragonal Z-phase is an ordered ternary nitride of Cr and V or Nb, whereas the cubic Z-phase is a disordered compound of the same elements. For both structures the generic formula Cr(V, Nb)N is used [3].

The presence of the two distinct cubic phases instead of an unique solid solution of the isomorphous and mutually miscible compounds VN and NbN is ascribed to the quenching and tempering procedure preceding the ageing treatments.

A first precipitation of the less soluble Nb-rich nitride during the early stages of the steel processing or during quenching is followed by that of the V-rich nitride during tempering. Simultanelously, also the Z-phase is found to be present in two different crystalline forms [3].

During ageing the chemical composition of the phases was found to be almost constant. In Table 2 the average atomic fraction of the metallic elements for samples treated at 650 °C for different times is reported. The averaging operation is justified by the low change in the composition of each phase during annealing. It has to be noticed that iron appears as impurity in all cases and similarly, Cr enters the fcc sublattice of metal atoms in the binary nitrides, On the other hand Nb and (primarily) V reside at Cr sites in Cr_2N.

3. Quantitative analysis

A specific quantitative X-ray analysis procedure was developed to estimate the relative volume fractions of the precipitate phases in the extracted powders.

Due to the overlapping of some of the X-ray reflections of phases with similar structures, a Rietveld-like algorithm [11-16] involving the fitting of the recorded diffractograms was applied.

The Rietveld method refines a set of user-selected parameters to minimize the difference between the experimental and a simulated diffractogram based on model crystal structures and instrumental parameters in a given angular range of the spectrum. Due to its ability to deal reliably with strongly overlapping reflections, it is particularly suitable in solving multiphase powder diffraction problems.

For the simulation of a diffractogram it is necessary to know the detailed crystal structure of all the phases, to assume a shape function for the diffracted peaks and a suitable background function. In the following, each of these issues is described in detail.

3.1 The diffracted intensity

All precipitates in the extracted powders are solid solutions of miscible “pure” precursors. Therefore, to calculate the theoretical diffracted intensities to be used in the Rietveld quantification algorithm the actual composition of the phases present should be taken into account.

To our knowledge, an assessed crystallographic structure of the newly proposed Z-phase is not currently available as standard CIF file (Crystallographic Information Files [17]), therefore an *ab-initio* approach was pursued to calculate the diffracted intensities of the phases according to the chemical compositions determined by TEM-EDS.

The intensity of the (hkl) diffraction peak of a pure phase *p* of known lattice structure as recorded by a diffractometer in Bragg-Brentano geometry can be expressed as [18]:

$$I^{0}_{hkl,p} \approx \frac{M_{hkl,p}}{V_p^2} \cdot \left|F_{hkl,p}\right|^2 \cdot \left(\frac{1+\cos^2(2\theta)}{\sin^2\theta \cdot \cos\theta}\right) \quad (1)$$

where $M_{hkl,p}$ is the multiplicity of the *hkl* reflection of phase *p*, V_p is the unit cell volume for phase *p*, θ the diffraction angle according to the selected wavelength and $F_{hkl,p}$ the structure factor for reflection *hkl* of phase *p*. The last factor in brackets accounts for the Lorentz and polarization effects.

The magnitude of the structure factor F_{hkl} for the crystal reflection *hkl* is calculated as:

$$\left|F_{hkl}\right|^2 = \left[\mathrm{Re}(F_{hkl})\right]^2 + \left[\mathrm{Im}(F_{hkl})\right]^2 \quad (2)$$

with the real and imaginary parts expressed as:

$$\mathrm{Re}(F_{hkl}) = \sum_{i}^{lattice\ sites} \sum_{j}^{atoms} \varphi_{i\,j} \cdot f_j \cdot \cos\left[2\pi(h\,x_i + k\,y_i + l\,z_i)\right] \quad (3a)$$

$$\mathrm{Im}(F_{hkl}) = \sum_{i}^{lattice\ sites} \sum_{j}^{atoms} \varphi_{i\,j} \cdot f_j \cdot \sin\left[2\pi(h\,x_i + k\,y_i + l\,z_i)\right] \quad (3b)$$

where φ_{ij} is the probability of finding an atom of type *j* in the *i*-th lattice site and f_j the atomic scattering factor. For a mixture of differently absorbing phases, each one present with a volume fraction ψ_V^p, the total intensity of the *hkl* diffraction peak of a single phase *p* is proportional to [19]:

$$I^{Mix}_{hkl,p} \approx \frac{M_{hkl,p}}{V_p^2} \cdot \left|F_{hkl,p}\right|^2 \cdot \left(\frac{1+\cos^2(2\theta)}{\sin^2\theta \cdot \cos\theta}\right) \cdot \left[\frac{\mu_p}{<\mu>}\right] \cdot \psi_V^p \quad (4)$$

where μ_p is the linear absorption coefficient of phase *p* and $<\mu>$ the average linear absorption coefficient of the mixture defined as [18]:

$$<\mu> = \frac{\sum_{p=1}^{phases} w_p \cdot \left(\mu/\rho\right)_p}{\sum_{p=1}^{phases} w_k/\rho_p} \quad (5)$$

w_p representing the weight fractions of the phases in the mixture and μ/ρ the mass absorption coefficients of the phases calculated from their chemical composition and the tabulated values of absorption for each element [20] according to the incident radiation wavelength:

$$\left(\mu/\rho\right)_p = \sum_{c=1}^{components} w_{c,p} \cdot \left(\mu/\rho\right)_c \quad ; \quad \sum_{c=1}^{components} w_{c,p} = 1 \quad (6)$$

In the Bragg-Brentano geometry the absorption correction factor $\mu_p/<\mu>$ in equation (4) is a constant specific of each phase since the scattering volume is constant and independent on the diffraction angle θ.

By converting the mass fractions into volume fractions according to:

$$\psi_V^p = w_p \cdot \frac{<\rho>}{\rho_p} \tag{7}$$

where the average density of all phases is

$$<\rho>= \sum_{p=1}^{phases} \psi_V^p \cdot \rho_k = \frac{1}{\sum_{p=1}^{phases} w_p / \rho_p} \tag{8}$$

one can write equation (4) for the total intensity of (hkl) diffraction peak of the phase *p* as:

$$I_{hkl,p}^{Mix} \approx \frac{M_{hkl,p}}{V_p^2} \cdot \left|F_{hkl,p}\right|^2 \cdot \left(\frac{1+\cos^2(2\theta)}{\sin^2\theta \cdot \cos\theta}\right) \cdot \left[\frac{\rho_p \cdot \left(\mu/\rho\right)_p}{\sum_{p=1}^{phases} \psi_V^p \cdot \rho_p \cdot \left(\mu/\rho\right)_p}\right] \cdot \psi_V^p \tag{9}$$

where the density of the phase ρ_p (g cm^{-3}), is:

$$\rho_p = 10^{24} \cdot \frac{\sum_{i}^{lattice\ sites} \sum_{j}^{atoms} \varphi_{ij} \cdot P_j}{N_A \cdot V_p} \tag{10}$$

with P_j the atomic weight of the element *j* (g mol^{-1}), N_A the Avogadro number (mol^{-1}), V_p the cell volume (Å^3) and φ_{ij} the probability of finding an atom of type *j* on the site *i* assuming a full occupancy.

3.2 The peak shape function

For fitting the peak shape, the Pearson VII function [21] in the reciprocal space *s* (s=2·sinθ/ λ) was modified in order to give the adjustable parameters *a* and *b*, which originally relate to the height and width of the profile, and *c*, a more physical meaning [22]:

$$\Phi(s-s_0;a,b,c) = a \cdot \frac{b}{\left\{1+\left[b \cdot B(c-\tfrac{1}{2},\tfrac{1}{2}) \cdot (s-s_0)\right]^2\right\}^c} \tag{11}$$

For a peak centred at s=s_0, the parameter *a* represents the integrated intensity:

$$a = \int_{-\infty}^{\infty} \Phi(s-s_0;a,b,c)ds = I_{hkl,p}^{Mix} \tag{12}$$

(unlike the original Pearson VII formulation, where it represents the maximum intensity, which is not a measurable quantity), *b* is the coherence length (and not simply the width of the profile), and $c \geq 1$ is still a peak shape factor used for fit optimisation. *B(x,y)* is the Eulerian Beta function. From a computational point of view the Pearson VII and the Φ profiles are identical. The function Φ retains

the same properties as the Pearson VII in the sense that it continuously changes from a Lorentz profile (c=1) to a Gaussian distribution ($c\to\infty$). Moreover, it approaches the delta function for an infinitely large crystal ($b\to\infty$).

3.3 Final equation for the whole spectrum fitting

Taking into account the presence of the $K_{\alpha1}$-$K_{\alpha2}$ doublet due to the experimental arrangement, the final equation is in the form:

$$I^{calculated}(s) = \beta(s) + \sum_{p}^{phases} \sum_{hkl} \left\{ I^{0}_{hkl,p} \cdot \left[\frac{\mu_p}{<\mu>} \right] \cdot \psi_V^p \right\} \cdot \cdot \left\{ \frac{b}{\left\{ 1 + \left[bB(c-\tfrac{1}{2}, \tfrac{1}{2})\,(s - s_0^{\alpha1}) \right]^2 \right\}^c} + \frac{R_{\alpha2/\alpha1} \cdot b}{\left\{ 1 + \left[bB(c-\tfrac{1}{2}, \tfrac{1}{2})\,(s - s_0^{\alpha2}) \right]^2 \right\}^c} \right\} \tag{13}$$

where $\beta(s)$ is the background correction in the form of a polynomial and $R_{\alpha2/\alpha1}$ is the intensity ratio between the $K_{\alpha2}$ and $K_{\alpha1}$ peaks, which typically is equal to 0.5. The adjustable parameters are the volume fractions (ψ_V^p), the coherence length of the reflections (for clarity $b=b_{hkl}^p$), the shape factor ($c=c_{hkl}^p$) and the lattice parameters which do not appear in equation (13) but determine the position of the peaks ($s_0^{\alpha1}=s_{0\,hkl}^{\;p}$). The term in the first braces of the right hand side of equation (13) is equivalent to the parameter *a* of the peak function Φ.

Since the reciprocal coordinate of the calculated spectrum is referred to the wavelength of the $K_{\alpha1}$ line, the position of the $K_{\alpha2}$ peak in each doublet has to be calculated relative to the reciprocal coordinate of the corresponding $K_{\alpha1}$ peak as:

$$s_0^{\alpha2} = \frac{\lambda_{\alpha2}}{\lambda_{\alpha1}} \cdot s_0^{\alpha1} \tag{14}$$

where $\lambda_{\alpha1}$ and $\lambda_{\alpha2}$ are the $K_{\alpha1}$ and $K_{\alpha2}$ wavelengths of the incident beam.

It has to be noticed that the quantity ψ_V^p is not exactly the volume fraction, but linearly proportional to it and requires a further normalization.

Finally, a least squares estimator was used to evaluate the goodness of the fit between the measured and the reconstructed diffractogram:

$$R = \sum_{i=1}^{N} \left(I_i^{observed} - I_i^{calculated} \right)^2 \tag{15}$$

where the index *i* spans over the *N* points of the spectrum, $I_i^{observed}$ and $I_i^{calculated}$ are the experimental and

theoretical diffracted intensities.

3.4 Crystal data

The arrangement of atoms in the model crystal structures has been taken from the available literature data together with the associated lattice parameters to be refined by the Rietveld procedure. The presence of lattice distortions in the real phases has been neglected. In reconstructing the diffractogram the atomic coordinates were kept fixed *i.e.* no refinement of the atomic positions within the cell was considered. The composition of the phases has been introduced in the model structures by modulating the occupancy fraction of the sites in accordance with the chemical data obtained from EDS.

Details concerning the crystal systems and the lattice parameters used as starting values for the refinement are collected in Table 3.

For the Nb-rich and V-rich binary nitrides a NaCl-type simple cubic lattice was adopted. The hexagonal structure chromium nitride, composed by a close-packed arrangement of the Cr atoms where nitrogen atoms occupy the interstitial sites with a partial disordering along the c-axis, were set according to reference [23].

The structure of the tetragonal Z-phase Cr(V, Nb)N was taken from reference [3], also taking into account the recent evaluation by Lazar *et al.* [16]. Finally, for the cubic Z-phase Cr(V, Nb)N, a NaCl-type structure was considered [3] with a random distribution of the present transition metal atoms over the sites of one of the two interpenetrating fcc lattices. According to the 2:1 stoichiometry, the N atoms were assumed to be distributed randomly over 50% of the sites of the other fcc sublattice.

4. Results and discussion

The density and the mass absorption coefficients of the phases were calculated from the crystal data, the chemical composition and the tabulated data of the mass absorption coefficients for the elements for the incident Co-K_α radiation [21]. The densities, calculated according to equation (10) are reported in Table 4; the mass absorption coefficients are listed in Table 5.

The refinement procedure was applied to all diffractograms to obtain the volume fractions of various phases in the extracted precipitates. A typical example of the good level of fit to the experimental spectrum is shown in Fig. 1 for the sample aged at 650 °C for 3000 h.

The volume fractions of the phases during the treatment at 650 °C are reported in Table 6 and plotted as a function of the ageing time in Fig. 2.

Taking into account all the possible uncertainties in the different elaboration steps, the total error of the fitting procedure can be estimated to be maximally ±3 units of volume percent. The results allow shed a

light on the transformation mechanism that leads to the development of Z-phase. It is interesting to observe that a completion of the precipitation of V-rich and Nb-rich nitrides occurs in the first 100 h ageing. Thereafter, as the Z-phase starts developing, the relative contents of V-rich and Nb-rich nitrides decrease along with the content of Cr_2N. The cubic form of Z-phase develops earlier than the tetragonal form, the latter, however, prevails for longer ageing times. This is in agreement with literature investigations indicating that the cubic structure is less stable than the tetragonal [9]. It is worth observing that, even after 10000 h of ageing at 650 °C, the cubic form is not completely dissolved but it reaches a constant volume fraction coexisting with the tetragonal form.

In the present case the absolute mass fractions of the precipitates with respect to the dissolved matrix could not be determined due to experimental difficulties. Despite the lack of an experimental confirmation, it is attempted to estimate the absolute mass fractions as a function of the ageing time at 650 °C by assuming that the residual amount of nitrogen in solid solution is negligible so that nitrogen can be considered completely bound to the precipitates. This is a reasonable assumption, because the nitrides have a very low solubility in bcc iron, The results of the calculations are given in Table 7.

The evolution of the total mass fraction of Z-phase at 650 °C, where the kinetics of Z-phase development is fastest [5], was obtained by considering the sum of the fractions of fcc and tetragonal components. The data was fitted with a Johnson-Mehl-Avrami-Kolmogorov (JMAK) kinetics [25-29]:

$$f_w(T,t) = f_w(T,t=\infty)\cdot\left[1 - \exp\left\{\ln(0.5)\cdot\left(t/t_{0.5}\right)^n\right\}\right] \qquad (16)$$

to extract the parameters, with particular reference to the time for 50% formation ($t_{0.5}$) and the order of the transformation (n). In Eq.(16) f_w is the mass fraction, T is temperature and t is time.

An optimum fit was obtained for: $f_w(T,t=\infty)$=0.0025, $t_{0.5}$=1572 h and n=1.09. A similar analysis was carried out at an ageing temperature of 700 °C up to 10000 h obtaining $f_w(T,t=\infty)$=0.0008, $t_{0.5}$=3889 h and n=1.11, which showed a similar value of the kinetic exponent. A comparative plot of the kinetic evolution of the total mass fraction of Z-phase at 650 °C and 700 °C and of the corresponding JMAK fits is shown in Fig. 3.

A kinetic exponent in the range from 1 to 1.5 is associated with a mechanism where the transformation proceeds by growth of particles of appreciable volume [30-32]. This is consistent with the transformation mechanism revealed by TEM which showed that NbN and VN particles are the sites where Z-phase develops by a conversion of these phases under the incorporation of Cr from the matrix (and dissolution of Cr_2N); the rate of nitride to Z-phase transformation is likely to be controlled by the diffusion kinetics of Cr atoms.

To be completed, this result requires an extension of the kinetic analysis at other ageing temperatures. On one hand, since the solubilization temperature of the Z-phase is slightly above 700 °C, an increase in the ageing temperature would imply a reduction in the equilibrium volume fraction of the phase. On the other hand, as the ageing temperature is decreased, the time required to achieve the equilibrium fraction will increase beyond the maximum ageing time of the present experiment, thus implying an onerous planning of the ageing treatments.

5. Conclusions

The aim of the present work is to develop a measurement procedure for studying the evolution of the Z-phase nitrides in a model alloy with composition similar to that of 12% Cr steels for high temperature applications during long time ageing.

The procedure consists of electrolytic extraction of the precipitates from the metallic matrix and quantitative X-ray diffraction determination of the volume fraction of second phases based on the Rietveld approach has provided consistent results.

The procedure accounts for the chemical composition of the phases involved, being (V, Nb)N, (Nb, V)N, Cr_2N and tetragonal and cubic Z-phase, which significantly affects the absolute intensity of the diffraction peaks, and by correcting the results of the Rietveld refinement by the not negligible absorption contributions in the extracted precipitates. The determination of the chemical composition is provided by other analysis techniques. The evolution of the total mass fraction of Z-phase described in terms of a Johnson-Mehl-Avrami-Kolmogorov analysis. The order of the transformation is in the range 1-1.5. This indicates that Z-phase formation is actually a transformation and growth of (V, Nb)N and (Nb, V)N into Z-phase by an exchange of substitutional elements, particularly Cr, with the surrounding matrix. This implies that all nuclei are available and have an appreciable size at the start of the transformation.

6. References

1. A. Strang, V. Vodarek, *Mater. Sci. Technol.*, 1996, 12, 552-556.
2. V. Vodarek and A. Strang, *J. Phys. IV France*, 2003, 112, 445-448.
3. H.K. Danielsen, J. Hald, F.B. Grumsen, M.A.J. Somers, *Metall. Mat. Trans. A*, 2006, 37A, 2633-2640.
4. H.K. Danielsen, J. Hald, *Calphad*, 2007, 31, 505-514.
5. K. Sawada, H. Kushima, K. Kimura, M. Tabuchi, *ISIJ Int.*, 2007, 47, 733-739.
6. A. Golpayegani, H.-O. Andrén, H. Danielsen, J. Hald, *Mater. Sci. Eng. A*, 2008, 489, 310-318.
7. K. Sawada, K. Suzuki, H. Kushima, M. Tabuchi, K. Kimura, *Mater. Sci. Eng. A*, 2008, 480, 558-563.
8. H.K. Danielsen, J. Hald, *Mater. Sci. Eng. A*, 2009, 505, 169-177.

9. V. Vodarek, H.K. Danielsen, F.B. Grumsen, J. Hald, A. Strang: Proc. 8th Liège Conference 'Materials for Advanced Power Engineering', (ed. J. Lecomte-Beckers et al.), Liège, B, September 2006, Forschungszentrum Jülich, p. 1251.
10. L. Cipolla, H.K. Danielsen, D. Venditti, P.E. Di Nunzio, J. Hald, M.A.J. Somers, *Acta Materialia*, 2009 (doi: 10.1016/j.actamat.2009.09.045).
11. H.M. Rietveld, *Acta Crystallogr.*, 1967, 22, 151-152.
12. H.M. Rietveld, *J. Appl. Crystallogr.*, 1969, 2, 65-71.
13. 'The Rietveld method, IUCr Monographs on Crystallography 5', (ed. R.A. Young), 1993, Oxford, U.K., Oxford Science Publishing.
14. L.S. Zevin, G. Kimmel, I. Mureinik, 'Quantitative X-Ray Diffractometry', 1995, New York, NY, Springer-Verlag.
15. L.B. McCusker, R.B. Von Dreele, D.E. Cox, D. Louër, P. Scardi, *J. Appl. Cryst.*, 1999, 32, 36-50.
16. V.K. Pecharsky, P.Y. Zavalij, 'Fundamentals of Powder Diffraction and Structural Characterization of Materials', The Netherlands, 2003, Kluwer Academic.
17. I.D. Brown, *J. Res. Natl. Inst. Stand. Technol.*, 1996, 101, 341-346.
18. H.P. Klug, L.E. Alexander, 'X-ray diffraction procedures for polycrystalline and amorphous materials', 1954, New York, NY, John Wiley & sons.
19. J. LeRoux, D.H. Lennox, K. Kay, *Anal. Chem.*, 1953, 25, 740–743.
20. 'Metals Reference Book' (ed. C.J. Smithells), 1976, London, U.K., Butterworths.
21. S.A. Howard, R.L. Snyder, *J. Appl. Cryst.*, 1989, 22, 238-243.
22. F. Rinaldi, F. Fabbri, S. Martelli, unpublished result.
23. T.-H. Lee, S.-J. Kim, S. Takaki, *Acta Cryst.*, 2006, B62, 190-196.
24. P. Lazar, R. Podloucky, E. Kozeschnik, J. Redinger, *Physical Review B*, 2008, 78, 134202.
25. W.A. Johnson, R.F. Mehl, *Trans. AIME*, 1939,135, 416-442.
26. M. Avrami, *J. Chem. Phys.*, 1939, 7, 1103-1122.
27. M. Avrami, *J. Chem. Phys.*, 1940, 8, 212-224.
28. M. Avrami, *J. Chem. Phys.*, 1941, 9, 177-184.
29. A.N. Kolmogorov, *Izv. Akad. Nauk SSSR, Ser. Mat.*, 1937, 3, 355-359.
30. F.J. Humphreys, M. Hatherly, 'Recrystallization and Related Annealing Phenomena', 1st edn., 1995, Oxford, U.K., Pergamon.
31. B. Ilschner, *Archiv für das Eisenhuttenwesen*, 1955, 26, 59-62.
32. J.W. Christian, 'The Theory of Transformations in Metals and Alloys', 3rd edn., 2002, Oxford, U.K., Pergamon.

TABLES

Table 1 Chemical composition of the 12% Cr model alloy in mass %.

C	Cr	Ni	Nb	V	N	Si	Mn	P	S
0.0045	11.9	1.15	0.07	0.19	0.061	0.35	0.32	0.003	0.0033

Table 2 Chemical composition of the metallic sub-lattice of the precipitate phases averaged over all the samples. Concentrations as determined by TEM-EDS measurements are expressed in atomic fraction.

Phase	***V***	***Nb***	***Cr***	***Fe***
Cr_2N	0.184	0.010	0.796	0.010
(Nb, V)N	0.358	0.480	0.146	0.016
(V, Nb)N	0.503	0.298	0.183	0.018
Cr(V, Nb)N*	0.714	0.286	1	-

* 2 atoms per formula.

Table 3 Crystal system and lattice parameters of the phases used for calculating the theoretical diffracted intensities.

Phase	***Crystal System***	***a (Å)***	***c (Å)***	***Reference***
Cr_2N	Hexagonal	4.811	4.484	JCPDS 35-803 [ref. 23]
(Nb, V)N	Cubic (NaCl)	4.394	-	JCPDS 71-162
(V, Nb)N	Cubic (NaCl)	4.139	-	JCPDS 35-768
Cr(V, Nb)N	fcc	4.045	-	[ref. 3]
Cr(V, Nb)N	Tetragonal	2.860	7.390	[ref. 3]

Table 4 Calculated density from crystallographic data and chemical composition (atoms per cell).

Phase	V	Nb	Cr+Fe	N	Cell Volume ($Å^3$)	Formula weight ($g\ mol^{-1}$)	ρ ($g\ cm^{-3}$)
Cr_2N	1.104	0.060	4.836	3	89.894	355.29	6.562
(Nb, V)N	1.432	1.920	0.648	4	80.790	341.05	7.009
(V, Nb)N	2.012	1.192	0.796	4	70.915	310.66	7.273
Z fcc	1.428	0.572	2	2	66.184	257.89	6.470
Z Tetragonal	1.428	0.572	2	2	60.447	257.89	7.084

Table 5 Calculated mass absorption coefficients of the precipitate phases for Co-K_α incident radiation.

Phase	μ/ρ ($cm^2\ g^{-1}$)
Cr_2N	328.93
(Nb, V)N	233.21
(V, Nb)N	248.01
Tetragonal and fcc Z-phase	299.04

Table 6 Volume percentage of the precipitate phases in the powders extracted from samples aged at 650 °C for different times as determined by the spectrum fitting procedure.
The time 0 h corresponds to the as-tempered material.

time (h)	Cr_2N	NbN	VN	Z-fcc	Z-Tetragonal
0	87.6	7.3	5.1	0.0	0.0
100	76.8	13.3	9.9	0.0	0.0
300	80.8	8.6	5.8	3.9	0.9
1000	72.1	6.6	3.4	3.6	14.3
3000	63.2	3.7	0.4	6.0	26.7
5300	54.0	2.4	0.3	7.4	35.9
10000	53.7	1.5	0.4	10.6	33.8

Table 7 Calculated evolution of the absolute mass fraction of the precipitate phases in the steel as a function of the ageing time at 650 °C.

Ageing time (h)	Cr_2N	NbN	VN	Z-fcc	Z-Tetragonal	Z-total
0	$4.22 \cdot 10^{-3}$	$3.78 \cdot 10^{-4}$	$2.70 \cdot 10^{-4}$	0	0	0
100	$3.50 \cdot 10^{-3}$	$6.46 \cdot 10^{-4}$	$5.00 \cdot 10^{-4}$	0	0	0
300	$3.87 \cdot 10^{-3}$	$4.38 \cdot 10^{-4}$	$3.05 \cdot 10^{-4}$	$1.86 \cdot 10^{-4}$	$4.92 \cdot 10^{-5}$	$2.36 \cdot 10^{-4}$
1000	$3.54 \cdot 10^{-3}$	$3.45 \cdot 10^{-4}$	$1.84 \cdot 10^{-4}$	$1.75 \cdot 10^{-4}$	$7.56 \cdot 10^{-4}$	$9.32 \cdot 10^{-4}$
3000	$3.22 \cdot 10^{-3}$	$2.02 \cdot 10^{-4}$	$2.15 \cdot 10^{-5}$	$3.01 \cdot 10^{-4}$	$1.47 \cdot 10^{-3}$	$1.77 \cdot 10^{-3}$
5300	$2.78 \cdot 10^{-3}$	$1.31 \cdot 10^{-4}$	$1.50 \cdot 10^{-5}$	$3.73 \cdot 10^{-4}$	$2.00 \cdot 10^{-3}$	$2.37 \cdot 10^{-3}$
10000	$2.78 \cdot 10^{-3}$	$8.18 \cdot 10^{-5}$	$2.35 \cdot 10^{-5}$	$5.39 \cdot 10^{-4}$	$1.89 \cdot 10^{-3}$	$2.43 \cdot 10^{-3}$

FIGURES

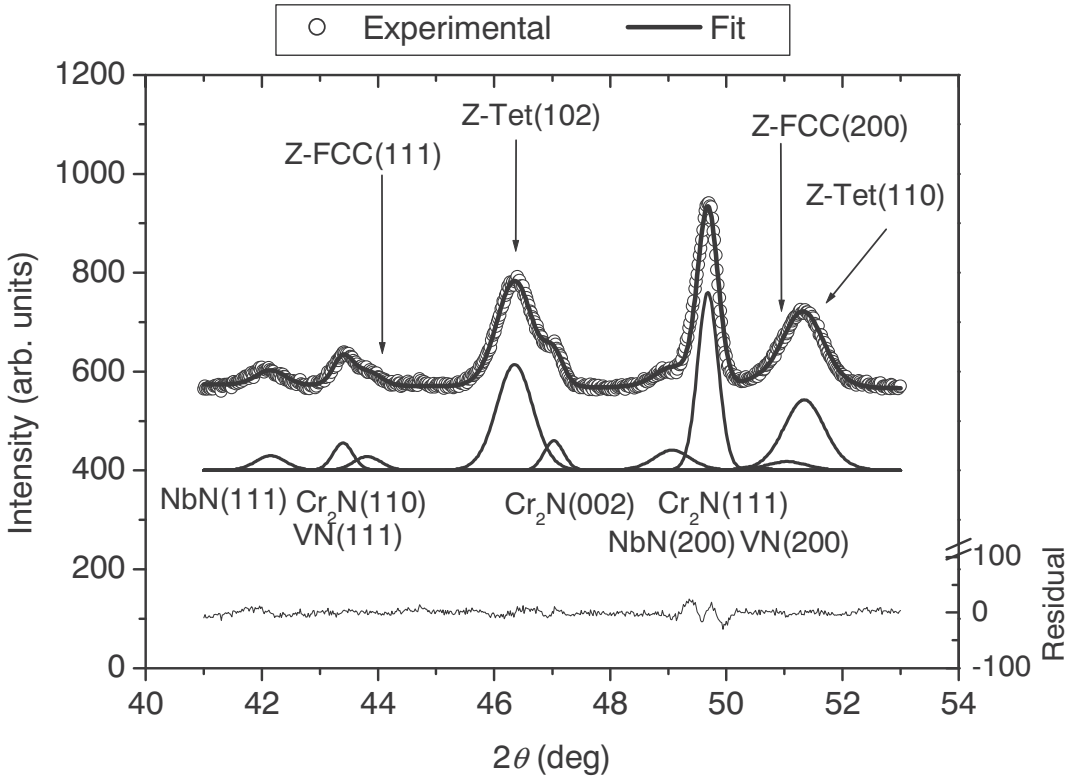

Figure 1 X-ray diffraction spectrum (Co-K_α incident radiation) of the sample aged for 3000 h at 650 °C and calculated spectrum after Rietveld refinement (solid line) superimposed to the measured data points (uppermost line), theoretical diffraction peaks of the phases (middle) and fitting residuals (lowermost line).

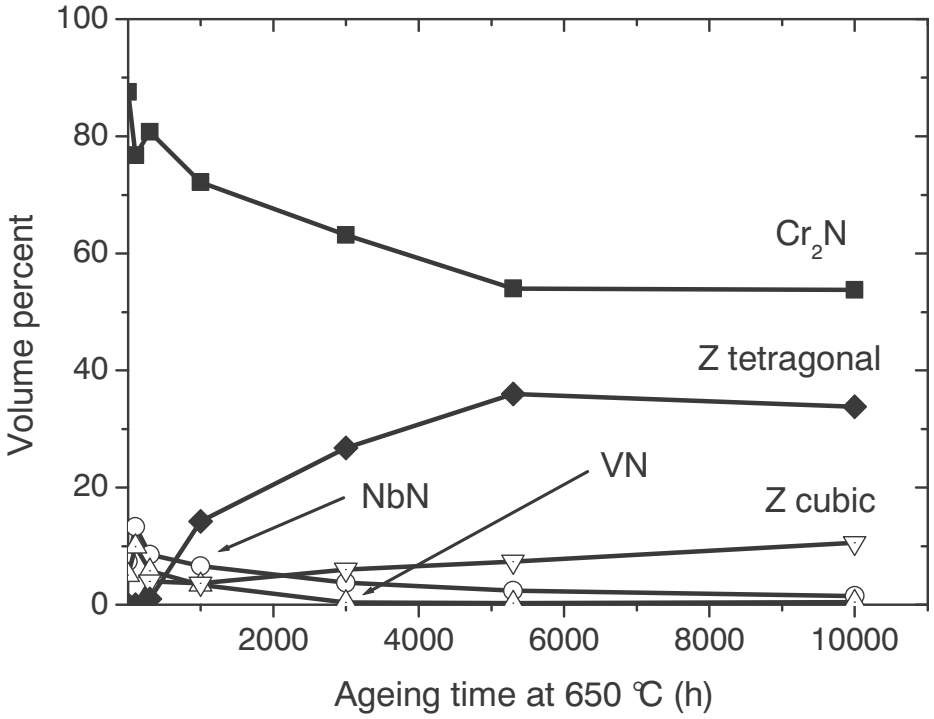

Figure 2 Evolution of the volume fractions of the phases in the powders extracted from samples aged at 650 °C.

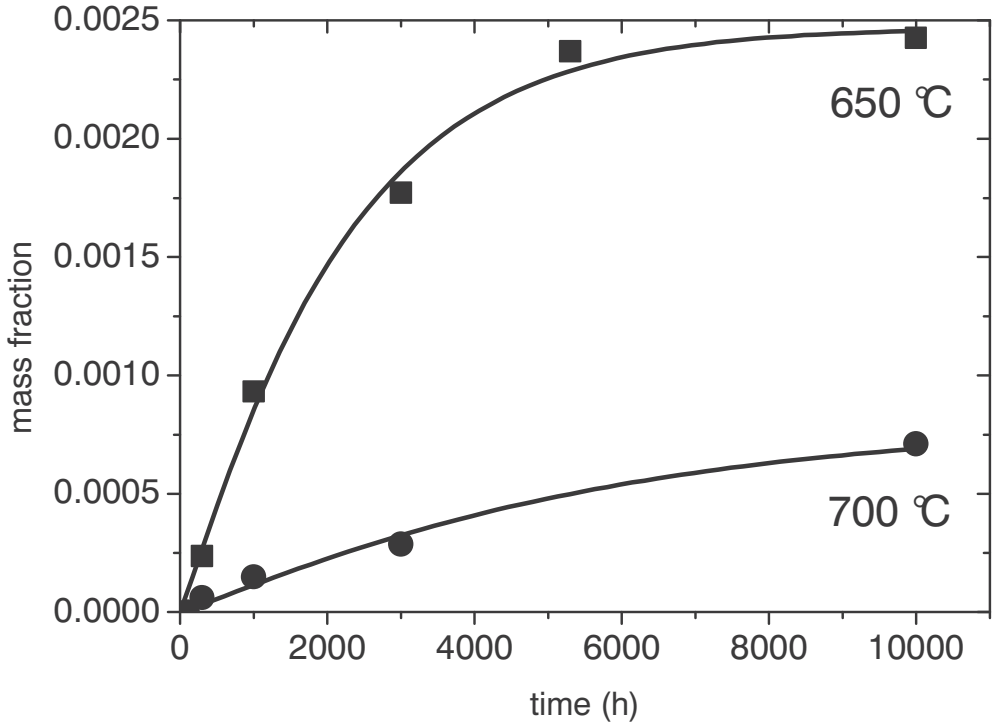

Figure 3 Evolution of the absolute total mass fraction of Z-phases (symbols) and JMAK fit of the overall fraction of Z-phase (solid line) for ageing at 650 °C and 700 °C.

This page was left blank on purpose

PAPER III

MICROSTRUCTURAL EVOLUTION OF ASTM P91 AFTER 100,000 HOURS EXPOSURE AT 550°C AND 600°C

L. Cipolla[1),*], S. Caminada[2),#], D. Venditti[1)], H. K. Danielsen[3)], A. Di Gianfrancesco[1)]

1) Centro Sviluppo Materiali SpA, Rome, Italy
2) TenarisDalmine, Dalmine, Italy
3) Technical University of Denmark, Lyngby, DTU, Denmark
* also Ph.D Student at Technical University of Denmark, DTU, Lyngby, Denmark
# also Ph.D Student at Politecnico di Milano, Mechanical Department, Milan, Italy

Paper accepted to 9th Liège Conference on Materials for Advanced Power Engineering, 27th-29th September 2010, Liège.

This page was left blank on purpose

MICROSTRUCTURAL EVOLUTION OF ASTM P91 AFTER 100,000 HOURS EXPOSURE AT 550°C AND 600°C

L. Cipolla[1),*], S. Caminada[2),#], D. Venditti[1)], H. K. Danielsen[3)], A. Di Gianfrancesco[1)]

1) Centro Sviluppo Materiali SpA, Rome, Italy
2) TenarisDalmine, Dalmine, Italy
3) Technical University of Denmark, Lyngby, DTU, Denmark
* also Ph.D Student at Technical University of Denmark, DTU, Lyngby, Denmark
# also Ph.D Student at Politecnico di Milano, Mechanical Department, Milan, Italy

Abstract

ASTM A335 P91 samples were investigated after creep testing at 550°C and 600°C for over 10^5 h.
X-Ray Diffraction, Scanning and Transmission Electron Microscopy were adopted to assess the microstructural evolution of the material in terms of precipitation changes during high temperature exposure. Mean equivalent diameters and average chemical compositions of MX and $M_{23}C_6$ precipitates and Laves phases were assessed through the analysis of a large number of particles. Their growth and coarsening kinetics were determined at 600°C on many samples with increasing exposure times up to 100,000 hours. Also the presence of modified Z-phase, Cr(V,Nb)N, was investigated.
The high microstructural stability of Grade 91 is related to the presence of fine and distributed MX carbonitrides, always present even after very long term temperature exposure. The mean size of MX carbonitrides remains almost constant and stays below 45 nm after 10^5 h at 600°C.
Although MX particles exhibit a Cr enrichment with increasing ageing times, indicating that they are absorbing Cr atoms from the surrounding matrix, their transformation into Z-phase is still at a very preliminary stage: only a few hybrid MX/Z particles and a few Z-phase precipitates were identified in the most aged sample after 10^5 h at 600°C.
Coarsening of $M_{23}C_6$ occurs during thermal exposure, but their average equivalent diameter, initially of 140 nm in the as-treated material, remains below 200 nm after 10^5 h at 600°C.
Laves particles form at grain boundaries after a relatively short time and soon become the largest precipitates.

Keywords: 9%Cr steels, long-term creep, microstructure evolution, Z-phase.

1. Introduction

In the last two decades several advanced 9%Cr ferritic steels were developed and some of them, such as ASTM Grades 91 and 92, are currently used in modern power plants [1, 2]. This has allowed the service pressure and temperature of components for advanced power plants to be increased significantly and more severe requirements on strength, oxidation resistance and creep properties to be imposed on high temperature steels.
Long term creep tests, even longer than 100,000 hours, are available today and reliable long term creep strength values have been established, based on comprehensive creep databases [3, 4]. The average 100,000 hours creep rupture strength values at 600°C of ASTM Grades 91 and 92 were recently assessed by the European Creep Collaborative Committee (ECCC) as 90 MPa [3] and 113 MPa, respectively [4].
A key element for the creep strengthening of the advanced 9%Cr steels is the formation of a fine dispersion of small MX carbonitrides, (V,Nb)(C,N), which are very stable against coarsening and thus provide a fundamental contribution to the creep resistance by means of precipitation hardening [5]. It has been well established that the main microstructural evolution mechanisms during high temperature exposure of 9%Cr steels are the coarsening of

carbides, $Cr_{23}C_6$, and the precipitation, growth and coarsening of Laves phase particles, $Fe_2(Mo,W)$ [5, 6, 7].
It has been found that the modified Z-phase, a complex nitride Cr(V,Nb)N, develops in 9-12%Cr steels during thermal exposure in the temperature range 600°C-700°C [8, 9, 10]. The formation of Z-phase has been associated with a dissolution of the fine dispersion of small MX nitrides, (V,Nb)N. Unfortunately, Z-phase particles grow much larger than MX precipitates and, thus the Z-phase formation results in a quick and severe loss of creep strength [6, 9], especially for 12%Cr steels.
A thermodynamic model of the Z-phase has recently been developed [11]. It predicts that in the 9-12%Cr steels Z-phase is the most stable nitride in the temperature range 600°C-700°C and, accordingly, at equilibrium it fully replaces the finely dispersed MX nitrides which precipitate during normalising and tempering heat treatment. It has been found that in advanced 12%Cr steels, such as P122, Z-phase formation occurs much faster than in 9%Cr steels and large colonies of Z-phase are observed in 12%Cr samples exposed for few thousand hours at 650°C [10]. It was concluded by model studies that the chromium content has a major influence on the driving force for Z-phase formation and on its growth rate, which explains why 12%Cr steels suffer from rapid and abundant formation of Z-phase, while this occurs much more slowly in 9%Cr steels [11].
Recently, it was explained that the formation of Z-phase occurs by Cr diffusion from the matrix into the original V- and Nb-nitrides, through the formation of metastable hybrid MX/Z particles [12, 13, 14].
The aim of this paper is to investigate the microstructural evolution of an industrial P91 by analysing several aged samples up to 100,000 hours at 550°C and 600°C.
In particular, the precipitate evolution at increasing times and temperatures are described and discussed in the paper, in order to demonstrate the high microstructural stability of Grade 91 even after long-term thermal exposures.
This work also investigates the presence of Z-phase in aged samples and the mechanism of its formation by means of hybrid MX/Z particles.

2. Material

An industrial ASTM A335 P91 seamless pipe produced by TenarisDalmine (heat 28145), with an outside diameter (OD) of 355 mm and a wall thickness (WT) of 35 mm, was extensively characterised in terms of microstructural, mechanical and creep properties after long-term thermal exposure. The chemical composition of the investigated pipe is reported in Table 1, compared with the requirements of ASTM A335-06. This pipe was normalised at 1040°C and tempered at 760°C.
Samples from a second industrial pipe from TenarisDalmine (heat 801141), 343mm OD and 74mm WT, were investigated after 7,000h and 58,000h at 600°C. This pipe was also normalised at 1040°C and tempered at 760°C. Its chemical composition is also shown in Table 1.
Both as-treated pipes fulfil the ASTM mechanical requirements.
The microstructure of the 355mm OD as-treated pipe consists of fully tempered martensite, with an average hardness of 230 HV_{10}.
The creep resistance of the 355mm OD pipe was extensively tested in the range of 550°C-650°C; in particular three creep specimens from this batch broke after 110,301h at 550°C and 150 MPa, 104,076h at 600°C and 90 MPa and 115,808h at 650°C and 50 MPa; the first two

specimens were selected for the extensive microstructural characterization reported in this work.
Figure 1 shows the comparison among all the creep rupture data from the 355mm OD pipe and the average creep-rupture strength of ASTM A335 P91, assessed by ECCC in 2009 [3]. This confirms that the creep strength of the industrial pipe selected in this work is in line with the ECCC creep rupture assessment for Grade 91.
The samples broken at longest times show the typical low values of elongation to rupture observed in 9-12%Cr steels [15]: 20%, 4% and 5%, respectively after 110,301h at 550°C, 104,076h at 600°C and 115,808h at 650°C.

3. Experimental

All the microstructural investigations were conducted on the heads of the broken creep specimens, since it was demonstrated that no differences in the precipitation occur between gauge and grip portion of the same crept specimen for 9%Cr steels [16, 17].
In addition to Light Microscopy (LM), Scanning Electron Microscope (SEM) investigations were carried out using a JEOL 5900, with a tungsten filament. As Laves phase is a Mo-based particle, this was easily identified by Back Scattered Electron (BSE) images. BSE images were processed adopting an Automatic Image Analysis (AIA) procedure, coupling particle size with chemical composition. During each SEM session, several hundred random particles from 50 random frames at 3000X magnification were identified, for a total scattered area of 3150 μm^2. A cut-off of particles with mean diameter less than 200 nm and a Mo content less than 5 wt% was imposed.
The morphology and the composition of finest precipitates were investigated with a Field Emission Gun Transmission Electron Microscope (FEG-TEM), JEOL 3000F, operating at 300kV and equipped with an Oxford Instruments Inca Link ISIS Energy Dispersive Spectroscopy (EDS) unit and a Gatan Imaging Filtered (GIF) Electron Energy Loss Spectroscopy (EELS).
A 200kV Scanning/Transmission Electron Microscope (STEM), JEOL 200CX, equipped with an EDS Noran Instruments was also used.
Occasionally, a FEG-TEM, FEI TITAN 80-300, operating at 300kV, has been used.
TEM observations were carried out on carbon extraction replicas as well as on thin foils. The replicas were prepared by a chemical etching with Vilella's reagent (1% picric acid and 5% hydrochloric acid in ethanol).
Several particles from each extraction replica were analysed in order to determine their equivalent diameter and, through EDS, their average chemical composition; only the particles above 10 nm and sufficiently far from each other to avoid overlapping were analysed.
This methodology was applied also to identify the presence of Z-phase precipitates; the following compositional criterion was adopted to discriminate Z-phase: $Fe(at\%)+Cr(at\%) \approx V(at\%)+Nb(at\%)$, with $40 \leq Cr(at\%)+Fe(at\%) \leq 60$.
A Selected Area Diffraction (SAD) analysis was performed on a limited number of particles, in order to couple lattice parameters with the chemical composition obtained through EDS.
The average dislocation density and the average sub-grain size were measured with a standard procedure based on the intercept method applied on thin foils [18].
For the determination of the different phases, X-Ray powder Diffraction (XRD) was also applied, using a Siemens D500 X-Ray Diffractometer equipped with Co-radiation source. The step size was 0.2° in 2θ and the counting time was 34s per step. In order to avoid interference from matrix reflections, the precipitates were extracted from the bulk by electrolysis in an

acidic solution of 5% HCl in 95% ethanol to dissolve the matrix. The solution thus obtained was filtered through a 20 nm Millipore filter to capture the extracted powders. The dissolution of samples for XRD investigation involved at least 10g of material from each sample.

4. Results

4.1 Microstructure evolution

The microstructure of both crept samples after 100,000h at 550°C and 600°C consists of tempered martensite with average hardness values of 225 HV_{10} and 224 HV_{10}, respectively. The microstructure by LM of the sample after 104,076 hours at 600°C is shown in Figure 2-a. Figure 2-b shows the same sample by SEM: grain boundaries and tempered martensite laths are decorated by precipitates.
TEM investigations by thin foils allowed to get information on the substructure evolution after long term exposure, without straining (specimens were taken from the heads of creep specimens). The thin foil images of as-treated, 550°C/110kh and 600°C/104kh samples are presented in Figure 3.
The as-treated material exhibits a well recovered matrix with polygonized structures. Precipitates at grain boundaries and laths were identified as $M_{23}C_6$ carbides (see section 4.2).
After long exposure at 550°C and 600°C, the substructure does not exhibit significant changes, being the tempered martensite lath still recognized in many regions.
The mean subgrain size of 600°C/104kh aged sample was found to be close to that of the as-treated material. Also the dislocation density values of the as-treated and 600°C/104kh samples are similar.

4.2 Precipitation evolution

The evolution of precipitates of the aged samples with increasing exposure times at high temperature is a diffusion controlled mechanism. The microstructural changes, in terms of progressive variation of precipitate morphology and their chemical composition, are described and quantified, as a function of temperature and time, adopting the Larson Miller Parameter (LMP) using a constant equal to 20.
The mean equivalent diameters and average chemical compositions (at%) of MX, $M_{23}C_6$ and Laves particles in the aged samples are reported in Table 2, where crept samples are sorted by Larson-Miller Parameter (LMP) values. Two samples, 600°C/7kh and 600°C/58kh, belong to heat 801141; they have been included in Table 2 to offer a complete view of the microstructural evolution of P91 over time.

TEM investigations enabled to detect very fine MX particles (mean size of 36 nm) in the as-treated material. TEM analyses on exposed samples showed that many fine particles, smaller than 40 nm, are still present in the matrix even after 100,000h at 550°C and 600°C.
EDS and Energy Filtered (EF) TEM investigations demonstrated that these fine precipitates, distributed within laths, are V- and Nb- rich carbo-nitrides. Figure 4 shows the precipitates extracted by carbon replica in the 600°C/104kh sample at higher magnification: in particular MX carbonitrides are indicated. Table 3 reports the EDS analyses (at%) of the main chemical elements found in some particles shown in Figure 4. MX carbo-nitrides contain mainly V (57-75 at%), Cr (14-30 at%) and Nb (3-29 at%). The presence of V, Nb and N as constitutional elements of MX is shown also in Figure 5, together with the zero loss image and the jump ratio images of Cr, N and V of the frame, which enabled to identify several small (V,Nb)N particles, together with a larger Cr carbide ($M_{23}C_6$ type).

Although hundreds of particles were analyzed on each sample, no traces of Z-phase were identified in the 550°C/113kh and 600°C/58kh samples. Only seven modified Z-phase particles, Cr(V,Nb)N, were detected in the 600°C/104kh sample (Figure 6) over several hundred investigated particles. Table 4 reports the EDS chemical compositions (at%) of some particles visible in Figure 6. An average equivalent diameter of 140 nm and the following average chemical composition (at%): 50%Cr, 33%V, 12%Nb, 4%Fe, 1%Mo were measured. Modified Z-phase is not included in Table 2, since the number of identified particles is too small for a reliable data assessment.

In addition to the well known MX and Cr(V,Nb)N phases, particles with a "hybrid" (V,Nb)N and Cr(V,Nb)N composition were also identified in the 600°C/104kh crept sample. A small hybrid particle with a V-rich core and a Cr-rich rim is shown in Figure 7. In addition to the High Annular Angular Dark Field (HAADF) image of the particle (Figure 7-a), the EF-TEM thickness map and the vanadium map of the hybrid particle are shown in Figures 7-b and 7-c, respectively. The variation in composition within the particle was also investigated using an EDS linescan with 50 measurements (Figure 8). The chemical composition gradually varies within the precipitate: there is an area with a MX-like composition in the middle, (V:~50 at%; Cr:~30 at%), while the "wings" of the particle have a Z-phase like composition (V:~35 at%; Cr:~55 at%). Between the core and the outer particle surface a relatively smooth Cr and V gradient was measured.
No such hybrid particles were found in the samples aged at 550°C for 110kh and at 600°C for 58kh.

$M_{23}C_6$ carbides are Cr-rich (72-80 at%) and contain also Fe (13-18 at%) and Mo (5-6 at%).
TEM investigations on the as-treated sample showed small $M_{23}C_6$ carbides distributed along grain boundaries and martensite laths (Figure 3-a).
Slightly coarser $M_{23}C_6$ carbides were observed in both 550°C/110kh and 600°C/104kh aged samples, mainly along grain boundaries and tempered martensite laths (Figures 3-b, 3-c and Figure 4).

No Laves phases are present in the as-treated material, confirming that it nucleates and precipitates during the exposure at service temperature, well below the tempering temperature at which it is not a stable phase.
Figures 3-b, 3-c and 4 show that large Laves phase particles are found in aged specimens. Figure 9 shows a SEM image of Laves particles at high magnification and their typical EDS spectrum. Size distribution of Laves particles from 600°C/104kh sample, measured by SEM-AIA, is shown in Figure 10: the highest frequency corresponds to an equivalent diameter of 450 nm (the standard deviation of the distribution is 290 nm). This value is in agreement with literature results from the investigation of an industrial P91 exposed 113,431h at 600°C (where the highest frequency corresponds to an equivalent diameter of 400 nm) [16].

Results from X-Ray powder Diffraction for 600°C/104kh sample are in line with the TEM results: $Cr_{23}C_6$, MX and Fe_2Mo phases were identified by means of their crystallographic reflections in the 2θ range (40°-60°), see Figure 11. The main Z-phase peak at $2\theta \approx 46.5$ is visible albeit quite small, and the MX peaks are still relatively large. The presence of Cr-nitrides in the sample, Cr_2N type, was also revealed by the diffractogram of Figure 11, although this could be not verified by electron microscopy.

5. Discussion

At the present time the samples investigated in this paper are among the most aged P91 crept specimens described in literature and represent an important opportunity to assess the microstructural evolution of this material up to 100,000 hours at 550°C and 600°C, especially because all the samples come from the same production batch.
The evolution of the average size of the detected precipitates (MX, $M_{23}C_6$ and Laves phases) at different exposure times at 600°C is shown in Figure 12-a and 12-b (average equivalent diameters are taken from Table 2). Fitting curves in Figure 12-a and 12-b have been traced adopting the calculated values of coarsening rate coefficient, K_d, according to the equation of Ostwald ripening kinetics [19, 20]

$$d^3 - d_0^3 = K_d \cdot t \qquad (1)$$

where d [m] is the average diameter of the particles at time t [s] and d_0 [m] is the initial average diameter of the particle before the coarsening process starts; K_d [m^3/s] is the coarsening rate coefficient.
It can be noticed that the average dimension of MX carbonitrides, which precipitate during the tempering treatment, remains almost constant during exposure and stays below 45 nm; the average diameter of $M_{23}C_6$ carbides, which are also formed during the tempering, remains below 200 nm. On the contrary Laves particles, which are not present in the normalized and tempered pipe, but precipitate during the exposure at service temperature, reach an average diameter of about 450 nm after 100,000 hours.
Literature results show that VN and NbN are not thermodynamically stable in 9-12%Cr steels and tend to transform at equilibrium into Cr(V,Nb)N, modified Z-phase [11]. From the analysis of the data reported in Table 2, it can be noticed that the average Cr content in MX particles increases progressively with increasing exposure at temperature. The average Cr content of MX particles passes from 11-at% in the as-treated sample to 13/17-at% in the samples exposed between 7kh and 58kh at 600°C up to 25-at% in the 600°C/104kh sample.
The increased average Cr content in MX particles indicates that the nitrides in the 600°C/104kh sample are absorbing Cr atoms from the surrounding matrix. This can be interpreted as the start of a slow conversion process into Z-phase through hybrid particles. Such effect is also seen for 12%Cr steel at shorter exposures [21]. The authors believe therefore that hybrid particles represent the nucleation stage of Cr(V,Nb)N particles, formed by Cr diffusion from the matrix into the original MX particle, as described also in [12, 13, 14].
However, it can not be predicted how long the transformation of all MX nitrides into Z-phase will take, because the available kinetic models do not account for a MX/Z conversion.
The experimental results show that Z-phase formation at the expense of V- and Nb-nitrides cannot be listed among the degradation mechanisms of the microstructure after 100,000 hours at 600°C, since just few particles of this phase were found (less than 1% of total investigated particles) and even fewer hybrid particles were identified in the 600°C/104kh sample, while many fine and distributed MX particles are still present.
Surely it can be stated that, due to their small size, MX precipitates found after exposure for 104kh at 600°C are still effective for strengthening the matrix against creep deformation.

Literature results indicate two main microstructural evolution mechanisms for 9%Cr grades after long exposure times [5, 6]: 1) coarsening of $M_{23}C_6$ carbides; 2) precipitation, growth and coarsening of Laves phases.
Coarsening of $M_{23}C_6$, is listed among the degradation processes, because Cr concentration will be depleted in the matrix around the particles and the pinning force for the boundary migration will be also reduced. However, the experimental results on long term exposed samples show that coarsening of $M_{23}C_6$ is relatively limited: the average equivalent diameter, initially of 140 nm in the as-treated material, remains below 200 nm after 100 kh at 600°C, thus still contributing to hinder the boundaries movement and giving some creep strengthening in any case.
On the other hand, the nucleation, growth and coarsening of Laves phases (Fe_2Mo) produce large particles at grain boundaries after a relatively short time which reach an average diameter of about 450 nm after 100,000 hours. Laves phase coarsens faster than all the other phases present and some of the particles reach a size of few micrometers after 100,000 hours at 600°C. The precipitation, growth and coarsening of Laves phase can be definitely accounted as a degradation mechanism of the microstructure.

However, the experimental observations of the limited coarsening of $M_{23}C_6$ and the high stability of MX allow to state that Grade 91 steel, even after more than 100kh of exposure at 600°C, shows a precipitation state still very effective for creep strengthening, due to the presence of many and diffuse fine precipitates.

6. Conclusions

Crept samples taken from a TenarisDalmine ASTM P91, 355mm OD pipe, exposed for over 100,000 hours at 550°C and 600°C, were extensively investigated in terms of microstructural evolution by Electron Microscopy and X-Ray Powder Diffraction.
The creep resistance of the pipe is in line with the average creep resistance of Grade 91, as recently assessed by the ECCC in 2009.

The high microstructural stability of Grade 91 is attributed to the presence of fine and uniformly distributed MX carbonitrides even after long term exposure. The mean size of MX carbonitrides remains almost constant and stays below 45 nm after 100 kh at 600°C.
Although MX particles exhibited a Cr enrichment with increasing ageing times, indicating that they are absorbing Cr atoms from the surrounding matrix, their transformation into Z-phase, is still at a very preliminary stage since only a limited number of hybrid MX/Z particles and Z-phase precipitates were detected in the most aged sample after 104kh at 600°C.

Coarsening of $M_{23}C_6$ occurs, but does not play a primary role since the average equivalent diameter, initially of 140 nm in the as-treated material, remains below 200 nm after 100 kh at 600°C.
The formation of Laves phase at grain boundaries and its coarsening is the main microstructure evolution mechanism. Laves particles form after a relatively short time and soon become the largest precipitates.
However, it is the presence of many and diffuse fine MX precipitates, even after more than 100kh of exposure at 600°C that determines a precipitation state still very effective for creep strengthening.

7. Acknowledgement

The authors wish to acknowledge their colleagues M. Ballone (CSM) and F. B. Grumsen (DTU) for excellent support during TEM analyses, as well as J. Hald (DONG/DTU) and M. A. J. Somers (DTU) for their supervision of the research activity.
Silvia Tiberi Vipraio (CSM) and Paolo Emilio di Nunzio (CSM) are thanked for their technical help during the research activities. We thank also E. Anelli (TenarisDalmine) for his precious suggestions during the research activities.
A. Carlsson (FEI Company) is kindly acknowledged for her precious support during TEM sessions.
This paper is published under authorization of Tenaris Dalmine R&D, directed by M.A. Rossi.

8. References

[1] J. Hald, Steel Research Journal 67 (1996) 369-374.
[2] L. Cipolla, A. Di Gianfrancesco, D. Venditti, G. Cumino, S. Caminada, Microstructural Evolution during Long Term Creep Tests of 9%Cr Steel Grades, Proceedings of the ASME Pressure Vessels and Piping Conference - 8th International Conference on Creep and Fatigue at Elevated Temperatures - CREEP8, July 22-26, 2007, San Antonio, Texas, USA.
[3] W. Bendick, L. Cipolla, J. Gabrel, J. Hald, New ECCC Assessment of Creep Rupture Strength for Steel Grade X10CrMoVNb9-1 (Grade 91), Proceedings of the Creep & Fracture in High Temperature Components – Design & Life Assessment Issues, April 21-23, 2009, Zurich, CH.
[4] W. Bendick, J. Gabrel, Assessment of Creep Rupture Strength for the New Martensitic 9%Cr Steels E911 and T/P92, Proceedings of the Creep & Fracture in High Temperature Components – Design & Life Assessment Issues, September 12-14, 2005, London, UK.
[5] V. Foldina, Microstructural Stability of Ferritic 9-12% Chromium Steels, COST Report No. COST-94-0076-CZ (DG 12CSMC).
[6] F. Abe, Strengthening Mechanisms in Steel for Creep and Creep Ruptures, Creep-Resistant Steels, F. Abe, T-U. Kern, R. Viswanathan editors, 279-304, ISBN-10: 1845691784.
[7] J. Hald, International Journal of Pressure Vessels and Piping 85 (2008) 30-37.
[8] E. Schnabel, P. Schwaab and H. Weber: Stahl Eisen 107 691 (1987).
[9] A. Strang and V. Vodarek: Material Science and Technology 12 (1996) 552.
[10] H. K. Danielsen, J. Hald, Energy Materials 1 (2006) 49-57.
[11] H. K. Danielsen, J. Hald, Computer Coupling of Phase Diagrams and Thermochemistry 31 (2007) 505-514.
[12] H. K. Danielsen, J.Hald, Materials Science and Engineering A 205 (2009) 169-177.
[13] H. K. Danielsen, J. Hald, F. B. Grumsen, M. A. J. Somers. Metallurgical and Materials Transactiona A 37A (2006), 2633-2640.
[14] L. Cipolla, H. K. Danielsen, D. Venditti, P. E. Di Nunzio, J. Hald, M. A.J. Somers, Acta Materialia 58 (2010) 669-679.
[15] J. Hald, Creep Strength and Ductility of 9 to 12% Chromium Steels, ECCC Seminar: Advanced Creep Data, 26 September 2003, SVUM, Prague, Czech Republic.
[16] C. Panait, W. Bendick, A. Fuchsmann, A.F. Gourgues-Lorenzon, J. Besson, Study of the Microstructure of the Grade 91 Steel after more than 100,000h of Creep Exposure at 600°C, Proceedings of the Creep & Fracture in High Temperature Components – Design & Life Assessment Issues, April 21-23, 2009, Zurich, CH.

[17] Ennis P. Creep Strengthening mechanisms in 9-12% Chromium Steels. EPRI 4th International Conference on Advances in Materials Technology for Fossil Power Plants 2004;1120-1133. USA: Hilton Head Island.
[18] P. Hirsch, A. Howie, R. Nicholson, W. Pashley, M.J. Whelan, Electron Microscopy of Thin Crystals, second edition, Krieger Publishing Company, Malabar, Florida, 1977.
[19] C. Wagner, Z. Elektrochem 65 (1961) 581.
[20] J. M. Lifshiz, V. V. Sloyzov, J. Phys. Chem. Solids 14 (1961) 35.
[21] M. Yoshizawa; M. Igarashi; K. Moriguchi; A. Iseda, H.G. Armaki; K. Maruyama: *Effect of Precipitates on Long Term Creep Deformation Properties of P92 and P122 Type Advanced Ferritic Steels for USC Power Plan*, Materials Science and Engineering A 510–511 (2009) 162–168 doi:10.1016/j.msea.2008.05.055.

Table 1 – Chemical composition of the investigated materials, compared with ASTM A335-06 P91 compositional range (wt%).

		C	Mn	P	S	Si	Cr	Mo	V	N	Ni	Al	Nb	Ti	Zr
ASTM A335-06	Min	0.08	0.3	-	-	0.2	8.0	0.85	0.18	0.03	-	-	0.06	-	-
	Max	0.12	0.6	0.02	0.01	0.5	9.5	1.05	0.25	0.07	0.4	0.02	0.10	0.01	0.01
Heat 28145		0.12	0.52	0.01	0.003	0.27	8.52	0.98	0.21	0.051	0.12	0.007	0.08	0.005	0.002
Heat 801141		0.093	0.46	0.02	0.002	0.40	9.12	0.94	0.19	0.038	0.07	0.004	0.05	-	-

Table 2 – Mean diameters and average chemical compositions (at%) of MX, $M_{23}C_6$ and Laves particles in long-term aged P91 samples.

Particle Type	LMP (C=20)	Sample	Number of particles	Mean diameter (nm)	Cr at-%	Mo at-%	Fe at-%	V at-%	Nb at-%
MX	-	As-treated♦	16	36	11	4	3	61	21
	20.6	550°C/110kh♦	39	44	13	2	1	59	25
	20.8	600°C/7kh♣	46	40	15	3	1	65	16
	21.2	600°C/20kh♦	20	36	17	3	1	59	20
	21.5	600°C/41kh♦	Not available (n.a.)	n.a.	15	4	2	60	19
	21.6	600°C/58kh♣	29	41	17	3	2	62	16
	21.8	600°C/104kh♦	21	39	25	5	4	45	21
$M_{23}C_6$	-	As-treated♦	34	139	73	6	18	2	1
	20.6	550°C/110kh♦	42	151	73	7	17	1	2
	20.8	600°C/7kh♣	30	145	78	4	16	1	1
	21.2	600°C/20kh♦	15	154	75	7	17	1	0
	21.5	600°C/41kh♦	21	160	78	7	15	0	0
	21.6	600°C/58kh♣	48	189	75	5	18	1	1
	21.8	600°C/104kh♦	40	200	75	7	14	3	1
Fe_2Mo	-	As-treated♦	0	not present	/	/	/	/	/
	20.6	550°C/110kh♦	15	325	16	39	43	1	1
	20.8	600°C/7kh♣	8	130	14	41	45	0	0
	21.2	600°C/20kh♦	n.a.	n.a.	n.a.	n.a.	n.a.	n.a.	n.a.
	21.5	600°C/41kh♦	15	375	10	46	43	1	0
	21.6	600°C/58kh♣	20	421	15	47	38	0	0
	21.8	600°C/104kh♦	15	464	11	50	37	1	1

♦: the sample belongs to heat number 28145. ♣: the sample belongs to heat number 801141.

Table 3 – Chemical composition (at%) of particles in Figure 4.

	Cr at%	V at%	Nb at%	Fe at%	Mo at%	Precipitate type
Site 1	72	6	1	16	5	$M_{23}C_6$
Site 2	80	1	1	13	5	$M_{23}C_6$
Site 3	77	0	0	17	6	$M_{23}C_6$
Site 4	16	68	11	4	1	MX
Site 5	16	75	7	1	1	MX
Site 6	30	56	8	5	1	MX
Site 7	77	0	0	18	5	$M_{23}C_6$
Site 8	17	72	7	3	1	MX
Site 9	20	63	14	2	1	MX
Site 10	25	57	12	4	2	MX
Site 11	30	31	29	7	3	MX
Site 12	14	62	22	2	0	MX
Site 13	26	53	14	4	3	MX
Site 14	15	65	16	4	0	MX
Site 15	29	55	7	5	4	MX
Site 16	76	0	0	19	5	$M_{23}C_6$
Site 17	24	69	3	3	1	MX
Site 18	21	74	4	0	1	MX

Table 4 – Chemical composition (at%) of particles in Figure 6.

	Cr at%	V at%	Nb at%	Fe at%	Mo at%	Precipitate type
Site 1	50	35	9	4	1	Cr(V,Nb)N
Site 2	51	30	13	6	1	Cr(V,Nb)N
Site 3	49	28	17	4	2	Cr(V,Nb)N
Site 4	50	32	13	5	0	Cr(V,Nb)N
Site 5	77	0	0	17	4	$M_{23}C_6$
Site 6	80	0	0	17	3	$M_{23}C_6$
Site 7	23	71	2	4	0	MX
Site 8	77	1	1	17	4	$M_{23}C_6$

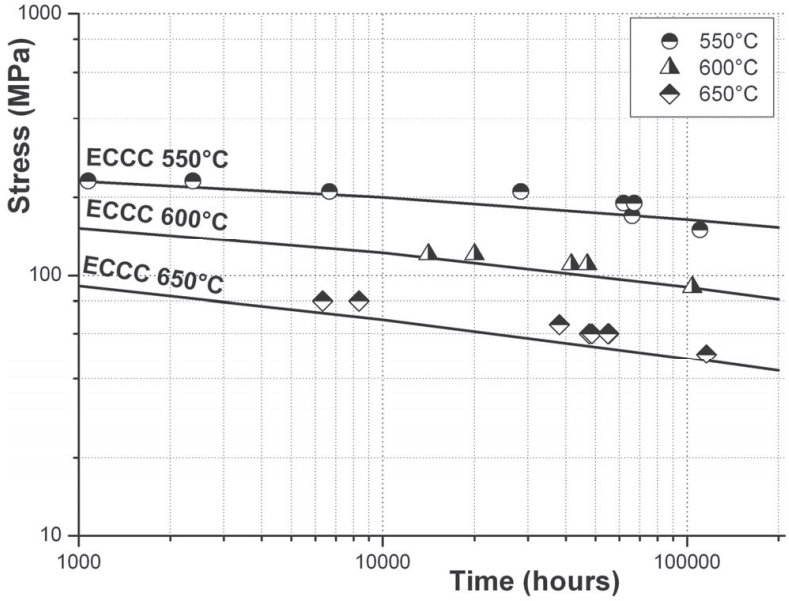

Figure 1 – Creep rupture tests from the 355mm OD pipe. Solid lines are the ECCC isotherms (year 2009) [3].

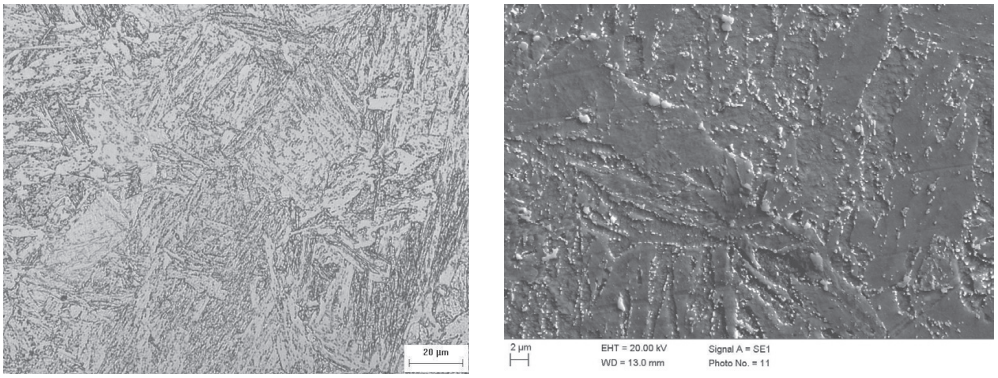

a) *b)*

Figure 2 – Microstructure of 600°C/104kh sample at (a) LM and (b) SEM.

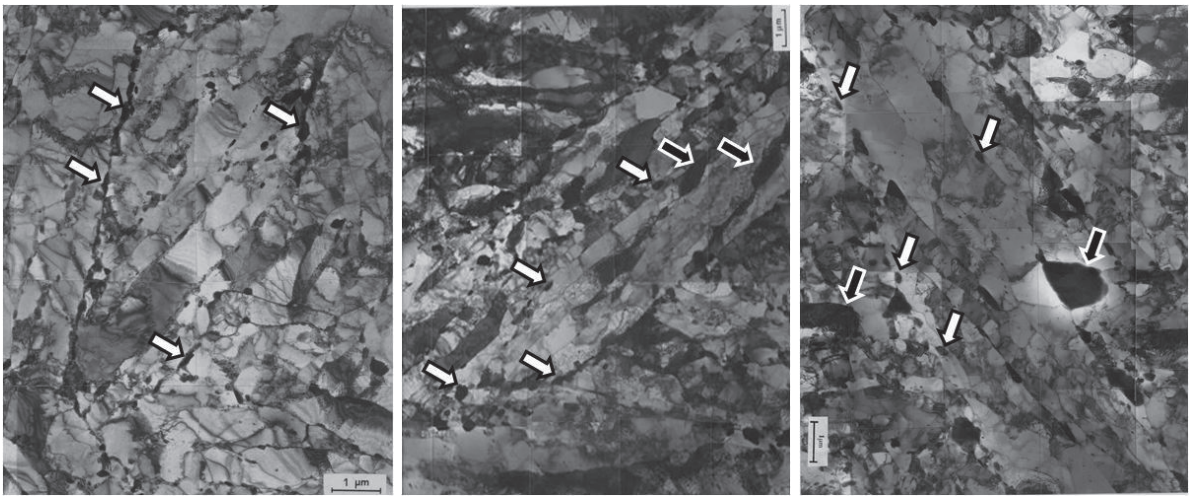

a) As-treated *b) 550°C – 110kh* *c) 600°C – 104kh*

Figure 3 – Evolution of substructure: thin foils taken from the heads of crept specimen. Also precipitates are indicated: black arrows: Laves phase; white arrows: $M_{23}C_6$.

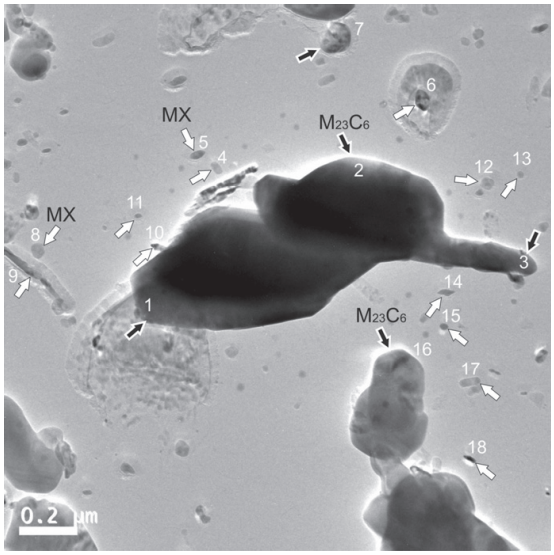

Figure 4 – Precipitates in the 600°C/104kh sample; white arrows: MX; black arrows: $M_{23}C_6$.

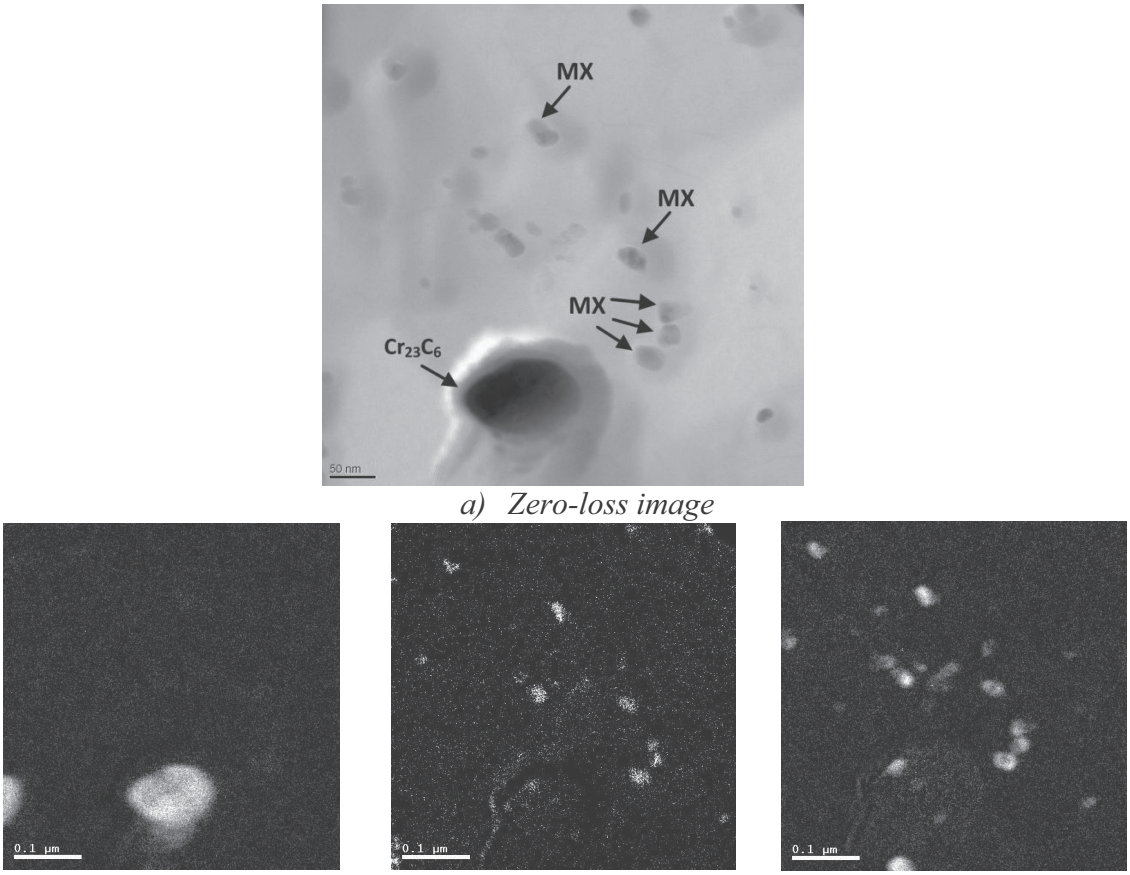

a) Zero-loss image

b) Cr-map *c) N-map* *d) V-map*

Figure 5 – a) Zero loss Image and jump ratio images of b) chromium, c) nitrogen, d) vanadium map on a frame of 600°C/104kh aged sample (investigation carried out on extraction replica).

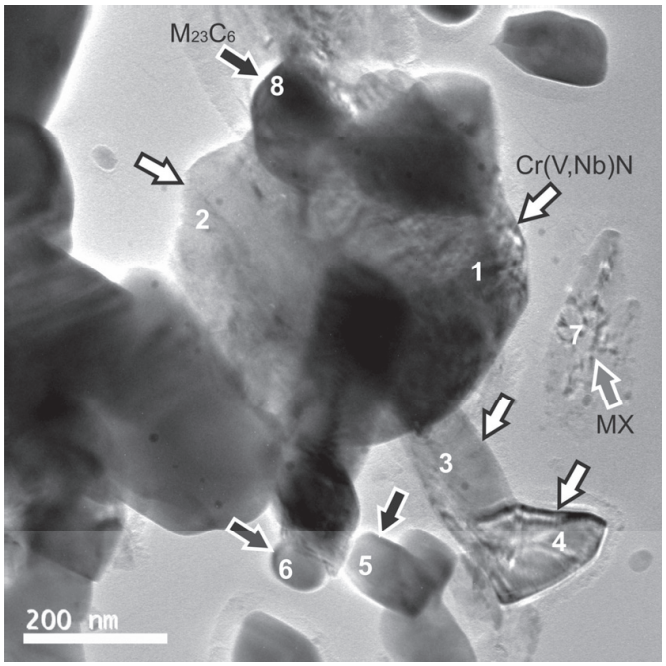

Figure 6 – Z-phase particles in 600°C/104k sample. Grey arrow: MX; black arrows: $M_{23}C_6$; white arrows: Cr(V,Nb)N.

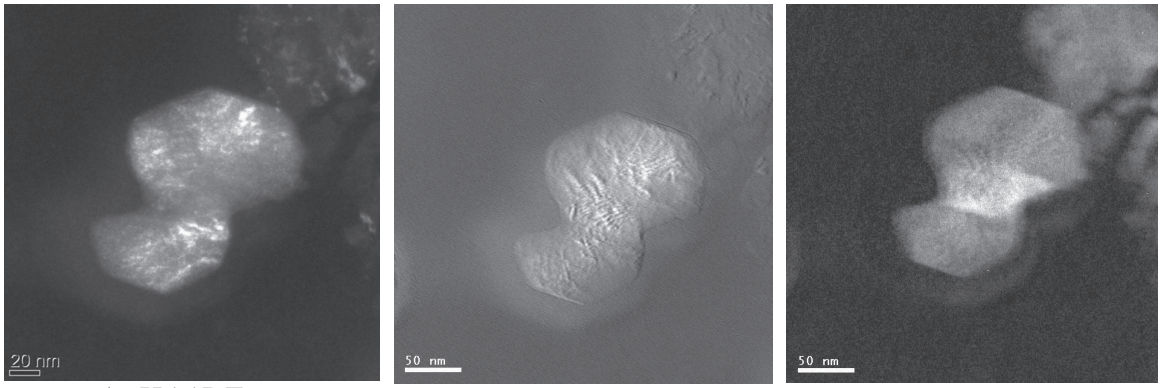

a) HAADF-image *b) Thickness-map* *c) V-map*

Figure 7 – Hybrid MX/Z-phase particle in P91 600°C/104kh sample: a) HAADF image, b) thickness map, c) vanadium map of the particle (investigation carried out on extraction replica).

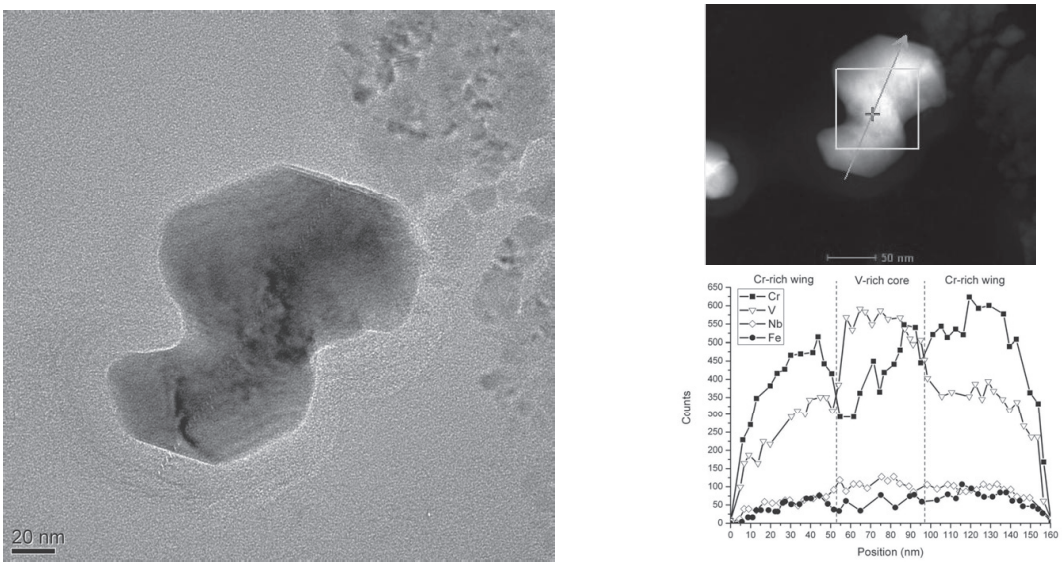

a) Bright field image. *b) EDS linescan.*

Figure 8 – a) Bright Field image of the hybrid particle in 600°C/104kh sample; b) linescan along main particle axis: Nb, Fe, Cr and V EDS counts.

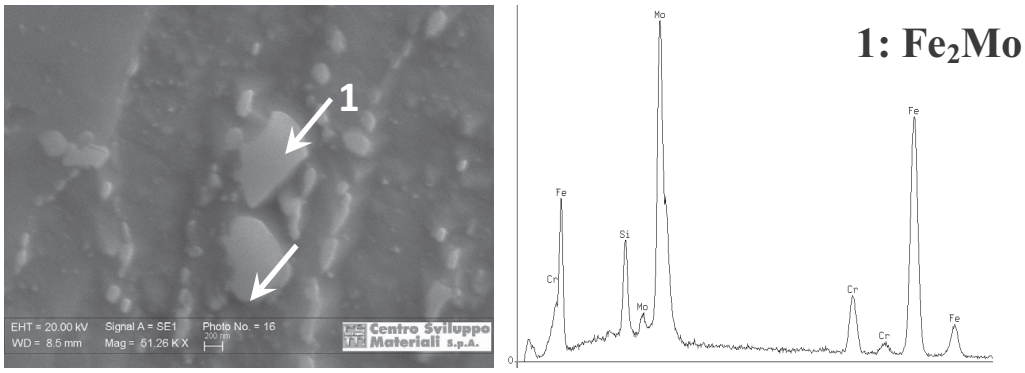

a) *b)*

Figure 9 – (a) Laves phase particles of 600°C/104kh sample and (b) their typical EDS spectrum by SEM.

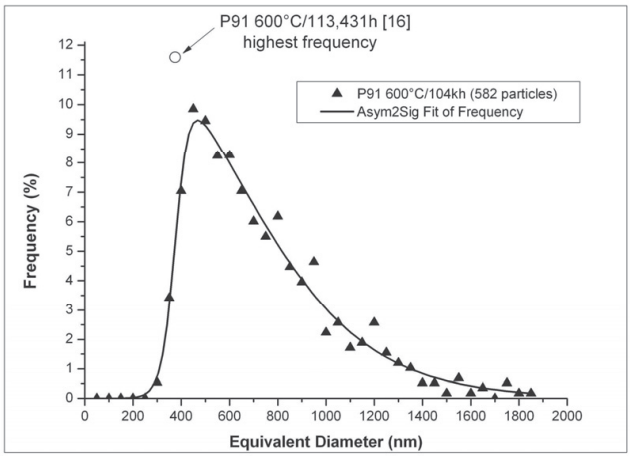

Figure 10 – Size distribution of Laves phase particles in the P91 600°C/104kh sample by SEM Automatic Image Analysis. Particles below 200nm were not detected. Comparison with data from literature [16].

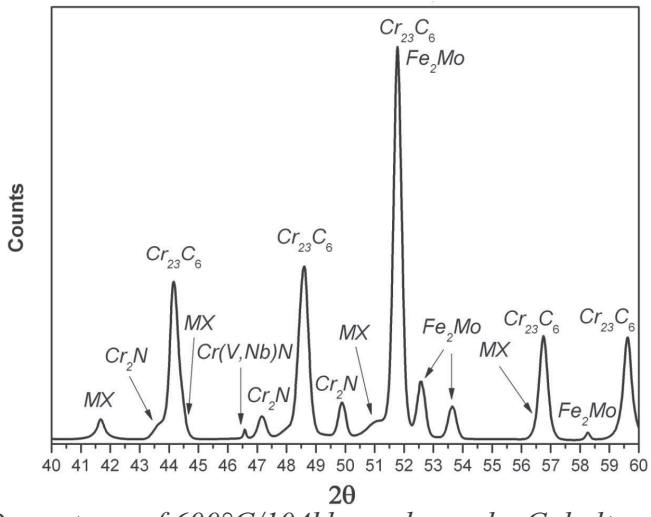

Figure 11 – XRD spectrum of 600°C/104kh aged sample. Cobalt radiation was used.

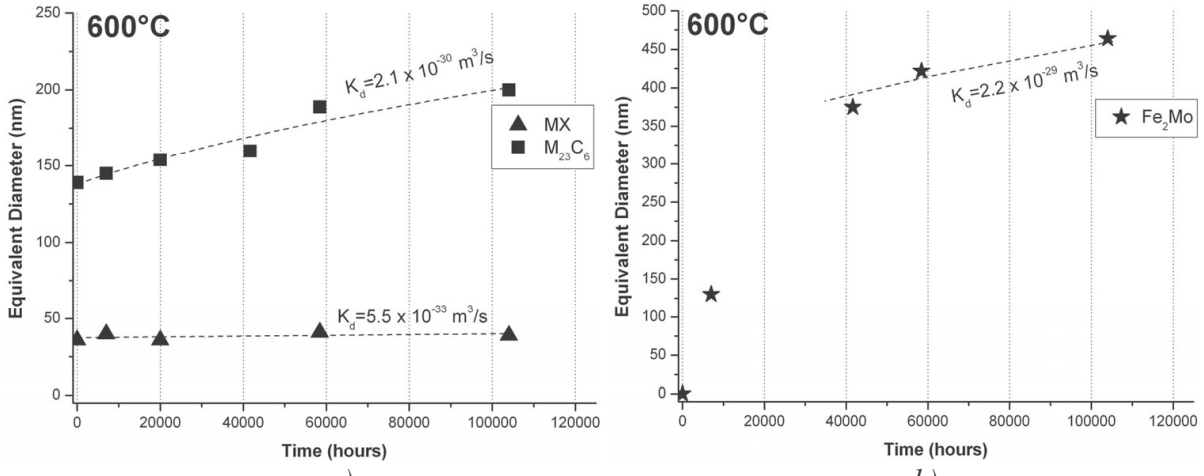

a) *b)*

Figure 12 – Evolution of equivalent diameter of a) MX, $M_{23}C_6$ and b) Fe_2Mo precipitates of Grade P91 at 600°C (data from Table 2).

PAPER IV

ELSEVIER

Available online at www.sciencedirect.com

ScienceDirect

Scripta Materialia 63 (2010) 324–327

Scripta MATERIALIA

www.elsevier.com/locate/scriptamat

On the role of Nb in Z-phase formation in a 12% Cr steel

L. Cipolla,[a,b,*] H.K. Danielsen,[b] P.E. Di Nunzio,[a] D. Venditti,[a] J. Hald[c] and M.A.J. Somers[b]

[a] *Centro Sviluppo Materiali, Via di Castel Romano 100, 00128 Rome, Italy*
[b] *Technical University of Denmark, Department of Mechanical Engineering, Kemitorvet b.204, DK 2800 Kgs. Lyngby, Denmark*
[c] *DONG Energy, Kraftværksvej 53 – Skærbæk, 7000 Fredericia, Denmark*

Received 21 March 2010; revised 16 April 2010; accepted 16 April 2010
Available online 21 April 2010

Z-phase precipitation in two model alloys, 12CrVNbN and 12CrVN, has been investigated. The alloys were aged up to 10^4 h and their precipitate evolution was followed by X-ray diffraction and transmission electron microscopy. The formation rate of Z-phase from vanadium-based nitrides, (V,Nb)N, in the Nb-containing alloy was observed to proceed considerably faster than in the Nb-free alloy. A hypothesis is put forward that explains the enhanced stability of VN in terms of changes in the interfacial energy of VN with the ferrite matrix.

Keywords: TEM; XRD; Creep-resistant steels; Nitrides

This page was left blank on purpose

Available online at www.sciencedirect.com
ScienceDirect
Scripta Materialia 63 (2010) 324–327
Scripta MATERIALIA
www.elsevier.com/locate/scriptamat

On the role of Nb in Z-phase formation in a 12% Cr steel

L. Cipolla,[a,b,*] H.K. Danielsen,[b] P.E. Di Nunzio,[a] D. Venditti,[a] J. Hald[c] and M.A.J. Somers[b]

[a] *Centro Sviluppo Materiali, Via di Castel Romano 100, 00128 Rome, Italy*
[b] *Technical University of Denmark, Department of Mechanical Engineering, Kemitorvet b.204, DK 2800 Kgs. Lyngby, Denmark*
[c] *DONG Energy, Kraftværksvej 53 – Skærbæk, 7000 Fredericia, Denmark*

Received 21 March 2010; revised 16 April 2010; accepted 16 April 2010
Available online 21 April 2010

Z-phase precipitation in two model alloys, 12CrVNbN and 12CrVN, has been investigated. The alloys were aged up to 10^4 h and their precipitate evolution was followed by X-ray diffraction and transmission electron microscopy. The formation rate of Z-phase from vanadium-based nitrides, (V,Nb)N, in the Nb-containing alloy was observed to proceed considerably faster than in the Nb-free alloy. A hypothesis is put forward that explains the enhanced stability of VN in terms of changes in the interfacial energy of VN with the ferrite matrix.

Keywords: TEM; XRD; Creep-resistant steels; Nitrides

Martensitic steels with 9 wt.% Cr, used for steam power plant applications, allow the use of steam temperature and pressure up to 600 °C and 300 bar, respectively [1]. The favourable mechanical performance of these steels relies on a fine distribution of MX-type particles, (V,Nb)N. An increase in the steam temperature up to 650 °C requires a Cr content of at least 12 wt.% Cr in ferritic steels for improved oxidation resistance [2]. However, attempts to apply 12% Cr steels at 650 °C have largely failed, because under these conditions the fine distribution of MX particles providing strength transforms into relatively coarse Z-phase, Cr(V,Nb)N particles, and an associated detrimental extension of the interparticle spacing occurs, and thus a net loss of the creep strength follows [3–5]. Hence, a combination of good creep properties and oxidation resistance is not achieved simply by increasing the Cr content [6].

Recently, an investigation of the conversion of MX nitrides into Z-phase was published for a model ferritic 12% Cr alloy, 12CrVNbN steel [7]. The chemical composition of the alloy investigated, coded M1, was designed on the basis of the thermodynamic model proposed in Ref. [8] and tailored in order to develop modified Z-phase Cr(V,Nb)N as fast as possible. This composition (see Table 1) has a very low C content to avoid precipitation of carbides and no W or Mo was added so as to avoid the development of Laves phase.

It was observed from quantitative X-ray diffraction analysis and transmission electron microscopy of extraction replicas that the tempered martensitic matrix contains the following nitrides: $(Cr,V)_2N$, V-rich (V,Nb)N and Nb-rich (Nb,V)N. Upon annealing at 650 °C for up to 10,000 h the MN-type nitrides were converted into both tetragonal and cubic Z-phase, Cr(V,Nb)N. The transformation mechanism of Z-phase was confirmed to be a diffusion of Cr into MX particles, physically transforming them into Z-phases as previously stated in Ref. [6].

In the present work the Nb-free pendant of the above-mentioned alloy was investigated (alloy M2 in Table 1). The M2 model alloy, 12CrVN steel, was designed to investigate the role of Nb in Z-phase formation. As compared to model alloy M1, the atomic fraction of Nb in M2 has been replaced by the same atomic fraction of V (which corresponds to about 0.05 wt.% V). The higher nitrogen content of M2 was unintentional.

All experimental details on alloy and sample preparation of the M2 alloy were identical to those described for the M1 alloy in Ref. [7].

* Corresponding author at: Centro Sviluppo Materiali SpA, Rome, Italy. Tel.: +39 065055275; fax: +39 065055461; e-mail: l.cipolla@c-s-m.it

1359-6462/$ - see front matter © 2010 Acta Materialia Inc. Published by Elsevier Ltd. All rights reserved.
doi:10.1016/j.scriptamat.2010.04.025

Table 1. Chemical composition of investigated materials (wt.%).

	C	Mn	Si	Cr	V	N	Ni	Nb
M1	0.0048	0.32	0.40	11.85	0.18	0.061	1.29	0.08
M2	0.0017	0.31	0.35	11.57	0.23	0.088	1.27	/

X-ray diffractograms of the extracted precipitates from as-treated and aged samples from the M1 and M2 alloys after annealing at 650 °C for up to 10,000 h are shown in Figure 1. For facilitating comparison of the M1 and M2 series, the diffractograms were normalized with respect to the highest peak, Cr_2N {1 1 1}, of each series, since the quantity of chromium nitride is relatively stable compared to that of the other precipitates.

In the as-treated samples no Z-phase, Cr(V,Nb)N, was present. After 300 h ageing the primary Z-phase peak (~46.3° 2θ; tetragonal Z-phase) was clearly distinguishable in alloy M1 (see [7]) and this is particularly well developed after 3000 h (Fig. 1); the VN and NbN peaks have disappeared completely after 10,000 h.

Clearly, the content of VN in the M2 alloy decreases relative to the content of Cr_2N, as indicated by the reduction of the peak intensity for VN. However, the VN peaks are also clearly present for ageing up to 10,000 h and no indication of the development of Z-phase is observed. The observations demonstrate that the alloy M1 exhibits a very fast rate of Z-phase formation as compared to alloy M2. Furthermore, the X-ray diffractograms show that the peaks for VN in alloy M2 are shifted to higher Bragg angles with respect to the corresponding (V,Nb)N peaks in alloy M1, indicating a difference in lattice parameter between VN and (V,Nb)N.

The quantitative assessment of phase fractions was carried out by reconstructing the spectra by a Rietveld-like algorithm previously developed for the M1 alloy [7,9] in the 2θ range from 42° to 55° where the diffraction peaks {1 1 0}, {0 0 2} and {1 1 1} of Cr_2N, {1 1 1} and {2 0 0} of VN are located. The absolute intensity of the peaks of the precipitate phases was calculated from their average chemical composition of the metallic sublattice and from the crystal structure, considering for Cr_2N a hexagonal lattice (JCPDS 35-803) and for VN a NaCl-type lattice (JCPDS 35-768). Further details are provided in Ref. [9].

The relative volume fractions determined for the alloy M2 as a function of the ageing time at 650 °C are reported in Table 2, together with the weight fractions calculated from the density of phases. The absolute overall volume fraction of second phases, also shown in Table 2, was estimated from the mass fractions based on the assumption that all nitrogen is present in the detected nitrides, recognizing that these nitrides have a very low solubility in body-centred cubic iron.

Transmission electron microscopy (TEM) on extraction replicas allowed an investigation of the evolution of the particle sizes of Cr_2N and VN nitrides in the alloy M2 as well as an energy-dispersive spectroscopy (EDS) assessment of the metallic fractions in the nitrides. The average particle size of the Cr_2N precipitates increases dramatically with time, while the size of the VN nitrides increases at a much lower rate (Table 3). This result is

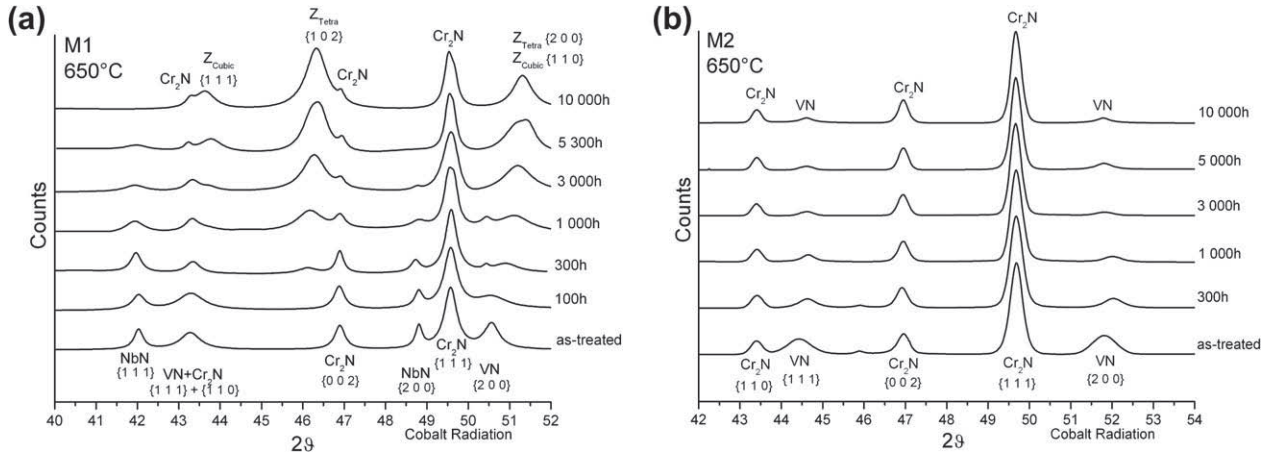

Figure 1. X-ray diffractograms (Co Kα incident radiation) of (a) M1 and (b) M2 series in as-treated and aged conditions.

Table 2. Relative volume fractions assessed by quantitative X-ray diffraction on the extracted powders and calculated mass fractions of Cr_2N and VN as a function of ageing time. The absolute overall volume fraction of second phases has been estimated from the mass fractions assuming complete binding of nitrogen.

Ageing time at 650 °C (h)	Cr_2N (vol.%)	VN (vol.%)	Cr_2N (mass%)	VN (mass%)	Absolute overall volume fraction of precipitates
0	81.2	18.8	75.5	24.5	0.0062
300	90.1	9.9	86.6	13.4	0.0067
1000	94.3	5.7	92.1	7.9	0.0069
3000	95.2	4.8	93.4	6.6	0.0070
5000	94.7	5.3	92.7	7.3	0.0070
10,000	94.3	5.7	92.1	7.9	0.0069

Table 3. Average metallic compositions and average equivalent diameter of VN and Cr_2N particles in as-treated and aged samples of M2 alloy.

Sample	Particle type	Number of analyzed particles	Average equivalent diameter (nm)	Average chemical composition (at.%)		
				Cr	V	Fe
As-treated (78 particles)	VN	46	60	30	69	1
	Cr_2N	32	124	81	18	1
650 °C/1000 h (85 particles)	VN	40	70	27	72	1
	Cr_2N	45	155	80	19	1
650 °C/5000 h (115 particles)	VN	55	75	22	77	1
	Cr_2N	60	250	78	21	1
650 °C/10,000 h (127 particles)	VN	54	80	18	81	1
	Cr_2N	73	377	77	22	1
Calculated equilibrium at 750 °C	VN	–	–	40	60	0
	Cr_2N	–	–	85	15	0
Calculated equilibrium at 650 °C	VN	–	–	30	70	0
	Cr_2N	–	–	80	20	0

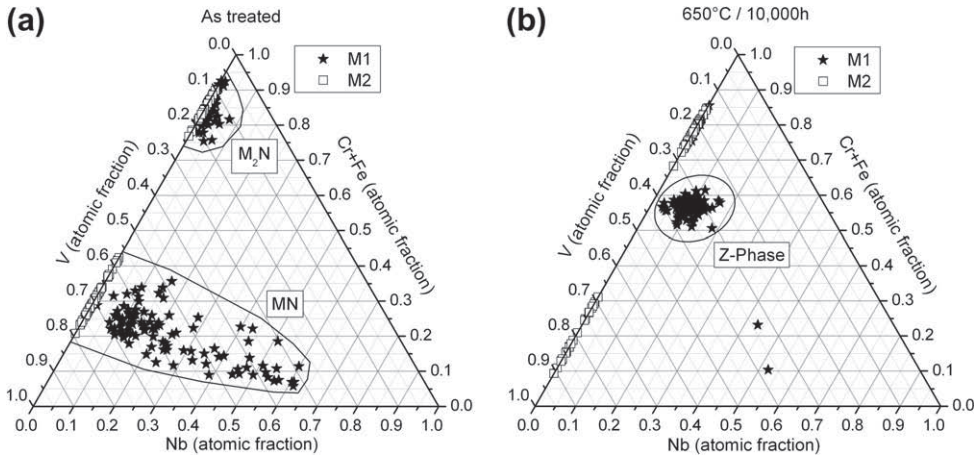

Figure 2. Ternary diagrams of precipitate composition in M1 and M2 in as-treated (a) and aged 10,000 h (b) conditions.

consistent with a relative reduction of the intensity of the line profiles of VN on ageing of M2 (cf. Fig. 1).

Average compositions measured for Cr_2N and VN precipitates in M2 are collected in Table 3. The data reflect that the content of Cr in both Cr_2N and VN is reduced on prolonged ageing. A similar decrease in the Cr content in Cr_2N was also observed in M1, while (V,Nb)N became enriched in Cr and gradually transformed into Cr(V,Nb)N particles [7]. The compositions of the precipitates in the extraction replicas for M1 and M2 alloys in the as-tempered condition and after ageing for 10,000 h are presented in the ternary diagrams of Figure 2. The regions for M_2N, MN and Z-phase are marked. In the M2 alloy no particles were found with a Cr:V ratio comparable with that of Z-phase, but only particles consistent with the composition M_2N and MN. Only occasionally were particles in the 10,000 h specimen identified with a morphology and composition similar to that of hybrid particles, i.e. particles of VN onto which Z-phase develops at the rim and where the average Cr content is in the range 30–40 at.% with respect to metal atoms in the precipitate [7]. An example of such a particle is shown in Figure 3: the core of the particle is V-rich (VN composition), while the wings of the particle are Cr-rich (Z-phase composition). The core/wing particles were identified as hybrids solely based on composition (particles with similar composition/morphology have previously been identified as such by electron diffraction [6]).

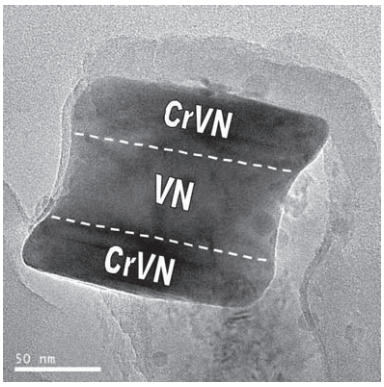

Figure 3. Hybrid MX/Z-phase particle with "H" morphology. The core of the particle is V-rich (metallic composition (at.%): V 83; Cr 16; Fe 1), while the wings of the particle are Cr-rich (metallic compositions (at.%): V 54; Cr 42; Fe 4 (upper) and V 53; Cr 43; Fe 4 (lower).

X-ray diffraction data show that the fraction of VN in M2 decreases as ageing proceeds until it reaches a constant value. Thermodynamically this change is explained in terms of the different equilibrium contents of VN and Cr_2N at the tempering temperature of 750 °C, where Cr_2N is not very stable, and the ageing temperature of 650 °C. Assuming all N is bound in nitrides and that its residual amount in solid solution is negligible at both 650 and 750 °C, the decrease in amount of MN and increase of M_2N on changing from 750 to 650 °C implies the transfer of V and N from VN to Cr_2N (see Table 3). The equilibrium compositions of Cr_2N and VN at 650 and 750 °C as calculated by the JMatPro software [11] are given in Table 3 together with the compositions determined with TEM–EDS, and indicate that the Cr content in both Cr_2N and VN is smaller at the lower temperature.

From a direct inspection of the diffractograms it has been observed that while the position of the peaks associated with Cr_2N remained largely unchanged, that of VN varied with time. Although this is mainly ascribed to the variation of the chemical composition of the phase, as mentioned above, another possible explanation could be a slight tetragonal distortion of the cubic lattice. However, within the experimental accuracy, the latter hypothesis cannot be confirmed.

The most relevant difference in the microstructural evolution on ageing between the model alloys is the absence of Z-phase in the Nb-free M2 up to 10,000 h at 650 °C, as compared to the relatively fast Z-phase precipitation found in alloy M1. CrNbN is known to be more thermodynamically stable than CrVN [5]. It is not expected that this difference in stability can explain the difference in the Z-phase precipitation rate, as the M1 alloy only contains a small amount of Nb, and even the Z-phases in M1 do not have a high Nb content. An alternative explanation can be found in the significant difference between the peak positions of the V-rich MN precipitates, indicating that the lattice parameters at least are significantly different, such that, as a consequence of Nb dissolution, MN has a larger lattice parameter in M1 than in M2. The lattice parameter for VN in alloy M2 has a value $a = 4.08$ Å which allows a semicoherent interface of the type $(0\,0\,1)_{\alpha\text{-Fe}}//(0\,0\,1)_{VN}$ and $[1\,0\,0]_{\alpha\text{-Fe}}//[1\,1\,0]_{VN}$ between the tempered martensite matrix and the precipitates with a misfit of only 0.65% [10]. On the other hand the lattice parameter in (V,Nb)N of about $a = 4.20$ Å would be associated with a coherency misfit of about 3.6% if the above-mentioned Baker–Nutting orientation relation applied. This difference in coherency misfit implies that the interfacial energy for (V,Nb)N in alloy M1 is higher than for VN in alloy M2. Accordingly, in order to explain the role of Nb in the occurrence of Z-phase, the following hypothesis is proposed.

The development of hybrid particles where Z-phase develops at the rim of (V,Nb)N precipitates, as observed in alloy M1 [7], is associated with a lowering of the interfacial energy of these particles, because, at these locations, the lattice parameter is reduced by the incorporation of Cr in the lattice of (V,Nb)N (cf. composition data for (V,Nb)N in Ref. [7]). A similar reduction in the lattice parameter by Cr incorporation does not occur for VN particles in alloy M2 as the atomic radii of V and Cr are almost identical, and different to that of Nb. In fact, the Cr content in the VN particles is slightly reduced on ageing (see Table 3).

The M2 alloy has a higher nitrogen content than alloy M1 (Table 1). This might affect the observed stabilities of Cr_2N and VN, as N stabilizes Cr_2N rather than VN. In spite of this there are many VN precipitates left after 10,000 h of ageing, while no Z-phase was identified; only a few hybrids were observed. It is therefore concluded that this enhanced stability of Cr_2N plays a minor role and that the major role of Nb on Z-phase formation is enhancing the interfacial energy between (V,Nb)N and ferrite, which is reduced by incorporation of Cr and the development of hybrid particles.

The results discussed above are consistent with past investigations on aged X20 steel grade (an old Nb-free 12% Cr steel grade), where it was shown that Z-phase precipitates very slowly as compared with other Nb-containing 12% Cr steels [5]. In X20, the Z-phases present have the CrVN composition. The reason that X20 first develops Z-phase after prolonged ageing is likely to be the absence of Nb. These insights could in principle pave the way for the development of oxidation-resistant Nb-free steels with a Cr content of 12%, with VN particles providing the strength.

Silvia Tiberi Vipraio from Centro Sviluppo Materiali is thanked for her valuable work and suggestions. Marcello Ballone from Centro Sviluppo Materiali is thanked for excellent TEM sample preparation.

[1] J. Hald, Steel Res. J. 67 (9) (1996) 369–374.
[2] K.H. Mayer, A. Scholz, Y. Wang, Materialwiss. Werkstofftech. 37 (10) (2006) 806–811.
[3] M. Yoshizawa, M. Igarashi, K. Moriguchi, A. Iseda, Hassan Ghassemi Armaki, K. Maruyama, Mater. Sci. Eng. A 510–511 (2009) 162–168.
[4] K. Sawada, H. Kushima, K. Kimura, ISIJ Int. 46 (5) (2006) 769–775.
[5] H.K. Danielsen, J. Hald, Energy Mater. 1 (1) (2006) 49–57.
[6] H.K. Danielsen, J. Hald, Mater. Sci. Eng. A 505 (2009) 169–177, doi:10.1016/j.msea.2008.11.019.
[7] L. Cipolla, H.K. Danielsen, D. Venditti, P.E. Di Nunzio, J. Hald, M.A.J. Somers, Acta Mater. 58 (2010) 669–679.
[8] H.K. Danielsen, J. Hald, Calphad 31 (4) (2007) 505–514, doi:10.1016/j.calphad.2007.04.001.
[9] P.E. Di Nunzio et al., Mater. Sci. Technol., in press, doi:10.1179/026708309X12567268926687.
[10] M.A.J. Somers, R.M. Lankreijer, E.J. Mittemeijer, Philos. Mag. A 59 (1989) 353–378.
[11] JMatPro: Practical Software for Materials Properties. Available from: http://www.sentesoftware.co.uk.

DTU Mechanical Engineering
Section of Solid Mechanics
Technical University of Denmark

Nils Koppels Allé, Bld. 404
DK- 2800 Kgs. Lyngby
Denmark
Phone (+45) 45 25 42 50
Fax (+45) 45 93 14 75
www.mek.dtu.dk
ISBN: 978-87-90416-29-4

DCAMM
Danish Center for Applied Mathematics and Mechanics

Nils Koppels Allé, Bld. 404
DK-2800 Kgs. Lyngby
Denmark
Phone (+45) 4525 4250
Fax (+45) 4593 1475
www.dcamm.dk
ISSN: 0903-1685